RESPONSE CHARACTERISATION OF NANOSTRUCTURES SUBJECTED TO UNCERTAIN LOADING AND MATERIAL CONDITIONS BY CONVEX MODELLING

Isaac Sfiso Radebe

In fulfillment of the
Master of Science in Enginering

College of Agriculture, Engineering and Science
University of KwaZulu-Natal

Supervisor: Professor S. Adali

December 2014

As the candidate's Supervisor I agree/do not agree to the submission of this thesis.

Date :

Professor S. Adali

DECLARATION 1 - PLAGIARISM

I.....declare that

(i) The research reported in this thesis, except where otherwise indicated, is my original work.

(ii) This thesis has not been submitted for any degree or examination at any other university.

(iii) This thesis does not contain other person's data, pictures, graphs or other information, unless specifically acknowledged as being sourced from other persons.

(iv) This thesis does not contain other person's writing, unless specifically acknowledged as being sourced from other researchers. Where other written sources have been quoted, then:

  a) their words have been re-written but the general information attributed to them has been referenced;

  b) where their exact words have been used, their writing has been placed inside quotation marks, and referenced.

(v) Where I have reproduced a publication of which I am an author, co-author or editor, I have indicated in detail which part of the publication was actually written by myself alone and have fully referenced such publications.

(vi) This thesis does not contain text, graphics or tables copied and pasted from the Internet, unless specifically acknowledged, and the source being detailed in the thesis and in the References sections.

Signed:

DECLARATION 2 - PUBLICATIONS

DETAILS OF CONTRIBUTION TO PUBLICATIONS that form part and/or include research presented in this thesis (include publications in preparation, submitted, *in press* and published and give details of the contribution of each author to the experimental work and writing of each publication)

1. Isaac Sfiso Radebe and Sarp Adali, "Buckling and sensitivity analysis of nonlocal orthotropic nanoplates with uncertain material properties", *Composites: Part B*, V. 56, 840-846, 2014.

2. Isaac Sfiso Radebe and Sarp Adali, "Effect of surface stress on the buckling of nonlocal nanoplates subject to material uncertainty", *accepted for publication in the Latin American Journal of Solids and Structures.*

3. Isaac Sfiso Radebe and Sarp Adali, "Static and sensitivity analysis of nonlocal nanobeams subject to load and material uncertainties by convex modelling", *accepted for publication in the Journal of Theoretical and Applied Mechanics.*

4. Isaac Sfiso Radebe and Sarp Adali, "Buckling of nonlocal orthotropic plates with uncertain material properties", (conference presentation), *17th International Conference on Composite Structures (ICCS 17)*, Porto, Portugal, 17-21 June 2013.

5. Isaac Sfiso Radebe and Sarp Adali, "Response characterisation of nanobeam to uncertain loading and appropriate modelling of boundary conditions", (conference presentation), *First International Conference on Composites, Biocomposites and Nanocomposites (ICCBN 2013)*, Durban, South Africa, 2-4 December 2013.

6. Isaac Sfiso Radebe, "Dynamic response characterisation of nanobeam subjected to uncertain loading", (conference presentation), *9th South African Conference on Computational and Applied Mechanics (SACAM 2014)*, Somerset West, South Africa, 14-16 January 2014.

Signed:

Abstract

Nanostructures are fast becoming the material of choice consequentially opening a new research frontier. Classical continuum computational techniques have proven insufficient in modelling the mechanical behaviour of these structures. The surface and nonlocal effects contributes to the size dependence of nanomaterial mechanical properties. Convex modelling techniques are employed in dealing with uncertainties associated with the lack of accurate measurements of nanostructures, molecular defects, and manufacturing anomalies. Numerical results are produced relating the level of uncertainty to maximum deflection for the nonlocal nanobeam, as well as determining the lowest buckling load subject to the effects of material uncertainty for nanoplates.

Acknowledgement

I would like to take this opportunity to express my special appreciation and gratitude to my supervisor Professor S. Adali, you have been an unparalleled mentor to me. Thank you for creating the space for my research and for your enduring patience and encouragement throughout all the phases of this project. I am indebted to your priceless mentorship on all aspect of my life, research and career. I would also like to thank Professor P. Tabakov for assisting with the necessary tools that made it possible for me to produce this report. I thank the University of kwaZulu Natal for the facilitating my registration. Thank you to my employer Durban University of Technology for sponsoring my studies. I would like to extend a special thanks to my children Wenzi and Khwezi as well as to the family at large. Lastly I would like to thank my beloved wife Ntombifuthi for all the sacrifices that she made and for being a pillar of strength to me. This has been a journey for all of us, your prayer is what sustained me thus far, thank you my love.

List of Figures

1.1 Line 8

1.2 Convex set 9

1.3 Hyperplanes 11

1.4 Epigraph 13

2.1 Atoms in array (a) Cubic array with a typical inter-atomic spacing r_0 of $0.2nm$. (b) Carbon atoms with each layer in a hexagonal array [10, 19]. 24

2.2 $2\boldsymbol{D}$ Half-space 26

2.3 Surface 27

3.1 Beam deformation 29

4.1 Plate deformation 35

4.2 Transverse loading 37

4.3 Moments 37

4.4 Lateral loads 38

4.5 Half-space (surface and cubic element) 42

Contents

DECLARATION 1 - PLAGIARISM ii

DECLARATION 2 - PUBLICATIONS iii

Abstract iv

Acknowledgement v

Introduction 1

Part I Theoretical Background 3

Chapter 1 Convex Space 4

1.1 Metric space 5

1.2 Concept of affine sets and functions 8

1.3 Convex sets 9

1.3.1 Cones 10

1.3.2 Hyperplanes and half-spaces 10

1.3.3 Euclidean ball 11

1.3.4 Ellipsoids 12

1.3.5 Polyhedron 12

1.4 Convex functions 12

1.5 Convex Models 14
1.6 Material uncertainty 16
1.7 Load uncertainty 17
1.8 Sensitivity analysis 18

Chapter 2 Small scale effects **20**

2.1 Nanotechnology 20
2.1.1 Carbon nanostructure composites 20
2.1.2 Growth and synthesis of nanostructures 21
2.1.3 Mechanical properties 22
2.2 Nonlocal theory 23
2.3 Surface effects 26

Chapter 3 Nonlocal Nanobeam **29**

3.1 Nano-beams 29
3.1.1 Governing equations 30
3.2 Principle of virtual work 32

Chapter 4 Small Scale Plate **35**

4.1 Plate theory 35
4.2 Governing equations 36
4.2.1 Classical plate equations 36
4.2.2 Nonlocal equations 40
4.2.3 Surface equations 41

Chapter 5 Final Discussion **44**

Bibliography **51**

Part II Publications **52**

Paper 1 Static and sensitivity analysis of nonlocal nanobeams subject to load and material uncertainties by convex modelling **53**

Paper 2 Buckling and sensitivity analysis of nonlocal orthotropic nanoplates with uncertain material properties **66**

Paper 3 Effect of surface stress on the buckling of nonlocal nanoplates subject to material uncertainty **74**

Introduction

The whole thrust of this dissertation is to contribute certain aspects towards a system that will serve as a framework in the description and analysis of nanostructures. Given the scale of nanostructures which is comparable to that of crystals, classical continuum modelling methods fail to factor in important phenomenons taking place in the system. Classical continuum techniques consider stress acting at a point to be a function of strain at that particular point. Further more there is no provision made to accommodate material property variations as well as loading anomalies which may prove to be detrimental to the structure in question.

At a small-scale structures tend to display exaggerated characteristics that are attributable to small-scale or even uniquely scale-dependant effects. Atomic arrangements or patterns near the surface of the structures are disrupted and anomalous when compared to the atoms in the body of the same structure. This in turn tends to give rise to the surface energy associated with the extension of the surface front, but more importantly bringing forth the surface stress that is responsible for the density arrangement of atoms near the surface. Material imperfections (i.e., inclusions, etc.) further complicates these structural arrangements. Added to this is the fact that the atomic length-scale is such that the stress at a point is a function of strain everywhere in the body of these nanostructures. The loading mechanism at this scale as well as the nature of the loads remain uncertain and indeterministic. Given all of the above a shift in the framework of the analysis of the small-scale structures becomes necessary, which proved to be the main motivation for this project.

The most distinguishing factor between what is covered in the literature and what is presented in this dissertation is the fact that material properties and the static loads are assumed to be uncertain but bounded in our study. Convex models of the uncertain parameters are proposed where the solution is attainable by using the method of Lagrange multipliers. The study covers the deflection of a nano-beam subject to small-scale effects, load and material property uncertainty. It also deals with the nonlocal and surface effects on the buckling of isotropic nanoplates together with nonlocal effects on the buckling of orthotropic nanoplates subject to the variation of the material properties. Analysis of the sensitivity of the deflection for the nanobeam and buckling load for nanoplates, to material uncertainty is also presented.

Dissertation overview

The structure of the dissertation follows this format;

Part I of the dissertation covers the back-ground theory and derivations of the equations used in the greater portion of the dissertation more especially the sections that do not appear in the papers.

Chapter 1 deals with convex modelling. Theoretical formalities around the development of a *metric space* are introduced followed by the description and attributes of the interval in an attempt to conceptually bridge the two spaces namely the Euclidean space and set-theoretic space. Essential characteristics of the set-theoretic space are sequentially constructed from the basic elementary sets to the complex convex sets. Convex models are covered culminating with materials and loading uncertainty models as well as a brief coverage of issues around sensitivity analysis.

Chapter 2 deals with small-scale effects. In this chapter aspects of nanotechnology are covered starting with the practical end-product related usage of nanostructures, followed by the process of synthesising nanostructures and the determination of the material properties. Theoretical back-ground of the nonlocal and surface effects in the context of nanostructures is also given.

Chapter 3 deals with the beam theory at a small-scale. The governing equations of the nonlocal beam are derived first via a static element model followed by the energy model.

Chapter 4 deals with plate theory at a small-scale. Classical governing equations for an orthotropic nanoplate are derived leading to their expansion covering nonlocal effects. In the last section the governing equation for an isotropic nanoplate subject to surface effects is derived.

Chapter 5 presents the final discussion of all the work covered in the dissertation and the summary of the results in the three papers.

Part II contains publications that serve as an anchor to this dissertation. The chapters are arranged in the following order;

Paper 1 Isaac Sfiso Radebe and Sarp Adali, "Static and sensitivity analysis of nonlocal nanobeams subject to load and material uncertainties by convex modelling", *accepted for publication in the Journal of Theoretical and Applied Mechanics*.

Paper 2 Isaac Sfiso Radebe and Sarp Adali, "Buckling and sensitivity analysis of nonlocal orthotropic nanoplates with uncertain material properties", *Composites: Part B*, V. 56, 840-846, 2014.

Paper 3 Isaac Sfiso Radebe and Sarp Adali, "Effect of surface stress on the buckling of nonlocal nanoplates subject to material uncertainty", *accepted for publication in the Latin American Journal of Solids and Structures*.

Part I

Theoretical Background

Chapter 1

Convex Space

Quality control and continuous evaluation of manufacturing processes involved in the production of various structural materials used in designing various products, have been steadily improving. Material testing under controlled environment and loading conditions have resulted in the production of large data banks pertaining to mechanical properties of various materials. However demands of exotic high end products coupled with competition amongst producers dictates that input materials and means of production be continuously renewed. Resulting from this venturesome exercise imperfections are bound to occur, be it in the modelling phase, or in producing required materials, or even at a fabrication stage. In production lines there is always going be some variation and inconsistencies taking place.

For precise analysis of any mechanical system the practitioner must have reliable tools at hand that will assist in giving a definitive understanding of the phenomena involved together with some prediction for the structural performance. There are numerous models that were developed in the past and have been used successfully for years with some degree of accuracy and reliability. Most of these models take it for granted that the information supplied in relation to the influences, external and internal, affecting the structure are certainly known and can be relied upon not to vary to the detriment of the structure. However if there is uncertainty [1,3,56] in relation to input information careful consideration of the modelling regime becomes necessary and can make or break the solution. Probabilistic models have been used extensively where data on random variables and functions were identifiable. Numerical characterisation that encompasses joint probability density functions relies on the data being known *a priori* if the model is to yield accurate outcome without distorting the results. Following this path normally leads to the determination of reliability of the structure or system in question as an end product [11,24]. In most applications this information is not readily available, thus presenting a problem in the implementation which cannot be trivialised.

On the other hand in cases where known data is insufficient for probabilistic analysis [2, 11, 24, 25], convex modelling has proven to be reliable. Convex modelling is a *set theory* based technique where in its formulation uncertain phenomena are modelled

and represented according to defined admissible convex sets and functions together with the extrema of convex sets and functions. The implications from this technique translate to the fact that it is not a prerequisite to have all the information beforehand. Solutions to difficult problems can be found by bounding uncertainties and matching them to specific perturbed solution sets . Thus a brief description of the set theory, conventions and topological properties of convexity applied to abstract *metric space* are presented.

1.1 Metric space

When constructing an abstract *metric space* or a distance function, elementary illustrations of the concepts and properties at play in the Euclidean $\mathcal{E}^n$ space which is understood and well established, can enhance our perspective at the same time serving as a bridge or some projection onto the characteristics of the former space. Einstein is recorded as having said [22]; *"A geometrical-physical theory as such is incapable of being directly pictured, being merely a system of concepts. But these concepts serve the purpose of bringing a multiplicity of real or imaginary sensory experience into connection in the mind. To "visualise" a theory, or bring it home to one's mind, therefore means to give a representation to that abundance of experiences for which the theory supplies the schematic arrangement"* As such the following definitions are important in understanding the structure of Euclidean space with respect to its basic subsets.

Take $\mathcal{E}$ to be a non-empty universal set with points as elements [38]

$$\{X_1, X_2, \ldots, X_n\} \tag{1.1}$$

such that its complement $\mathbf{cp}(\mathcal{E})$ is a null set $\emptyset$. If the ordered pairs associated with it have a real number

$$\{f(X_1, X_2) : (X_1, X_2) \in \mathcal{E},\ f \in \mathcal{E}\} \tag{1.2}$$

then the real valued function f is said to be a metric for $\mathcal{E}$ subject to the following restrictions and regulations;

i) $f(X_1, X_2) \geq 0$ equality if and only if $X_1 = X_2$.

ii) $f(X_1, X_2) = f(X_2, X_1)$ symmetry.

iii) $f(X_1, X_2) + f(X_2, X_3) \geq f(X_1, X_3)\ \forall \{X_1,\ X_2,\ X_3\} \in \mathcal{E}$ triangle inequality.

Thus set $\mathcal{E}$ and f make up the *metric space*. Following from this subsequent definitions apply.

Boundedness in the metric space: If a set $\mathcal{L}$ is bounded above [38], this translates to the set being contained in some ball

$$\left\{ \|X - X_n\| \ :\ \{\exists k \ :\ f(X_1, X_2) \leq k,\ k \in \mathcal{E}\},\ \forall \{X_1,\ X_2\} \in \mathcal{L} \right\} \tag{1.3}$$

where

$$\|X - X_n\| = \sqrt{(X_1 - X_2)^2} \tag{1.4}$$

is the Euclidean distance between points. Using above mentioned definitions further attributes and restrictions are deducible.

Connectedness in the Euclidean metric space $\mathcal{E}$: The concept of connectedness can be better explained by defaulting to the basic sets of the Euclidean space namely the intervals. The *bounded intervals* (for $a < b$) are defined with respect to real numbers if the sets are contained as follows;

a) *open interval*

$$(a,\, b) = \{x \,:\, a < x < b\} \tag{1.5}$$

with a typical example of the neighborhood in a following manner;

i) *neighborhood*

$$\mathbf{N}(x_c, \delta) = \{x :\, f(x_c, x) < \delta\} \tag{1.6}$$

$$\text{where} \qquad x_c = \frac{(a+b)}{2},\, \delta = \frac{(b-a)}{2}$$

ii) *deleted neighborhood*

$$\mathbf{N}_0(x_c, \delta) = \{x :\, 0 < f(x_c, x) < \delta\} \tag{1.7}$$

$$\text{where the } \textit{open interval} \text{ is} \qquad (x_c - \delta, x_c + \delta).$$

b) *closed interval*

$$[a,\, b] = \{x \,:\, a \leq x \leq b\} \tag{1.8}$$

with the *ball* as a prototype of a *closed interval*;

$$\textit{ball} \qquad \mathbf{B}(x_c, \delta) = \{x :\, f(x_c, x) \leq \delta\} \tag{1.9}$$

$$\text{where} \qquad x_c = \frac{(a+b)}{2},\, \delta = \frac{(b-a)}{2}$$

bounded above and below;

c) *endpoints interval* $\{a,\, b\}$ is the 1-dimensional sphere

$$\textit{sphere} \qquad \mathbf{S}(x_c, \delta) = \{x :\, f(x_c, x) = \delta\} \tag{1.10}$$

$$\text{where} \qquad x_c = \frac{(a+b)}{2},\, \delta = \frac{(b-a)}{2}$$

d) *half open interval*

$$\textit{greatest lower bound} \qquad [a,\, b) = \{x \,:\, a < x < b\} \tag{1.11}$$

$$\textit{least upper bound} \qquad (a,\, b] = \{x \,:\, a < x < b\} \tag{1.12}$$

e) *unbounded interval*

i)
$$(a,\, \infty) = \{x \,:\, a < x\} \tag{1.13}$$

ii)
$$[a,\, \infty) = \{x \,:\, a \leq x\} \tag{1.14}$$

iii)
$$(-\infty,\, a) = \{x \,:\, x < a\} \tag{1.15}$$

iv)
$$(-\infty,\, a] = \{x \,:\, x \leq a\} \tag{1.16}$$

v)
$$(-\infty,\, \infty] = \mathbf{R} \tag{1.17}$$

Compactness in Euclidean metric space $\mathcal{E}^n$: Following from the results already established it possible to describe the concept of set compactness using the following theorem.

Theorem 1 [38, p.49] A set of real numbers is compact and connected if and only if it is a closed, bounded interval.

Mappings of metric space:

Theorem 2 [38, p.50] If $f : \mathcal{D} \to \mathcal{R}$ is a continuous, real valued function, and $\mathcal{D}$ is a compact, connected subset of a metric space, then f achieves a minimum value, a maximum value, and every intermediate to these.

Linear function: $f : \mathcal{E}^n \to \mathcal{E}$ on a vector space $\mathcal{E}^n$ is the image under f of some $s \in \mathcal{E}^n$ linear combinations of vectors onto (surjective) [35] the same linear combinations $t \in \mathcal{E}$.

$$f(s) = \{t :\, f(s) \in \mathcal{E},\, s \in \mathcal{E}^n\} \tag{1.18}$$

Systems of linear inequalities possess functions that are bounded or sometimes unbounded where the governing boundary conditions have both strict $<, >$ or non-strict $\leq, \geq$ constraints. Simplified linear transformation can be explicitly characterised as a linear function if and only if there exist a unique vector a in vector space $\mathcal{E}^n$ such that

$$f(x) = a\, x. \tag{1.19}$$

where mapping in the linear subspace contains the origin. The general subspace of $\mathcal{E}^n$ *(affine space)* that does not include the origin relates to linear translation of $\mathcal{E}^n$

$$f(x) = a\, x + \upsilon \tag{1.20}$$

by a vector $\upsilon \in \mathcal{E}^n$. Therefore a general subspace of $\mathcal{E}^n$ is a translate of a n-dimensional linear subspace.

1.2 Concept of affine sets and functions

Affine sets: The basic concepts of affine combination of vectors [59] in vector space are best demonstrated by observing a group of transformations. Suppose there are two points with coordinates x_1 and x_2 in $\mathbf{R}^n$ space, joined together by some transformation in a form of

$$(1-\alpha)x_1 + \alpha x_2 \text{ where } \alpha \in \mathbf{R}$$

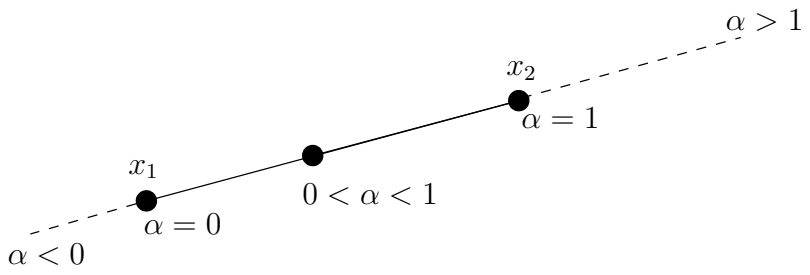

Figure 1.1: Line

generally referred to as a line through x_1 and x_2. A subset C of $\mathbf{R}^n$ in a form

$$\{(1-\alpha)x_1 + \alpha x_2 \in C : x_1 \in C, x_2 \in C, \alpha \in \mathbf{R}\}$$

is an affine set. An affine set must contain x_1 and x_2 as well as the entire line [13,38,55] through x_1 and x_2. Generally a subset C of $\mathbf{R}^n$ is affine if for every points $x_1, \ldots, x_n \in C$ and every number $\alpha_i \in \mathbf{R}$ contains every affine combination of points $\alpha_1 x_1 + \ldots + \alpha_n x_n \in C$ where the affine coefficients $\alpha_1 + \ldots + \alpha_n = 1$. Further more the affine set is closed under summation and scalar multiplication. The set $C \subseteq \mathbf{R}^n$ that contains all affine combinations of points in C,

$$\mathbf{aff}C = \left\{ \sum_{n=1}^{N} \alpha_n x_n \Big| x_n \in C,\ \left\{ \forall\, \alpha \in \mathbf{R} \Big| \sum_{n=1}^{N} \alpha_n = 1 \right\} \right\} \tag{1.21}$$

is called the *affine hull*. It is the smallest affine set that contains C, also defining the *affine dimension* of the same set.

Affine function: The same applies to a functional transformation where a function maps every affine combination of points x_n in $\mathbf{R}^n$ space, onto the same affine combination of their image.

$$f\left(\sum_{n=1}^{N} \alpha_n x_n \right) = \left\{ \sum_{n=1}^{N} \alpha_n f(x_n) \Big| x_n \in C,\ \left\{ \forall\, \alpha \in \mathbf{R} \Big| \sum_{n=1}^{N} \alpha_n = 1 \right\} \right\} \tag{1.22}$$

It has been shown again through theorems and proofs [11, 13, 55] that the following assertions are true. If $a \neq 0$ then the linear functional $f(x) = a\,x$ and the affine functional $g(x) = a\,x + \upsilon$ map bounded sets onto bounded sets, neighborhoods onto

neighborhoods, balls onto balls, and open sets onto open sets. Convex modelling is a generalisation of linear programming problems with special or unique restrictions. Every affine set is convex, and in the extreme cases it includes an empty set ϕ and sets that consist of solitary points of the $\mathbf{R}^n$ space.

1.3 Convex sets

A set $C \in \mathbf{R}^n$ is convex if for any points $x_1, \ldots, x_k \in C$ and any number $\alpha_i \in \mathbf{R}$ where $\alpha_1 + \ldots + \alpha_n = 1$ and $\alpha_i \geq 0, i = 1, \ldots, k$ it contains all convex combinations $\alpha_1 x_1 + \ldots + \alpha_n x_n \in C$ of elements within the set [13]. Similarly to the affine set discussed above, the *convex hull* of set C,

$$\mathbf{conv}C = \{\alpha_1 x_1 + \ldots + \alpha_k x_k \ : \ x_1, \ldots, x_k \in C, \alpha_i \geq 0, i = 1, \ldots, k, \alpha_1 + \ldots + \alpha_k = 1\}, \tag{1.23}$$

is the smallest set that contains all convex combinations of C. The distinguishing factor that makes convex sets more general than affine sets is the restriction imposed in its formulation i.e., $\{(1-\alpha)x_1 + \alpha x_2 \ : \ 0 \leq \alpha \leq 1\}$ which is referred to as the (closed) line segment between x_1 and x_2 [55].

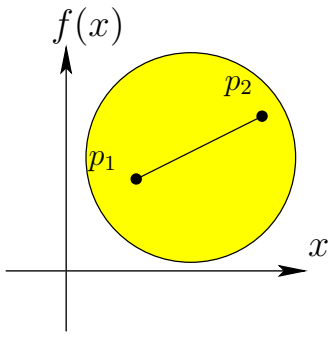

Figure 1.2: Convex set

Naturally the generalisation of convex combinations include infinite sums, such that $\alpha_1, \ldots, \alpha_\infty$ satisfy

$$\alpha_i, \qquad i = 1, 2, \ldots \qquad \sum_{i=1}^{\infty} \alpha_{i=} 1$$

and $x_1, x_2, \ldots \in C$ where $C \subseteq \mathbf{R}^n$ is convex. Then

$$\sum_{i=1}^{\infty} \alpha_i x_i \in C$$

provided the series converges [13].

They also cover integrals such that; $P : \mathbf{R}^n \to \mathbf{R}$ satisfies $P(x) \geq 0$ for all $x \in C$ and $\int_C P(x).dx = 1$, where $C \subseteq \mathbf{R}^n$ is convex. Then

$$\int_C P(x).x.dx \in C$$

if the integral exists [13].

Other convex sets of function [11, p.51] are:

$$\mathbf{A} = \{f : |f(x)| \leq 1\}$$

$$\mathbf{B} = \{f : |\frac{df}{dx}| \leq 1\}$$

$$\mathbf{C} = \{f : \int_{-\infty}^{\infty} f^2(x)dx \leq 1\}$$

of which the proof is shown in the above mentioned reference.

It has been shown through theorems and proofs that the following assertions are true [38]. Convex span of a finite set R is also its convex hull. The extreme point of convex set R belong to every finite subset of convex set R whose convex span is **conv**R. These extreme points of a convex set R are contained in every subset of R whose convex hull is R. If R is convexly independent, then R is the set of extreme points of **conv**R. The convex hull of any set $\mathcal{L}$ is the union of the convex spans of all the finite subsets of $\mathcal{L}$. Therefore the convex hull of any set $\mathcal{L}$ can be be built-up from inside by forming unions of convex spans of finite subsets of $\mathcal{L}$. If R is a convex, compact set then the convex hull of set R is a finite set of extreme points of R:- $R = \mathbf{conv}[\mathbf{extem}(R)]$.

1.3.1 Cones

The *conic hull* of a set C is convex if the *conic combinations or non-negative linear homogeneous combinations* is as follows,

$$\{\alpha_1 x_1 + \ldots + \alpha_k x_k \ : \ x_i \in C, \ \alpha_i \geq 0, \ i = 1, \ldots, k\} \tag{1.24}$$

the smallest convex cone containing C.

1.3.2 Hyperplanes and half-spaces

a) A hyperplane is a set of the following form

$$\{x : a^T x = b \ a \in \mathbf{R}^n, \ a \neq 0, \ b \in \mathbf{R}\} \tag{1.25}$$

Theorem 3 [38, p.94] Corresponding to a hyperplane $\mathcal{H}$, there exists a non-null vector $\mathbf{a}$ and a real number υ such that $\mathcal{H}$ is the graph of $\mathbf{a} \cdot x = \upsilon$. The vector $\mathbf{a}$ is orthogonal to $\mathbf{PQ}$ for all P, Q in $\mathcal{H}$, and $\mathbf{LS}(\mathbf{a})$ (linear span of $\mathbf{a}$) is precisely the set of vectors that have this property.

Theorem 4 [38, p.98] Each point P in space has a unique foot P_0 in a hyperplane; $\mathcal{H} : \ f(x) = \mathbf{a} \cdot x = \upsilon$, and

$$d(P, \mathcal{H}) = \frac{|f(p) - \upsilon|}{|\mathbf{a}|} \tag{1.26}$$

$$= \frac{|\mathbf{a} \cdot P - \upsilon|}{|\mathbf{a}|} \tag{1.27}$$

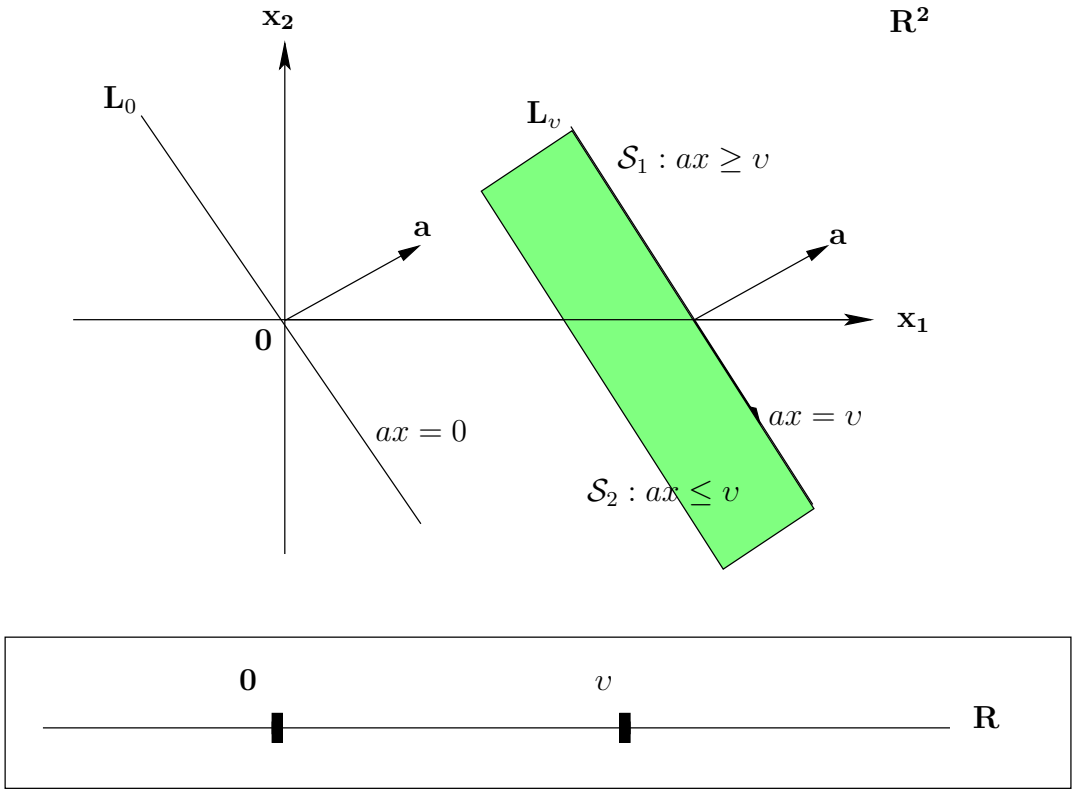

Figure 1.3: Hyperplanes

Then if there are two distinct parallel hyperplanes $\mathcal{H}_1 : f(x) = \mathbf{a} \cdot x = \upsilon_1$ and $\mathcal{H}_2 : f(x) = \mathbf{a} \cdot x = \upsilon_2$ with a common normal direction and same linear functional, the distance between them $d(\mathcal{H}_1, \mathcal{H}_2)$ is expressed as follows;

$$d(X_2, \mathcal{H}_1) = d(X_1, \mathcal{H}_2) = \left\{ \frac{|\upsilon_1 - \upsilon_2|}{|\mathbf{a}|} \qquad \forall\, X_1 \in \mathcal{H}_1 \,\text{and}\, X_2 \in \mathcal{H}_2 \right\} \tag{1.28}$$

Every supporting hyperplane to a convex body $\mathcal{K}$ contains an extreme point of $\mathcal{K}$.

b) Opposite sides of half-spaces are a *closed* sets of the form

$$\{x \,:\, a^T x \leq b \text{ or } a^T x \geq b,\ a \in \mathbf{R}^n,\ a \neq 0,\ b \in \mathbf{R}\} \tag{1.29}$$

c) opposite sides of half-spaces are *open* sets represented as follows

$$\{x \,:\, a^T x < b \text{ or } a^T x > b,\ a \in \mathbf{R}^n,\ a \neq 0,\ b \in \mathbf{R}\} \tag{1.30}$$

1.3.3 Euclidean ball

An Euclidean ball is of the following form

$$\mathbf{B}\,(x_c, r) = \{x \,:\, \| \, x - x_c \, \|_2 \leq r\} = \{x_c + ru \,:\, \| \, u \, \|_2 \leq 1\}$$

where the radius $r > 0$, x_c the center of the ball and $\| \ \|_2$ the L_2 norm,i.e., $\| \ u \ \|_2 = \sqrt{(u^T u)}$. Convex norm ball with r as the radius, x_c the center is represented as follows $\{x : \| \ x - x_c \ \| \leq r\}$.

1.3.4 Ellipsoids

Ellipsoids are of the following form

$$\varepsilon = \{x_c + \mathbf{A}u : \| \ u \ \|_2 \leq 1\}$$

where $\mathbf{A}$ is assumed to be a symmetric and positive definite matrix.

1.3.5 Polyhedron

A polyhedron is the following

$$\mathcal{P} = \{x : \mathbf{A}x \preceq b, \ \mathbf{C}x \preceq d\}$$

$$\text{where} \qquad \mathbf{A} = \begin{bmatrix} a_1^T \\ \vdots \\ a_m^T \end{bmatrix}, \quad \mathbf{C} = \begin{bmatrix} c_1^T \\ \vdots \\ c_m^T \end{bmatrix}$$

$\preceq$ denotes *componentwise vector inequality.*

1.4 Convex functions

For a convex function the domain of a function $\mathbf{dom}f$ specifies the range for which $f(x)$ is defined.

$$f : R^n \to R \text{ then } f \text{ is convex if for the coefficients } \{\alpha_1, \ \alpha_2, \ldots, \alpha_n\}$$
$$f\left(\sum_{n=1}^{N} \alpha_n \, x_n\right) \leq \sum_{n=1}^{N} \alpha_n \, f(x_n)$$

Topological expressions of a convex function serves to further enhance the understanding of issues at play. Suppose there is a function with an epigraph $\mathbf{epi}f$ as shown in Figure 1.4. This is a set R^{n+1} that contains [55] all the points on or above the surface f.

$$\mathbf{epi}f = \{(x, y) : x \in \mathcal{D}, \, y \in R, \, y \geq f(x)\} \qquad \text{where } \mathcal{D} \subset R^n$$

Conditions imposed on a proper epigraph $\mathbf{epi}f$ are:

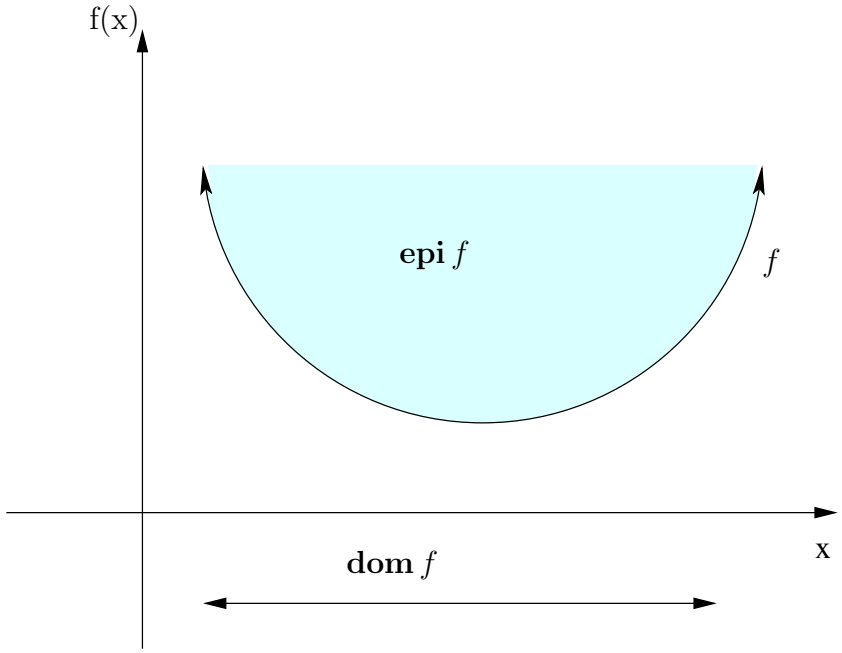

Figure 1.4: Epigraph

a) $\mathbf{epi}f = (x, y) \neq 0$ and has no vertical lines.
b) $\mathbf{conv}f = \mathbf{dom}f \neq 0$ where

$$\mathbf{dom}f = \{x : \exists y, (x, y) \in \mathbf{epi}f\}$$

f is convex in $\mathcal{D}$ if and only if

$$(1-\alpha)(x_1, y_1) + \alpha(x_2, y_2) = \{(1-\alpha)x_1 + \alpha\, x_2,\ (1-\alpha)y_1 + \alpha\, y_2\}$$

belongs to $\mathbf{epi}f$ whenever (x_1, y_1) and $(x_2,\ y_2)$ belongs to $\mathbf{epi}f$ and $0 \leq \alpha \leq 1$. This condition is equivalent to

$((1-\alpha)x_1 + \alpha x_2) \in R$ and
$((1-\alpha)x_1 + \alpha x_2) \leq ((1-\alpha)y_1 + \alpha\, y_2)$ whenever
$x_1 \in \mathcal{D},\ x_2 \in \mathcal{D},\ f(x_1) \leq y_1 \in R,\ f(x_2) \leq y_2 \in R$ and
$0 \leq \alpha \leq 1$

It has been shown again through theorems and proofs [13, 38, 55] that the following assertions are true. If the domain $\mathbf{dom}f$ of an affine functional f is a compact, convex set, then f achieves its maximum values and its values on the set $\mathbf{extrem}\{\mathbf{dom}f\}$.

Useful variances of functional convexity subject to different constraints [55]
a) Let $f : \mathcal{D} \to (-\infty, +\infty]$ where $\mathcal{D}$ is a convex set, then f is convex on $\mathcal{D}$ subject to the following restriction;

$$f\left(\sum_{n=1}^{N} \alpha_n x_n\right) \leq \sum_{n=1}^{N} \alpha_n f(x_n), \qquad 0 < \alpha < 1$$

whenever $x \in \mathcal{D}$.

b) Let $f : R \to [-\infty, +\infty]$, then f is convex subject to the following restriction;

$$f\left(\sum_{n=1}^{N} \alpha_n x_n\right) < \sum_{n=1}^{N} \alpha_n y_n, \qquad 0 < \alpha < 1$$

whenever $f(x_n) < y_n$.

c) (Jensen's Inequality). Let $f : R \to (-\infty, +\infty]$, then f is convex subject to the following restriction;

$$f\left(\sum_{n=1}^{N} \alpha_n x_n\right) \leq \sum_{n=1}^{N} \alpha_n f(x_n)$$

whenever $\alpha_n \geq 0,\ \sum_{n=1}^{N} \alpha_n = 1$.

1.5 Convex Models

Convex modelling is a process [11, 23, 25, 50] where a set of vectors or functions are specified using deterministic basis characteristics to estimate some uncertain quantity of the phenomenon in question. These quantities [24] of uncertainty can be stated and classified as sets of variables in groups bounded as follows;

a)

$$|x| \leq a \tag{1.31}$$

where x is the uncertain parameter and a is a constant,

b)

$$x_{lower}(t) \leq x(t) \leq x_{upper}(t) \tag{1.32}$$

where $x_{lower}(t)$ and $x_{upper}(t)$ are the deterministic functions,

c)

$$\int_{-\infty}^{\infty} x^2(t)\ dt \leq a \tag{1.33}$$

where the uncertain function $x(t)$ has an integral square bound. When modelling the uncertainty of the vector or function space [11], quantities of its definition are formulated in terms of a convex set $\mathbf{R}$ of allowed functions. A set of linear functions $\mathbf{E}$ whose convex hull is $\mathbf{R}$, is then used to maximise the set of allowed functions. This set is not restricted to having only the extremum of $\mathbf{R}$, but can contain just the fundamental functions of $\mathbf{R}$. The vector function quantities can also be modelled using set-theoretic method as follows [50];

$$F_n = \left\{ f : f(t) = \frac{1}{n} \sum_{i=1}^{n} g_i(t),\ g_i(t) \in \Gamma,\ i = 1, 2, \ldots, n \right\} \tag{1.34}$$

where F_n is the set of n-fold averages of vector functions in Γ. Various convex models are available and cover probably most applications to a certain degree. They are listed [11] as follows;

a) **Density functions**
Set of density functions of unit mass,

$$R_{df} = \left\{ f : f(x) \geq 0 \text{ and } \int_J f(x)dx = 1 \right\}, \tag{1.35}$$

and the extreme points are

$$E_{df} = \left\{ f : f(x) = \delta(x - \xi) \text{ for } \xi \in J \right\}, \tag{1.36}$$

where δ is the Dirac-function.

b) **Monotonic functions**
Set of real functions monotonically increasing

$$R_{mf} = \left\{ f : f(0) = 0,\ f(1) = 1, f(x) \leq\ f(y) \text{ for } 0 \leq x \leq y \leq 1 \right\}, \tag{1.37}$$

and the extreme points are

$$E_{mf} = \left\{ f : f(x) = K_{[0,\xi]}(x) \text{ for } 0 \leq \xi \leq 1 \right\}, \tag{1.38}$$

where

$$K_V(x) = \begin{cases} 1 & \text{if } x \in V, \qquad V \subset \mathcal{E}^n, \\ 0 & \text{otherwise.} \end{cases}$$

c) **Uniformly bounded functions**
Set of functions defined on a domain $J \in \mathcal{E}^n$

$$R_{ubf} = \left\{ f : |f(x)| \leq 1 \right\}, \tag{1.39}$$

and the extreme points are

$$E_{ubf} = \left\{ f : f(x) = K_U(x) - K_V(x) \text{ for } U \cap V = J,\ U \cup V = \emptyset,\ \{U,\ V\} \subset \mathcal{E}^n \right\}, \tag{1.40}$$

d) **Envelope bounded functions**

$$R_{ebf} = \left\{ f : f_{min}(x) \leq f(x) \leq f_{max}(x) \right\}, \tag{1.41}$$

where $f_{min}(x)$ and $f_{max}(x)$ are specified functions. The extreme points are

$$E_{ebf} = \left\{ f : f(x) = K_V(x)\, f_{max}(x) + K_U(x)\, f_{min}(x) \text{ for } U \cup V = J,\ U \cap V = \emptyset \right\} \tag{1.42}$$

e) **Functions of bounded energy**
Set of uniformly bounded functions,

$$R_{fbe} = \left\{ f : \int_J f^2(x)\, dx \leq 1 \right\}, \tag{1.43}$$

and the extreme points are

$$E_{fbe} = \left\{ f : \int_J f^2(x) dx = 1 \right\}, \tag{1.44}$$

f) **Frequency bounded functions**
Set of uniformly bounded functions,

$$R_{fbf} = \left\{ f : f = \sum_{n=1}^{N} c_n\, \varphi_n(x) \text{ for } c \in A \right\}, \tag{1.45}$$

if A is the solid ellipsoid then

$$A = \left\{ c = (c_1, \ldots, c_n) : \sum_{n=1}^{N} \left(\frac{c_n}{\omega_n} \right)^2 \leq 1 \right\}, \tag{1.46}$$

with the convex hull

$$B = \left\{ c = (c_1, \ldots, c_n) : \sum_{n=1}^{N} \left(\frac{c_n}{\omega_n} \right)^2 = 1 \right\}, \tag{1.47}$$

and the extreme points are

$$E_{fbf} = \left\{ f : f = \sum_{n=1}^{N} c_n\, \varphi_n(x) \text{ for } c \in B \right\} \tag{1.48}$$

1.6 Material uncertainty

Assuming that material property scatter on average are limited or bounded in some neighbourhood such that;

$$S(E, \delta) = \{ \tilde{E} \,:\, d(E, e) \leq \delta \} \tag{1.49}$$

where E is the uncertain elastic moduli and radius δ. Thus the buckling load N_{cr} can be perturbed [1] with respect to uncertain quantity $\tilde{E}$,such that;

$$N_{cr} = N_{cr}(E^0) + \left(\nabla N_{cr}(E^0),\, [\tilde{E}] \right) \tag{1.50}$$

where E^0 is the deterministic elastic moduli. Due to the convexity of this formulation the minimum value of N_{cr} is the hull of S such that;

$$N^*_{cr}(E^0, e) = \min \left\{ N_{cr}(E) \,:\, \sum_{i=1}^{k} \left(\frac{\tilde{E}_i}{e_i} \right)^2 = \alpha^2,\, \tilde{E} \in \partial S \right\} \tag{1.51}$$

where ∂S is the boundary of the convex set S with first partial derivatives at relative minimum. Because the variables $\tilde{E}_i (i = 1, 2, \ldots, k)$ are not independent but must satisfy a condition of constraints α the extremum can be found using a method of **Lagrange multipliers** such that;

$$\mathcal{L}\left(\tilde{E}, \Lambda\right) = \left(\nabla N_{cr}(E^0),\, [\tilde{E}]\right) + \Lambda \left(\sum_{i=1}^{k} \left(\frac{\tilde{E}_i}{e_i}\right)^2 - \alpha^2\right) \tag{1.52}$$

subject to

$$\frac{\partial \mathcal{L}}{\partial \tilde{E}} = 0 \tag{1.53}$$

which is a sufficient condition for the extremum points. Evaluating the partial differential the following equation is obtained

$$\frac{\partial \mathcal{L}}{\partial \tilde{E}} = \nabla N_{cr}(E^0) + 2\Lambda[\tilde{E}] = 0 \tag{1.54}$$

$$\tilde{E} = -(2\Lambda)^{-1} \nabla N_{cr}(E^0) \tag{1.55}$$

where Λ is the **Lagrange multiplier** with the following value;

$$\Lambda = -\frac{1}{4\alpha^2} \nabla^T N_{cr}(E^0)\, \xi^{-1} \nabla\, N_{cr}(E^0) \tag{1.56}$$

letting

$$\xi = \frac{\delta_{ij}}{e_i^2}, \qquad \text{with} \qquad (i, j) = (1, \text{ or } 2, \ldots, \text{or } 4) \tag{1.57}$$

where δ is the Dirac-function.

Then by substitution equation(1.56) into equation(1.52) and evaluating it terms of N_{cr}^*, the least favourable buckling load subject to constraint is obtained having the following value;

$$N_{cr}^* = N_c r(E^0) - \alpha \left(\sum_{i=1}^{k} \left(e_i \frac{\partial N_{cr}(E^0)}{\partial E_i}\right)^2\right)^{\frac{1}{2}} \tag{1.58}$$

which is the [1] semi-axis of the uncertain ellipsoid e_i linked with the scatter in the i-th elastic modulus.

1.7 Load uncertainty

When assessing structures for their inherent material properties it is common practice to subject them to various loading conditions. Variations in the loads (distribution, orientation, etc) result in different reactions within the material which can be correlated to the type of the applied load. However when there is uncertainty with respect to the nature of the load, modelling becomes difficult and unpredictable. On the other hand convex modelling in its formulation presents a mechanism of factoring into the

model elements of uncertainty with the solution providing a glimpse to the worst case scenario.

Assuming that load bearing $f^j(x_i)$ on the structure is bounded with variations confined within a neighbourhood. The load is then divided [1] into two components namely the deterministic $f_0^j(x_i)$ and uncertain component $\tilde{f}^j(x_i)$ as follows;

$$f^j(x_i) = \{f_0^j(x_i) + \tilde{f}^j(x_i) : \|\tilde{f}^j(x_i)\|_2^2 \leq \varepsilon_j^2,\ i = 1, 2, 3,\ j = 1, 2, \ldots, \zeta\} \tag{1.59}$$

where ε_j is the prescribed level of uncertainty for the j-th loading, ζ denoting the number of loads, i representing the orientation, and the L_2 norm$\|\ \|_2^2$ defined as follows;

$$\|\tilde{f}^j(x_i)\|_2^2 = \int_0^1 |\tilde{f}^j(x_i)|^2\ dx_i \tag{1.60}$$

the extremum values are when

$$\sum_{n=1}^{N} \left[\tilde{f}^j(x_i)\right]^2 = \varepsilon_j^2 \tag{1.61}$$

Utilising the method of Lagrange multiplier for the extremum the procedure work as follows;

$$\mathcal{L}(x_0,\ \tilde{f}^j) = \varphi\left(x_0; \tilde{f}^j(x_0)\right) + \lambda\left(\sum_{n=1}^{N}(\tilde{f}^j)^2 - \varepsilon_j^2\right) \tag{1.62}$$

where φ denotes the deflection of the structure in question. The extremum condition for the Lagrangian is as follows;

$$\frac{\partial \mathcal{L}(x_0,\ \tilde{f}^j)}{\partial \tilde{f}^j} = 0 \tag{1.63}$$

The solution in terms of unknown coefficients at a particular position x_0 is the following;

$$\tilde{f}^j(x_0) = -\frac{1}{2\lambda}\frac{\varphi\left(x_0; \tilde{f}^j(x_0)\right)}{\partial \tilde{f}^j} \tag{1.64}$$

where x_0 is to be determined with respect to the maximum deflection subject to the load.

1.8 Sensitivity analysis

Sensitivity analysis is an attempt to assess the response of perturbed design parameters relative to the overall system performance. Perturbation means gradual and continuous modification of the easy original problem and its solution so that difficult problems in the neighbourhood can be solved or approximated closely [29]. In order for this to occur there must be an explicit solution to the original problem. The difficulty

associated with problems of material uncertainty is that, it is not easy to identify actual solutions thus making it even more difficult to properly formulate the domain for parameterised solution. Sensitivity analysis with respect to the set of possible solution is often used and preferred for identifying optimality. The structure of convex problems is such that points satisfying a first-order necessary conditions for optimality are sufficient and are a true solution [41]. That has proven to be beneficial in a sense that numerous first order conditions can be formulated into generalised equations where a quasi-solution can be tested for stability.

Numerous authors contributed in developing formal theories that attempt to deal decisively with the issue of stability. For instance Robinson's work [54] deals with B-derivatives, strong-derivatives and strong B-derivatives. The culmination of this work was to set on a strong footing the implicit function theorem and a theorem on approximation of implicit-function using simpler functions with an extension covering the non-linear approximating functions. The interpretation of these results is given by Rockafellar [41] in terms of the sensitivity to perturbation as follows;

$$S(\gamma_i) = \{x \in C : -f(\gamma_i, x) \in H(x)\} \tag{1.65}$$

where C is a bounded convex set in the Hilbert space, $f(\gamma_i, x)$ is the single -valued mapping and $H(x)$ is the input multifunction. Theories relating to the stability of various formulations of the sensitivity analysis together with the alignment of these to the systems in question are important but beyond the scope of the thesis. However the technique adopted in this report is the *relative sensitivity* approach [14] which is based on linear statistical analysis. Relative sensitivity evaluates the covariance-variance matrix of the input parameters such that the high quantity of relative sensitivity results in elevating the importance of the stated specific input parameter. The system formulation is as follows;

$$\frac{\partial \varphi^*}{\partial x_i} = \left|\frac{\partial \varphi}{\partial x_i}\right| \left|\frac{x_i^0}{\varphi^0}\right| \tag{1.66}$$

such that it compares relative importance of input parameters on the response. If on the other hand the concept is constructed using the buckling load the procedure work as follows;

$$N_{cr} = N_{cr}(\beta)$$
$$\Phi = \{\gamma_1, \gamma_2, \ldots, \gamma_k\}$$

where Φ is the k-dimensional uncertain vector belonging to a convex set S, and γ_i being the material uncertain parameters.

$$f(\gamma_i) = \left|\frac{\partial N_c r(\beta)}{\partial \gamma_i}\right| \left|\frac{\gamma_i^0}{N_c r(0)}\right| \tag{1.67}$$

If the quantity of the value is such that $\frac{\partial N_c r(\beta)}{\partial \gamma_i} > 0$, then the system's response is monotone increased around γ_i, and if the opposite is true then the system is monotonic degressive around the same parameter.

Chapter 2

Small scale effects

The size dependence of nanostructure material properties makes it necessary to utilise a modelling mechanism sensitive to their unique attributes. Therefore combining the nonlocal effects and surface effect in the theory of analysis of nanostructures is important. Several authors [9, 44, 67] have in the past worked with both nonlocal and surface effects showing improvement in the theoretical analysis. The lack of precise stress-strain measuring mechanism at nanoscale, combined with molecular defects and manufacturing variances for nanostructure further complicates modelling and create uncertainty.

2.1 Nanotechnology

Generally most materials can be synthesised into nanostructures to a varying degree. Eutectic microstructures can be tailored by modification resulting with materials characterised by mechanical, electrical, chemical, and optical properties at various levels. However carbon nanostructures get most of the attention due to their potential offering in relation to numerous physical properties. The are possibilities of developing these [17,30,42] nanostructures into nano-electronics and micro-electromechanical devices based on mechanical and electrical properties which can be modulated through various synthesis techniques. Nanostructures have proven to be reliable [69] and stable to perform as expected when subjected to various loading conditions.

2.1.1 Carbon nanostructure composites

Over the past few years composite materials have been projected as an important alternative to the traditional materials [61]. This is due to fact that they possess unique material properties that can be tailor made to suit almost any loading environment. There are various types of composite materials, which in the main consist of two or more distinct materials. Commonly a matrix of some kind (natural or synthetic) is used

together with some load bearing reinforcement in a form of short or long fibres or particles of some kind. The cost and the working environment usually dictates the specifics when it comes to the choice of materials used for the composite in question. With the advent of nanotechnology the scope for choosing materials has widened. Problems associated with manufacturing and load bearing capacity of composite materials [6] can now be addressed by manipulating constituents at a macroscopic, microscopic as well as at nanoscale.

One attractive feature that resonates with most designers when using composites is the high-strength to mass ratio. To achieve this property the reinforcement should have high strength together with high aspect ratio in order to facilitate optimal load transfer between the matrix and stiffner. Carbon nanotubes present [4, 5, 12] a perfect model, structurally, in fulfilling some of these demands if not all of them in the foreseeable future. They consist of a single-walled or multi-walled hollow rolled graphite sheets [37]. Carbon chains form molecules and are covalently bonded producing a structure with high specific thermal and electrical conductivity ratio as well as mechanical properties superior to traditional filler reinforcements [8, 42, 60].

Manufacturing nanostructures consistently into continuous long fibres has some challenges [6, 10] and this has limited the use of these fibres to just being matrix modifiers. As a function of their size they inherently have a tendency to agglomerate and cluster into bundles and fail to disperse homogeneously in the matrix. Given the large surface area of nanotubes per volume of mixture, normally there is poor solubility of nanofibre in the matrix resulting in these composites tending to be very viscous and not easy to process or mould. Although the increased surface area of nanotubes can cause difficulties it's also an attractive feature that can be exploited for other gains. For example, due to their high aspect ratio together with their tendency percolate in the matrix this serves as a mechanical strengthening character for composites and it facilitates an electrical conductivity property which can be modulated by applying mechanical stress in the composite. Nanotubes can be arranged in a three dimensional array in the matrix resulting in the improvement of material properties in all planes. Numerous issues [6] related to mechanical bonds at the interface between the matrix and nanofibres have caused some challenges and have to be sorted out before making these composites cost effective and widely available.

2.1.2 Growth and synthesis of nanostructures

The uniqueness of carbon to assimilate numerous structural forms helped in facilitating the possibility for the discovery of nano-tubes accredited to Iijima in 1991 [37]. Since their discovery a lot off activity in the research area of nano-tube composites has been inspired. There are various techniques [17, 30, 48] that are currently being investigated and utilised to produce carbon nano-tubes. A full understanding of the mechanism involved in the production of these fibres is imperative, as this will in turn aid consistency in producing these nano-structures with predictable mechanical properties [5].

Materials with eutectic composition have a low melting point [10] and are easily infused as the Greek word *eutectos* suggests. The freezing range for these materials transforms them from liquid state to solid state at a constant temperature called eutectic temperature. The end product is a function of the distribution of atoms characteristic to a specific eutectic system resulting with either a tubular structure or a laminar microstructure. The shapes of the primary phases plays an important role and the surface energy helps in retaining this shape whilst the interaction between the phases are progressing. Nanowires are synthesised in the same manner taking advantage of the low melting temperature associated with eutectic reactions.

It is understood that Iijima [4, 5, 37] used carbon arc process where a direct current is passed between two carbon electrodes in chamber saturated with inert gas at an elevated temperature above the eutectic temperature levels. Gas in the atmosphere decomposes and is absorbed in the carbon electrode and diffuses resulting in the formation of nanoparticles. These particles are then held at a constant temperature whilst increasing the gas content. This gas continuously diffuses into the rod until the nanoparticles are completely molten. Then the increased gas content that is continuously diffused into the catalyst reacts resulting with the formation a solid phase. This interaction between the catalyst and the anode gas facilitates the precipitation of graphite sheets shaped into a multiwalled nanotubes. It is also understood that by incorporating various types of metal catalyst single walled nanotubes can be produced. The nanostructure will continues to grow with the liquid leading edge producing the nanowire, as long as the environment provides sufficient reaction to facilitate precipitation.

Accordingly it has been established that nanofibre growth is dependent on the abrupt shape in the catalyst particle to which in turn depends on the reaction between the catalyst and vapour [5]. Helveg *et al.* [34] reckons that *"step edges act as growth centres for graphene growth mainly because carbon binds more strongly to such sites than to sites at the closed-packed facets on Ni"*. The typical dimension [6, 12, 48] of these multiwalled nanotubes (with slight variation from one reference text to another) with $4 - 24$ concentric shells ranges between $2 - 50nm$ in diameter. On the other hand single walled nanotube consist of $0.5 - 2nm$ in terms of their diameter. Various other techniques are available for synthesising carbon nanotubes; i.e. laser evaporation, catalystic combustion, chemical vapour deposition and ion bombardment [12].

Once the process of producing nanotubes is done the system has to be purified from contaminants. Nanoparticles that did not form part of the beam or lamina structure are the main by-product [20] and constitute about one third in terms mass per production of the total nanostructure. An oxidation reaction at a slow rate is reported as the preferred technique in purifying nanostructures.

2.1.3 Mechanical properties

The literature is populated [12, 30, 48] with various methods used in determining mechanical properties of nanotubes. These properties are important for the practical

application of nanotubes, be it as matrix reinforcement, sensors or as nano-device actuators. Characterisation of the mechanical properties of structural materials is based on elastic modulus which is a relationship between stress and strain subject to predetermined loading conditions. The modulus of elasticity for homogeneous materials is understood to be an intensive property defined at arbitrary points in the material continuum. Due to the discrete nature of the composite material elements and the dependency of nano-composites to the properties of its constituents, characterisation of its modulus is an averaged quantity based on the relative fraction of each constituents referred to as the effective modulus.

The basic formation of carbon nanotubes can be viewed as a rolled tube of graphite sheet with caps that resemble half of a sphere at the ends [10, 15, 33, 44]. Graphene sheets can be rolled into single or multi-walled pattens resulting with different physical properties for the tube. As reinforcements and stiffeners for polymer matrix, its understood from material science that at the interface between the two phases atomic bond structure is interrupted and irregular. This phenomenon is a function of distribution of electrons at the surface of each phase which in turn affects the bond at the interface. Not only does it affect the relationship between the two phases but it also disrupts the even distribution of energy within each phase creating differences between energy associated with the surface atoms to those in the bulk of the material. Thus the elastic moduli of the surface region differs to that of the bulk region. This phenomenon is at the core of this study and the essence in terms of theoretical models that are going be subsequently implemented.

Further more the composition of these nano-sized structural materials is such that surface to volume ratio is high making it necessary to model these structures with the bias to surface energy and surface stress. Surface free energy (or surface tension) as a concept is credited to Gibbs [16] which is viewed as a thermodynamic quantity. It is thought of as reversible work responsible for creating or extending by filling new surface lattice sites with atoms at constant temperature and volume without changing the density of atoms at the surface. Surface stress on the other hand is responsible for stretching the substrate thus changing the density of surface atoms but keeping the same quantity of atoms at the surface.

2.2 Nonlocal theory

Structures [19] in general can be examined at five different scale levels namely;

a) atomic scale $1\mathring{\mathbf{A}}$,

b) short and long-range atomic arrangement scale $1 - 10\mathring{\mathbf{A}}$,

c) nanostructure $1 - 100nm$,

d) microstructure (single crystal or grain size) $0.1 - 100\mu m$,

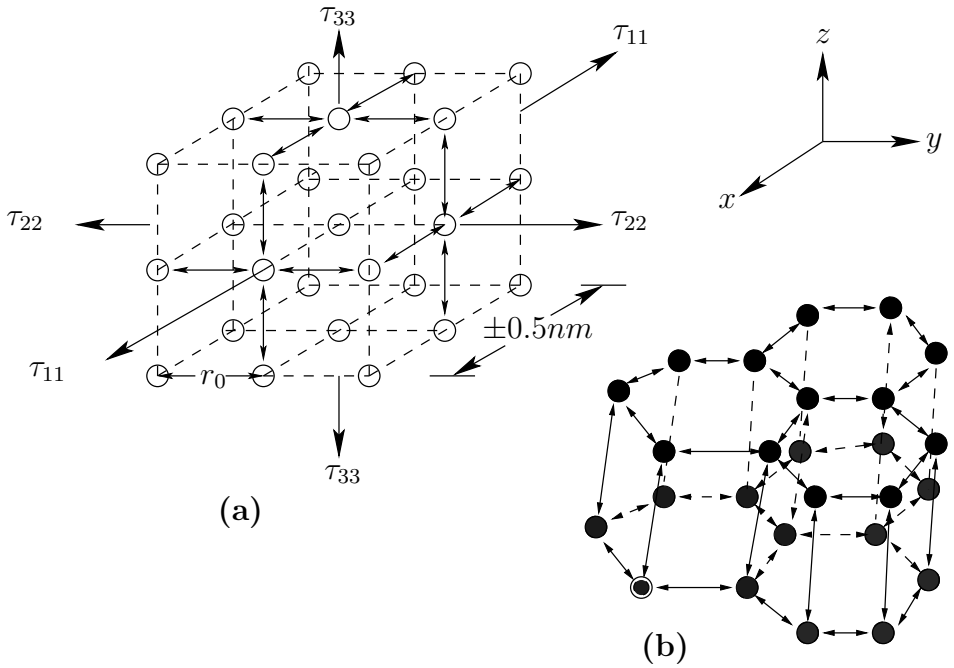

Figure 2.1: Atoms in array (a) Cubic array with a typical inter-atomic spacing r_0 of $0.2nm$. (b) Carbon atoms with each layer in a hexagonal array [10, 19].

e) macrostructure $> 100\mu m$.

Material features at these levels have a distinct and profound influence on the properties or behaviour of the material. Atomic structure also affects the types of material bonds be it covalent bonding or otherwise. The response of solid materials to external stimuli or loading mechanism (point loads, distributed loads, etc.) at an atomic scale is dependant on the nature and magnitude of the force as well as material properties of the solid in question. The material may fracture if the intensity of the load exceeds the internal tolerable limit or may deform permanently without fracture for a lesser magnitude or might just elastically deform. Thus it is important to properly quantify linear elasticity using a model that best fits the scale effects of the object concerned.

The classical theory of elasticity works well at macroscopic level since in its formulation long range effects are catered for. However the applicability of the same theory at a nanoscale or even at microstructure scale is seriously doubted [21,66,68,70]. Atomic or molecular simulation models are available for undertaking this analysis but computational costs may prove to be a deterrent. Responding to the short comings of classical continuum mechanics, Eringen *et al*, [26–28], introduced the nonlocal theory of elasticity. The postulation forwarded by nonlocal continuum mechanics asserts that stress at a point in the body is a function of strain in all other points in the body [26, 28, 53]. Theoretical formulation proceeds as follows;

$$\tau_{ij,j} + \rho(f_i - \ddot{u}_i) = 0 \tag{2.1}$$

where τ_{ij}, ρ, f_i, and u_i are, respectively, the stress tensor, mass density, body force density and the displacement vector at a reference point in the body, at time t. The nonlocal tensor is defined by

$$\tau_{ij}(\mathbf{x}) = \int_V \kappa(\|\mathbf{x} - \mathbf{x}'\|, \xi)\sigma_{ij}(\mathbf{x})d\mathbf{x} \tag{2.2}$$

The kernel function $\kappa(\|\mathbf{x} - \mathbf{x}'\|, \xi)$ constitutes the nonlocal modulus, together with the norm $\|\mathbf{x} - \mathbf{x}'\|$. This integral computes an averaged strain quantity at all the points in the body for the stress at a referenced point [51, 53]. ξ is the material constant derived from internal and external characteristic lengths (e.g. lattice spacing and wavelength), and $\sigma_{ij}(\mathbf{x}')$ is the macroscopic classical stress tensor at point $\mathbf{x}$ in accordance with generalised Hooke's law

$$\sigma_{ij}(\mathbf{x}) = \mathbf{C}_{ijkl}(\mathbf{x})\varepsilon_{kl}(\mathbf{x}) \tag{2.3}$$

$$\varepsilon_{kl}(\mathbf{x}) = \frac{1}{2}\left(\frac{\partial u_k(\mathbf{x})}{\partial \mathbf{x}_l} + \frac{\partial u_l(\mathbf{x})}{\partial \mathbf{x}_k}\right) \tag{2.4}$$

where $\mathbf{C}_{ijkl}$ are the elastic modulus components.

In determining the properties of the nonlocal modulus for homogeneous and isotropic elastic solids, Eringen [27] made the following observations:

i) The modulus $\kappa(\|\mathbf{x} - \mathbf{x}'\|, \xi)$ attains its maximum value when the norm $\|\mathbf{x} - \mathbf{x}'\|$ is minimised such that $\mathbf{x} = \mathbf{x}'$.

$$\vartheta = \kappa(\|\mathbf{x} - \mathbf{x}'\|, \xi) \qquad \text{where} \qquad \xi = \frac{e_0 a}{l} \tag{2.5}$$

where e_0, a, l is the material constant, internal and external characteristics respectively, for the specific material in question.

ii) To cater for the inclusion of the classical elastic limit the material constant for internal characteristic length must vanish i.e.; $\xi \to 0$,

$$\lim_{\xi \to 0} \kappa(\|\mathbf{x} - \mathbf{x}'\|, \xi) = \delta(\|\mathbf{x} - \mathbf{x}'\|) \tag{2.6}$$

where $\delta(\|\mathbf{x} - \mathbf{x}'\|)$ is the Dirac delta function.

iii) For $\xi \to 1$ (small scale), nonlocal theory should approximate atomic lattice dynamics.

iv) ϑ for various materials can be determined by matching dispersion curves of plane waves with those of atomic lattice dynamics. To this end Eringen [27] experimented by matching the dispersion curve of one -dimensional plane wave based on the nonlocal elasticity and the Born-Kármán model of the atomic lattice dynamics, two-dimensional and three dimensional lattices with minimal error levels.

v) Assuming ϑ to be the Green's function of a linear differential operator

$$\mathcal{L}\kappa(\|\mathbf{x}-\mathbf{x}'\|,\xi) = \delta(\|\mathbf{x}-\mathbf{x}'\|) \tag{2.7}$$

applying the the differential operator $\mathcal{L}$ to the nonlocal constitutive equation it reduces to;

$$\mathcal{L}\tau_{ij} = \sigma_{ij} \tag{2.8}$$

resulting in the simplification of the integropartial differential equation to having the partial differential equation;

$$\sigma_{ij} + \mathcal{L}(\rho f_i - \rho\ddot{u}_i) = 0 \tag{2.9}$$

vi) From matching dispersion curves with Born-Kármán model of the atomic lattice dynamics the differential operator $\mathcal{L}$ is;

$$\mathcal{L} = 1 - \xi^2 l^2 \nabla^2 \tag{2.10}$$

Substituting the relevant terms yields an equivalent simplified expression for the stress tensor given as follows;

$$\left(1 - \xi^2 l^2 \nabla^2\right)\tau_{ij} = \sigma_{ij} \tag{2.11}$$

.

2.3 Surface effects

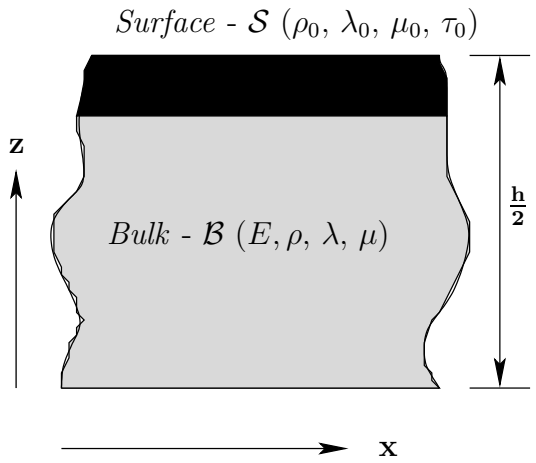

Figure 2.2: 2***D*** Half-space

It has been established that when the overall structural dimensions are at a scale comparable with the atomic scale, surface stress becomes prominent and cannot be ignored [15, 33, 44]. Nanostructure materials have a large surface area per unit mass as a result of a large number of atoms at the surface compared to those within the

body of the material. The anomalous arrangement of atoms at the surface dictates that equilibrium satisfaction for surface atoms be different to the atoms in the bulk of the structure. This phenomenon facilitates the development of different energy levels between the two spaces resulting with the occurrence of size dependant material properties giving rise to surface stress.

Classical continuum theories fail to factor this phenomenon and cannot therefore provide analysis acceptable at this scale. Gurtin and Murdoch [32, 33] realised this, thus presented a general continuum theory of surface stress that accommodates these residual stresses. Surface traction caused by the residual stresses affects the modelling of the small scale elements resulting with a coupled system of field equations that contain non-classical boundary conditions. In formulating the basic equations for surface effects Gurtin and Murdoch [33] considered the body as constituted by two distinct sections (bulk and the surface) Figure 2.2 with pronounced differences in terms of their material properties.

Consider the body $\mathcal{B}$ described in Figure 2.2 by a coordinate system $x_i (i = 1, 2, 3)$ which is bounded by the surface $\mathcal{S}$ regarded as having two dimensional $x_\alpha (\alpha = 1, 2)$ continuous structure. The surface structure is strained as a result of residual stresses but bonded to the bulk perfectly but still behaves like a surface region even if through the bulk is unstrained. The stress localised at the surface region is regarded as a tensor $\tau_{\alpha\beta}$ subject to the following ;

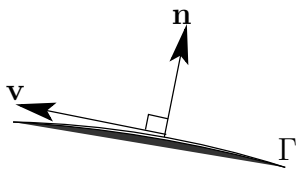

Figure 2.3: Surface

a) take Γ as the surface curvature (see Figure 2.3) with vector $\mathbf{v}$ acting tangential to Γ and is normalised;

b) $\mathcal{S}$ contains an orthogonal projection such that;

$$\{\mathbf{n}.\mathbf{v} = 0 \qquad \forall\, \Gamma \subset \mathcal{S}\} \tag{2.12}$$

c) then $\tau_{\alpha\beta}\,\mathbf{v}$ is the force per unit length produced by the residual stresses in the direction of the vector $\mathbf{v}$ projection;

d) both $\mathcal{S}$ and $\mathcal{B}$ are regarded as having homogeneous, linear elastic and isotropic material properties.

From the classical equations, equilibrium for the bulk stress tensor consists of the

following

$$\tau_{ij,j} = \rho\ddot{u} \tag{2.13}$$

$$\tau_{ij} = \lambda\delta_{ij}\varepsilon_{kk} + 2\mu\varepsilon_{ij} \tag{2.14}$$

$$\varepsilon_{ij} = \frac{1}{2}\left(u_{i,j} + u_{j,i}\right) \tag{2.15}$$

In the determination of the surface phenomenon the quantity γ represents surface free energy per unit area produced by surface effects. This quantity can be interpreted as reversible work per unit area needed to create a new surface through cleavage or creep [15].

$$dW = \gamma da \tag{2.16}$$

Work needed to elastically stretch the existing surface can be represented by a surface stress tensor $\tau_{\alpha\beta}$ with $d\varepsilon_{\alpha\beta}$ representing a small variation of the area. Relating the two quantities yields;

$$d(\gamma A) = A\tau_{\alpha\beta}d\varepsilon_{\alpha\beta} \tag{2.17}$$

from calculus we know that

$$d(\gamma A) = \gamma dA + Ad\gamma \tag{2.18}$$

and $dA = A\delta_{\alpha\beta}d\varepsilon_{\alpha\beta}$ where $\delta_{\alpha\beta} \rightarrow$ Kronecker delta. Then the surface stress constitutive relation becomes

$$\tau_{\alpha\beta} = \gamma\delta_{\alpha\beta} + \frac{\partial\gamma}{\partial\varepsilon_{\alpha\beta}} \tag{2.19}$$

The surface stress tensor as a linear function of strain tensor is expressed as follows

$$\tau_{\alpha\beta} = \tau_0 + \mathbf{K}_{\alpha\beta r\varphi}\ \varepsilon_{r\varphi} \tag{2.20}$$

where τ_0 is the surface stress tensor when the bulk is unstrained (see Shenoy [44]) and $\mathbf{K}_{\alpha\beta r\varphi}$ is the *surface elastic modulus* tensor.
The expanded format of the surface stress tensor constitutive relation (see Gurtin Murdoch [33]) is formulated as follows:

$$\tau_{i\alpha,\alpha} + \sigma_{i3} = \rho_0\ddot{u}_i \tag{2.21}$$

$$\tau_{\alpha\beta} = \tau_0\delta_{\alpha\beta} + (\mu_0 - \tau_0)\left(u_{\alpha,\beta} - u_{\beta,\alpha}\right) + (\lambda_0 + \tau_0)\ u_{r,r}\delta_{\alpha\beta} + \tau_0\ u_{\alpha,\beta} \tag{2.22}$$

$$\tau_{3\beta} = \tau_0\ u_{3,\beta} \tag{2.23}$$

where μ_0, γ_0, σ_{i3} are the Lamé moduli and traction in the direction of α respectively, with α, β, $r = 1$ and 2.

Chapter 3

Nonlocal Nanobeam

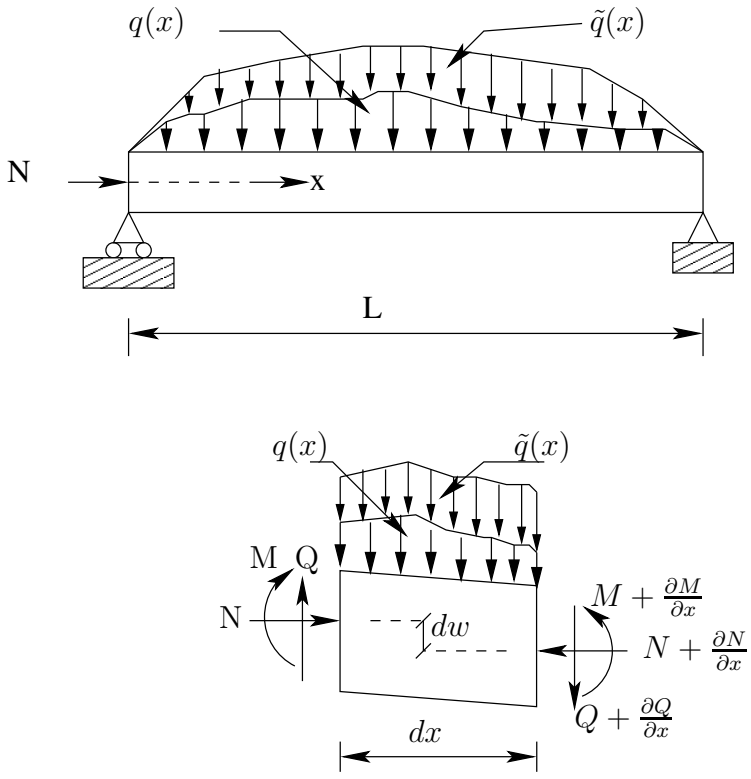

Figure 3.1: Beam deformation

3.1 Nano-beams

Technological advancement has resulted in the design and production of numerous nano-devices that are used for various applications. Devices such as atomic force microscope employ micro-cantilever-tip systems, together with numerous other critical

parts such as nano-tubes, nano-wires, and cantilever actuators being used in micro-electromechanical systems. It is imperative therefore to utilise models that are accurate in the analysis of the deformation properties of these structures. There are numerous classical beam theories [2,36,62,63], going as far back as the 18th century, attempting to appropriately model the mechanics of beam deformation under various loads. The Euler-Bernoullis formulation is based on the assumption that the transverse plane remains plane and perpendicular to the neutral axis under small elastic deformation of bending. Timoshenko beam theory on the other hand takes into account the effects shear deformation and rotary inertia. The latter [40] is regarded as more accurate and an improvement of the former.

Developments of nanotechnology and advancements have created a necessity for the adaptation of these classical macro-scale theories to micro-to-nanoscale theories. Other than classical continuum mechanics there are other options namely the atomic or molecular models. However these models are very complex computationally and difficult to accurately formulate [70]. The nonlocal theory [21,31,45,66,68] was developed to link the atomic theory of lattice mechanics with the classical continuum mechanics. In classical continuum mechanics it is postulated that the stress at a point **x** is a functional of strain at point **x**. Eringens nonlocal theory postulates that stress at a reference point **x** is a functional of the strain field at every point **x'** in the small scale body. Application of this theory by various authors has demonstrated it is effectiveness on a wide range of physical phenomenon spanning micro-to-nanoscale and even convertible to classical local theories.

In its essence the nonlocal kernel function factors in the influences of strain on all locations of the small scale volume. Naturally accurate determination of buckling, deflection, and vibration of various structural elements require compliance with boundary conditions. Due to difficulties in solving mathematically the nonlocal integropartial differential equations little progress has been made in acquiring knowledge of the interaction between this function and the boundary value problems. In this paper, convex modelling is proposed in handling not only uncertainties in the boundary condition but even the effects of uncertain loading and displacement.

3.1.1 Governing equations

The derivations of the governing equations [52, 53] are based on the Euler-Bernoulli beam theory where the displacement field are modelled as follows;

$$u_1 = u(x) - z\frac{\partial w}{\partial x} \tag{3.1}$$

$$u_2 = 0 \tag{3.2}$$

$$u_3 = w(x) \tag{3.3}$$

where u is the axial displacement and w the transverse displacement of the point from

the mid-plane position of the beam. The constitutive relations for the nonlocal stress tensor τ_{ij} at point $\mathbf{x}$ are defined as [26–28];

$$\tau_{ij}(\mathbf{x}) = \int_V \kappa(\|\mathbf{x} - \mathbf{x}'\|, \xi)\sigma_{ij}(\mathbf{x})d\mathbf{x} \tag{3.4}$$

The nonlocal integropartial is replaced by the equivalent differential form expressed as follows

$$\left(1 - \tau^2 l^2 \nabla^2\right)\tau_{ij} = \sigma_{ij},\ \tau = \frac{e_0\, a}{l} \tag{3.5}$$

Uniaxial Hook's law taking into account the nonlocal equivalent differential form equation (3.5) yields

$$\sigma - \frac{(e_0\, a)^2 \partial^2 \sigma}{\partial x^2} = E\, \varepsilon \tag{3.6}$$

Euler-Bernoulli axial and curvature strain relations yields the following expression;

$$\varepsilon = \frac{\partial u_1}{\partial x} \tag{3.7}$$

$$\varepsilon = \frac{\partial u}{\partial x} - z\frac{\partial^2 w}{\partial x^2} \tag{3.8}$$

Substituting in the stress equation (3.6), the following equation is obtained;

$$\sigma - \frac{(e_0\, a)^2 \partial^2 \sigma}{\partial x^2} = E\left(\frac{\partial u}{\partial x} - z\frac{\partial^2 w}{\partial x^2}\right) \tag{3.9}$$

For the element shown in the Figure 3.1, the equilibrium of forces and moments is derived as follows;
In summing vertical forces $\sum F_v = 0$ the following equations are obtained

$$-\frac{\partial Q}{\partial x}\, dx - q\, dx = 0 \tag{3.10}$$

$$\frac{\partial Q}{\partial x} = -q \tag{3.11}$$

When summing moments $\sum M = 0$, and ignoring $(dx)^2$ or higher will result with the following;

$$N\, dw + Q\, dx - \frac{\partial M}{\partial x}\, dx = 0 \tag{3.12}$$

by differentiating equation (3.12) with respect to x once, substitution using equation (3.11) we get

$$\frac{\partial^2 M}{\partial x^2} = N\frac{\partial^2 w}{\partial x^2} - q \tag{3.13}$$

where N and M are the transverse load per unit length and bending moment respectively. They are defined as follows;

$$N = \int_A \sigma\, dA \tag{3.14}$$

$$M = \int_A z\, \sigma\, dA \tag{3.15}$$

If the stress equation is integrated for N and M as shown above respectively the following terms are obtained;

$$N = \int_A \sigma \, dA = E \, A \, \frac{\partial u}{\partial x} \tag{3.16}$$

$$M = \int_A z \, \sigma \, dA = -E \, I \, \frac{\partial^2 w}{\partial x^2} \tag{3.17}$$

Where I is defined as follows;

$$I = \int_A z \, dA \tag{3.18}$$

with

$$A = \int_A dA \tag{3.19}$$

Expanding the nonlocal stress equation (3.9) with respect to the moment equation (3.17) and differentiating it twice with respect to x, the following equations are obtained;

$$M - \mu^2 \frac{\partial^2 M}{\partial x^2} = -E \, I \, \frac{\partial^2 w}{\partial x^2} \tag{3.20}$$

$$\frac{\partial^2 M}{\partial x^2} - \mu^2 \, \nabla^2 \frac{\partial^2 M}{\partial x^2} = -E \, I \, \frac{\partial^4 w}{\partial x^4} \tag{3.21}$$

Substituting with the resultant moment equation (3.13) in the above equation (3.21), gives the following;

$$N \frac{\partial^2 w}{\partial x^2} - q - \mu^2 \, \nabla^2 \left(N \frac{\partial^2 w}{\partial x^2} - q \right) = -E \, I \, \frac{\partial^2 w}{\partial x^2} \tag{3.22}$$

where $\mu^2 = (e_0 \, a)^2$ and $\nabla^2 = \frac{\partial^2}{\partial x^2}$. Simplifying the expression yields;

$$E \, I \, w_{xxxx} + \left(1 - \mu^2 \nabla^2\right) \left(N \, w_{xx} - q\right) = 0 \tag{3.23}$$

3.2 Principle of virtual work

An alternative method [52, 64] for deriving the governing equations is based on the principle of virtual work. Assuming that the particle is in equilibrium then the total work of all the forces acting on it (forces are assumed to be constant and preserving their line of action), in any virtual displacement is zero or vanishes. If δu, δv, and δw are components of virtual displacement in the x, y, and z directions and $\sum X$, $\sum Y$, and $\sum Z$ are sums of projected forces in the same direction as the coordinates system on the particle, then by applying the principle of virtual work the following is obtained:

$$\sum X \, \delta u = 0 \tag{3.24}$$

$$\sum Y \, \delta v = 0 \tag{3.25}$$

$$\sum Z \, \delta w = 0 \tag{3.26}$$

satisfied for any virtual displacement if the projected forces are in equilibrium.

$$\sum X = 0, \sum Y = 0, \sum Z = 0 \tag{3.27}$$

Expressed differently if the forces in equilibrium in a system of equations are multiplied by their respective virtual displacements we obtain the virtual work equations. Relating these to strain the following is obtained

$$\delta\epsilon_{ij} = \frac{1}{2}(\delta u_{i,j} + \delta u_{j,i}) \tag{3.28}$$

Virtual work for the volume

$$\delta V_0 dx_i = \sum \tau_{ij}\, \delta\varepsilon_{ij}\, dx_i \tag{3.29}$$

where V_0 is the amount of the strain energy per unit volume. Work done by external forces consists of the surface forces $\bar{X}ds$, $\bar{Y}ds$, $\bar{Z}ds$ on the surface element ds. It also consists of body forces $\bar{X}dv$, $\bar{Y}dv$, and $\bar{Z}dv$ on the volume of the element $dv = dx$, dy, and dz. The change in strain energy measures the work done against mutual forces between the particle. To quantify work done by mutual forces on the particles the sign must be reversed.

$$\textit{surface forces} + \textit{body forces} - \textit{mutual forces} = 0 \tag{3.30}$$

$$\int \left(\bar{X}\delta u + \bar{Y}\delta v + \bar{Z}\delta w\right) ds + \int \left(X\delta u + Y\delta v + Z\delta w\right) dv - \int \delta V_0 dv = 0 \tag{3.31}$$

Applying the principle of virtual displacement with its formulation in terms of displacement for the nonlocal beam,

$$\delta U = \int_v \tau_{ij}\, \delta\varepsilon_{ij}\, dv \tag{3.32}$$

where δU is the strain energy variation in the beam, based on the Euler-Bernoulli beam theory

$$\delta U = \int_0^L \left\{ \int_A \sigma_x\, \delta\varepsilon_x da \right\} dx \tag{3.33}$$

$$= \int_0^L \left\{ \int_A \sigma_x \frac{\partial \delta u}{\partial x} da - z \int_A \sigma_x \frac{\partial^2 \delta w}{\partial x^2} da \right\} dx \tag{3.34}$$

$$= \int_0^L \left\{ N\frac{\partial \delta u}{\partial x} - M\frac{\partial^2 \delta w}{\partial x^2} \right\} dx \tag{3.35}$$

Variation of externally applied loads with respect to the displacement of the beam;

$$\delta W = \int_0^L \left[q\, \delta w + \vec{N}\frac{\partial \delta w}{\partial x} \right] dx \tag{3.36}$$

where $\vec{N} = N\frac{\partial w}{\partial x}$. Putting the terms together and integrating by parts, from the principle of virtual displacement the procedure is as follows;

$$= \int_0^L \left\{ N\frac{\partial \delta u}{\partial x} - M\frac{\partial^2 \delta w}{\partial x^2} \right\} dx - \int_0^L \left\{ q\, \delta w + \vec{N}\frac{\partial \delta w}{\partial x} \right\} dx \tag{3.37}$$

resulting with the following set of equations;

$$\int_0^L M\frac{\partial^2\delta w}{\partial x^2}dx = \left[M\frac{\partial\delta w}{\partial x} - \frac{\partial M}{\partial x}\delta w\right]_0^L + \int_0^L \frac{\partial^2 M}{\partial x^2}\delta w dx \tag{3.38}$$

$$\int_0^L \vec{N}\frac{\partial\delta w}{\partial x}dx = \vec{N}\delta w|_0^L - \int_0^L \frac{\partial\vec{N}}{\partial x}\delta w\, dx \tag{3.39}$$

$$\int_0^L N\frac{\partial\delta u}{\partial x}dx = N\delta u|_0^L - \int_0^L \frac{\partial N}{\partial x}\delta u\, dx \tag{3.40}$$

noting that there is no variation at the boundary, which translates to $\delta w(L) = \delta w(0) = 0$. From this the following is obtained;

$$\left[M\frac{\partial\delta w}{\partial x} - \frac{\partial M}{\partial x}\delta w\right]_0^L = 0 \tag{3.41}$$

$$\vec{N}\delta w|_0^L = 0 \tag{3.42}$$

$$N\delta u|_0^L = 0 \tag{3.43}$$

From the *fundamental lemma of the calculus of variations*: [18, 57]

$$\int_{x_0}^{x_1} \eta(x)\varphi(x)\, dx = 0 \qquad \forall\ \eta \in C^1 \tag{3.44}$$

where C^1 is the set of real valued functions defined and differentiable with continuous derivative on x. Simplifying by collecting terms with similar coefficients δu and δw,

$$\delta u: \qquad \int_0^L \delta u\left\{\frac{\partial N}{\partial x}\right\}dx = 0 \tag{3.45}$$

$$\delta w: \qquad \int_0^L \delta w\left\{\frac{\partial^2 M}{\partial x^2} - \frac{\partial\vec{N}}{\partial x} + q\right\}dx = 0 \tag{3.46}$$

obtaining the Euler-Lagrange equations which are;

$$\delta u: \qquad \frac{\partial N}{\partial x} = 0 \tag{3.47}$$

$$\delta w: \qquad \frac{\partial^2 M}{\partial x^2} - N\frac{\partial^2 w}{\partial x^2} + q = 0 \tag{3.48}$$

by substitution the nonlocal equation

$$E\,I\,w_{xxxx} + \left(1 - \mu^2\nabla^2\right)\left(N\,w_{xx} - q\right) = 0 \tag{3.49}$$

can be determined. When determining constants, boundary conditions in the beam can be specified in the span $0 \geq x \geq L$ with information relating to

$u \rightarrow$ axial deflection or $N \rightarrow$ axial force
$w \rightarrow$ transverse deflection or $Q \rightarrow$ shearing force
$\frac{dw}{dx} \rightarrow$ slope or $M \rightarrow$ bending moment

By setting $\mu = 0$, the classical local equation of motion can determined for the beam.

Chapter 4

Small Scale Plate

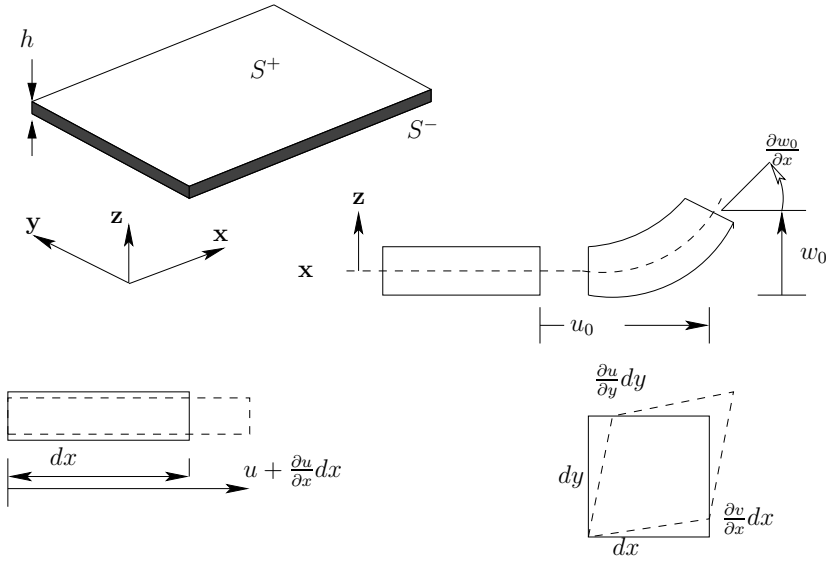

Figure 4.1: Plate deformation

4.1 Plate theory

The popularity of nanostructures as a relatively new class of material is due to their unique mechanical, electrical, electronic and thermal properties. These attributes are linked to the small scale effects of these structures [39, 46, 49]. Nanostructures specifically graphene sheets show promise of possible use in a variety of technological applications [7, 58]. It is imperative therefore to have a proper understanding of all the factors at play when modelling nanostructures subjected to various loads and environments.

For an expansion of a specific continuum theory governing structural deformation

[43,47,67] the study of the classical plate theory attributed to or known as Kirchhoff's hypothesis is considered. According to this theory it is assumed that the normal to the mid-plane remains normal even after small deformation and do not change in length. Obviously this is in contradiction to the fact that transverse strain exists ($\varepsilon_3 \neq 0$) if one were to consider the hygrothermal and Poissons ratio effects. However as a function of differences between lateral and transverse dimensions when considering pure bending, it is assumed that the middle surface is the neutral surface of the plate, implying that the direct stress is zero. This can only be true if the middle surface of the bent plate is a developable surface [64, 65] in a sense that:

a) The thickness of the plate is very small when compared with the radius of curvature

b) Deflection of the plate is very small when compared with the width of the plate

c) Deflection of the plate is very small when compared with the thickness of the plate.

The same understanding is used when analysing the response of nano-plates subjected to uncertain transverse and buckling loads. Using special cases [64,65] the investigation will be limited to the effects of stiffness and deflections. But first the general governing equations will be derived and later refined to suit the special cases investigated in this dissertation.

4.2 Governing equations

According to the classical theory [52, 64], the plane stress and strain system is sufficient for the analysis of rectangular thin plates. Loads are normally taken as acting parallel to the plane system referenced at mid-plane. The following stress components σ_z, τ_{xz}, τ_{yz} are regarded as negligible at the surface $\mathcal{S}$ as well as in the bulk $\mathcal{B}$. This implies that σ_x, τ_{xy}, σ_y are the only components required to determine the stress state in the plate.

4.2.1 Classical plate equations

Given the scenario where there are transverse loads, lateral loads as well as moments acting on the plate we have an option of proceeding as follows;

Summing vertical forces $\sum F_z = 0$ (see Figure 4.2) and then simplifying the equation we get:

$$\frac{\partial V_x}{\partial x} + \frac{\partial V_y}{\partial y} + q(x, y) = 0 \tag{4.1}$$

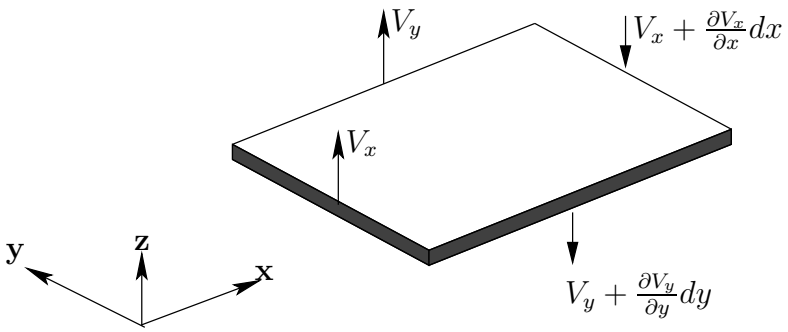

Figure 4.2: Transverse loading

where $\{q, V\}$ represents the distributed load and transverse shearing force/unit length respectively projected in the z-direction as:

$$V_x = \int_{-\frac{h}{2}}^{\frac{h}{2}} \tau_{xz} \, \mathrm{d}z \tag{4.2}$$

$$V_y = \int_{-\frac{h}{2}}^{\frac{h}{2}} \tau_{yz} \, \mathrm{d}z \tag{4.3}$$

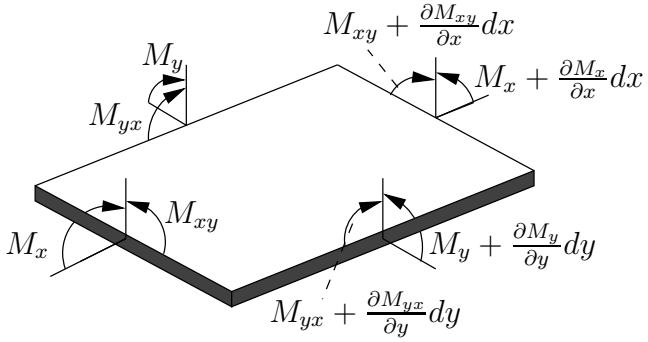

Figure 4.3: Moments

Summing moments $\sum M_{x_i} = 0$ with respect (see Figure 4.3) to the x and y axis respectively yields:

$$\frac{\partial M_{xy}}{\partial x} - \frac{\partial M_y}{\partial y} + V_y = 0 \tag{4.4}$$

$$\frac{\partial M_{xy}}{\partial y} - \frac{\partial M_y}{\partial x} + V_x = 0 \tag{4.5}$$

Given that $M_{yx} = -M_{xy}$, substituting equation (4.4) and (4.5) into equation (4.1) and simplifying yields:

$$\frac{\partial^2 M_x}{\partial x^2} + \frac{\partial^2 M_y}{\partial y^2} - 2\frac{\partial^2 M_{xy}}{\partial x \partial y} = -q \tag{4.6}$$

When considering the lateral loading (see Figure 4.4) the forces are first projected in the x and y directions yielding after simplification the following equations:

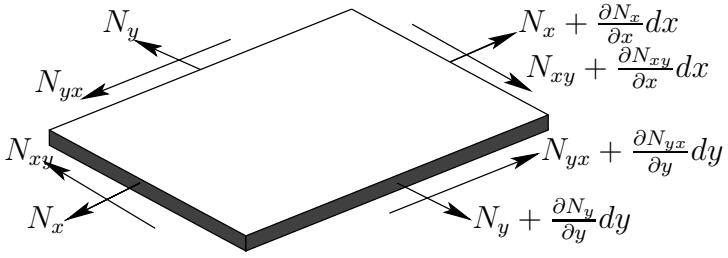

Figure 4.4: Lateral loads

$$\frac{\partial N_{xy}}{\partial y} + \frac{\partial N_x}{\partial x} = 0 \tag{4.7}$$

$$\frac{\partial N_{xy}}{\partial x} + \frac{\partial N_y}{\partial y} = 0 \tag{4.8}$$

Taking into account the curvature (see Figure 4.1) on the plate and projecting the lateral loads as well as the shearing forces in the z-direction, after simplification where second order and higher quantities are ignored, the following equations are obtained;

$$N_x \frac{\partial^2 w}{\partial x^2} dx\, dy + \frac{\partial N_x}{\partial x}\frac{\partial w}{\partial x} dx\, dy \tag{4.9}$$

$$N_y \frac{\partial^2 w}{\partial y^2} dx\, dy + \frac{\partial N_y}{\partial y}\frac{\partial w}{\partial y} dx\, dy \tag{4.10}$$

noting the fact that $N_{yx} = N_{xy}$ when shearing forces are projected on the z-axis, after simplification the following equation is obtained:

$$2N_{xy}\frac{\partial^2 w}{\partial x\, \partial y} dx\, dy + \frac{\partial N_{xy}}{\partial x}\frac{\partial w}{\partial y} dx\, dy + \frac{\partial N_{xy}}{\partial y}\frac{\partial w}{\partial x} dx\, dy \tag{4.11}$$

Summing all the vertical forces and simplifying the equation yields the following:

$$\frac{\partial^2 M_x}{\partial x^2} + \frac{\partial^2 M_y}{\partial y^2} - 2\frac{\partial^2 M_{xy}}{\partial x \partial y} = -\left(q(x,y) + N_x \frac{\partial^2 w}{\partial x^2} + N_y \frac{\partial^2 w}{\partial y^2} + 2N_{xy}\frac{\partial^2 w}{\partial x \partial y}\right) \tag{4.12}$$

where M represents the moments projected in the z-direction as:

$$\begin{Bmatrix} M_x \\ M_x \\ M_{xy} \end{Bmatrix} = \int_{-\frac{h}{2}}^{\frac{h}{2}} \begin{Bmatrix} \sigma_x \\ \sigma_y \\ \tau_{xy} \end{Bmatrix} z \, \mathrm{d}z \tag{4.13}$$

For small deflection (see Figure 4.1) implementing Kirchhoff's hypothesis the following is obtained;

$$\begin{Bmatrix} u \\ v \\ w \end{Bmatrix} = \begin{Bmatrix} u_0(x,\, y) - z\, \frac{\partial w}{\partial x} \\ v_0(x,\, y) - z\, \frac{\partial w}{\partial y} \\ w(x,\, y) \end{Bmatrix} \tag{4.14}$$

resulting with general strain components as follows;

$$\begin{Bmatrix} \varepsilon_x \\ \varepsilon_y \\ \gamma_{xy} \end{Bmatrix} = \begin{Bmatrix} \frac{\partial u}{\partial x} \\ \\ \frac{\partial v}{\partial y} \\ \\ \frac{\partial u}{\partial x} + \frac{\partial v}{\partial y} \end{Bmatrix} = \begin{Bmatrix} \frac{\partial u_0}{\partial x} - z\,\frac{\partial^2 w}{\partial x^2} \\ \\ \frac{\partial v_0}{\partial y} - z\,\frac{\partial^2 w}{\partial y^2} \\ \\ \frac{\partial u_0}{\partial x_1} + \frac{\partial v_0}{\partial y} - 2z\,\frac{\partial^2 w}{\partial x\,\partial y} \end{Bmatrix} \tag{4.15}$$

When considering the orthotropic case but ignoring hygrothermal effects the equation for constitutive relations is as follows;

$$\begin{Bmatrix} \sigma_x \\ \sigma_y \\ \tau_{xy} \end{Bmatrix} = \begin{bmatrix} \frac{E_x}{(1-\nu_{xy}\nu_{yx})} & \frac{\nu_{xy}E_y}{(1-\nu_{xy}\nu_{yx})} & 0 \\ \\ \frac{\nu_{xy}E_y}{(1-\nu_{xy}\nu_{yx}} & \frac{E_y}{(1-\nu_{xy}\nu_{yx})} & 0 \\ \\ 0 & 0 & G_{xy} \end{bmatrix} \begin{Bmatrix} \varepsilon_x \\ \varepsilon_y \\ \gamma_{xy} \end{Bmatrix} \tag{4.16}$$

Where E is the modulus of elasticity in x and y direction, G and ν being the modulus of rigidity and Poissons ratio, respectively. The strain components for pure bending are as follows;

$$\begin{Bmatrix} \kappa_x \\ \kappa_y \\ \kappa_{xy} \end{Bmatrix} = -\begin{Bmatrix} z\,\frac{\partial^2 w}{\partial x^2} \\ \\ z\,\frac{\partial^2 w}{\partial y^2} \\ \\ 2z\,\frac{\partial^2 w}{\partial x\,\partial y} \end{Bmatrix} \tag{4.17}$$

Expanding the moment terms the following are obtained;

$$\begin{Bmatrix} M_x \\ M_x \\ M_{xy} \end{Bmatrix} = \int_{-\frac{h}{2}}^{\frac{h}{2}} - \begin{bmatrix} \frac{E_x}{(1-\nu_{xy}\nu_{yx})} & \frac{\nu_{xy}E_y}{(1-\nu_{xy}\nu_{yx})} & 0 \\ \\ \frac{\nu_{xy}E_y}{(1-\nu_{xy}\nu_{yx}} & \frac{E_y}{(1-\nu_{xy}\nu_{yx})} & 0 \\ \\ 0 & 0 & G_{xy} \end{bmatrix} \begin{Bmatrix} \frac{\partial^2 w}{\partial x^2} \\ \\ \frac{\partial^2 w}{\partial y^2} \\ \\ 2\frac{\partial^2 w}{\partial x\,\partial y} \end{Bmatrix} z^2 \,\mathrm{d}z \tag{4.18}$$

Substituting the moment terms (4.18) into equation (4.12), the classical governing deflection is obtained as follows;

$$D_{11}\frac{\partial^4 w}{\partial x^4} + D_{22}\frac{\partial^4 w}{\partial y^4} + 2(D_{12}+D_{66})\frac{\partial^2 w}{\partial x^2 \partial y^2} + q(x,y) + N_x\frac{\partial^2 w}{\partial x^2} + N_y\frac{\partial^2 w}{\partial y^2} + 2N_{xy}\frac{\partial^2 w}{\partial x \partial y} = 0 \tag{4.19}$$

where the D's represents the stiffness coefficients as follows:

$$D_{11} = \frac{h^3\,E_x}{12(1-\nu_{xy}\nu_{yx})}, \qquad D_{12} = \frac{h^3\,\nu_{xy}E_y}{12(1-\nu_{xy}\nu_{yx})}$$

$$D_{22} = \frac{h^3\,E_y}{12(1-\nu_{xy}\nu_{yx})} \qquad D_{66} = \frac{h^3\,G_{xy}}{12}$$

4.2.2 Nonlocal equations

According to Eringen's nonlocal theory of elasticity, stress at a reference point is considered to be a function of strain field at every point in the bulk of the body [26–28]. This based on the fact that in the atomic theory of lattice dynamics long range cohesive forces are known to be active given the scale of these crystals. The same considerations are applicable to nanostructures as a function of their small scale comparable to that of crystals. However in the classical theory of elasticity the effects of this phenomenon are neglected. The basic formulation of the constitutive equation for nonlocal theory of linear elasticity in the continuum is given as follows;

$$\tau_{ij}(\mathbf{x}) = \int_V \kappa\left(|\mathbf{x}-\mathbf{x}'|,\, \xi\right) C_{ijkl}(\mathbf{x})\varepsilon(\mathbf{x})\, d\mathbf{x} \tag{4.20}$$

where C, $\kappa\left(|\mathbf{x}-\mathbf{x}'|,\, \xi\right)$ is the classical macroscopic tensor and the kernel function respectively, with $|\mathbf{x}-\mathbf{x}'|$ as the Euclidean norm and ξ the material constant. It is difficult to solve for the integral constitutive equation however it can be represented by its equivalent form as follows;

$$\left(1-\xi^2 l^2\nabla^2\right)\tau_{ij} = \mathbf{T}_{ij}, \qquad \xi = \frac{e_0 a}{l} \tag{4.21}$$

where e_0, a, l is the material constant, internal and external characteristics lengths respectively. By rearranging the compatibility equations in terms of stress for the orthotropic case a nonlocal stress-strain system is obtained in the following format;

$$\begin{Bmatrix}\sigma_x\\ \sigma_y\\ \tau_{xy}\end{Bmatrix} - \eta^2\nabla^2\begin{Bmatrix}\sigma_x\\ \sigma_y\\ \tau_{xy}\end{Bmatrix} = \begin{bmatrix}\frac{E_x}{(1-\nu_{xy}\nu_{yx})} & \frac{\nu_{xy}E_y}{(1-\nu_{xy}\nu_{yx})} & 0\\ \frac{\nu_{xy}E_y}{(1-\nu_{xy}\nu_{yx}} & \frac{E_y}{(1-\nu_{xy}\nu_{yx})} & 0\\ 0 & 0 & G_{xy}\end{bmatrix}\begin{Bmatrix}\varepsilon_x\\ \varepsilon_y\\ \gamma_{xy}\end{Bmatrix}, \qquad (\eta^2 = e_0^2 a^2) \tag{4.22}$$

Where $\nabla^2 = \frac{\partial^2}{\partial x_1^2} + \frac{\partial^2}{\partial x_2^2}$ and the matrix is symmetrical along the upper left to lower right diagonal. The moments equation then becomes;

$$\begin{Bmatrix}M_x\\ M_x\\ M_{xy}\end{Bmatrix} - \eta^2\nabla^2\begin{Bmatrix}M_x\\ M_x\\ M_{xy}\end{Bmatrix} = \int_{-\frac{h}{2}}^{\frac{h}{2}} -\begin{bmatrix}\frac{E_x}{(1-\nu_{xy}\nu_{yx})} & \frac{\nu_{xy}E_y}{(1-\nu_{xy}\nu_{yx})} & 0\\ \frac{\nu_{xy}E_y}{(1-\nu_{xy}\nu_{yx}} & \frac{E_y}{(1-\nu_{xy}\nu_{yx})} & 0\\ 0 & 0 & G_{xy}\end{bmatrix}\begin{Bmatrix}\frac{\partial^2 w}{\partial\, x^2}\\ \frac{\partial^2 w}{\partial\, y^2}\\ 2\frac{\partial^2 w}{\partial x\, \partial y}\end{Bmatrix} z^2\, \mathrm{d}z \tag{4.23}$$

The nonlocal governing deflection equation is obtained as follows;

$$\begin{gathered} D_{11}\frac{\partial^4 w}{\partial x^4} + D_{22}\frac{\partial^4 w}{\partial y^4} + 2(D_{12}+D_{66})\frac{\partial^2 w}{\partial x^2\partial y^2} = \\ (\tilde{\eta}^2\nabla^2 - 1)\left(q(x,y) + N_x\frac{\partial^2 w}{\partial x^2} + N_y\frac{\partial^2 w}{\partial y^2} + 2N_{xy}\frac{\partial^2 w}{\partial x\partial y}\right)\end{gathered} \tag{4.24}$$

4.2.3 Surface equations

When modelling for the surface effects [33] the thin plate is regarded as having two physically distinct material sections namely the surface $\mathcal{S}$ and the bulk $\mathcal{B}$. The surface area is considered to be a two dimensional continuum that adheres to the body without slipping with a coordinates system of Greek symbols ($x_{\{\alpha,\beta,\gamma\}} = x_{\{1,2\}}$). On the other hand the bulk complement is considered to be a three dimensional continuum with a coordinate system that uses Latin symbols ($x_{\{i,j,k\}} = x_{\{1,2,3\}}$), bounded by the surface. Neglecting body forces the state of stress in the bulk $\mathcal{B}$ is defined by the following differential equation;

$$\tau_{ij,j} = 0 \qquad \text{with} \qquad i,j = 1,2,\text{or}3. \tag{4.25}$$

where τ_{ij} denotes stress and commas implying differentiation with respect to the corresponding index. Applying the index system with the following definitions;

$$\begin{bmatrix} \sigma_{xx} & \tau_{xy} & \tau_{xz} \\ \tau_{yx} & \sigma_{yy} & \tau_{yz} \\ \tau_{zx} & \tau_{zy} & \sigma_{zz} \end{bmatrix} \qquad = \qquad \begin{bmatrix} \tau_{11} & \tau_{12} & \tau_{13} \\ \tau_{21} & \tau_{22} & \tau_{23} \\ \tau_{31} & \tau_{32} & \tau_{33} \end{bmatrix}$$

with the coordinate system working as follows;

$$\{x,\, y,\, z\} = \{x_1,\, x_2,\, x_3\}$$

Expanding the differential equation (4.25) based on the variation of stress in a three dimensional parallelepiped (see Figure 4.5) element the following equations are obtained;

$$\frac{\partial \tau_{11}}{\partial x_1} + \frac{\partial \tau_{12}}{\partial x_2} + \frac{\partial \tau_{13}}{\partial x_3} = 0 \tag{4.26}$$

$$\frac{\partial \tau_{22}}{\partial x_2} + \frac{\partial \tau_{12}}{\partial x_1} + \frac{\partial \tau_{23}}{\partial x_3} = 0 \tag{4.27}$$

$$\frac{\partial \tau_{33}}{\partial x_3} + \frac{\partial \tau_{13}}{\partial x_1} + \frac{\partial \tau_{23}}{\partial x_2} = 0 \tag{4.28}$$

As shown in Figure 4.1, h in the z or x_3 direction is the thickness of the plate and is taken as significantly small in comparison to the x and y dimensions. Based on this assumption and applying integration through the thickness [43, 47, 67] the resultant forces and moments can be concisely specified in the following manner;

$$N_{ij} = \int_{-\frac{h}{2}}^{\frac{h}{2}} (\tau_{ij})\, \mathrm{d}x_3 \tag{4.29}$$

$$M_{ij} = \int_{-\frac{h}{2}}^{\frac{h}{2}} (\tau_{ij})\, x_3\, \mathrm{d}x_3 \tag{4.30}$$

Multiplying equation 4.25 by $\mathrm{d}x_3$ and subsequently by $x_3\,\mathrm{d}x_3$ respectively and integrating through the thickness the following is obtained;

$$N_{i\beta,\beta} + \tau^{+}_{i3} - \tau^{-}_{i3} = 0, \tag{4.31}$$

$$M_{i\beta,\beta} - N_{i3} + \frac{h}{2}(\tau^{+}_{i3} + \tau^{-}_{i3}) = 0 \tag{4.32}$$

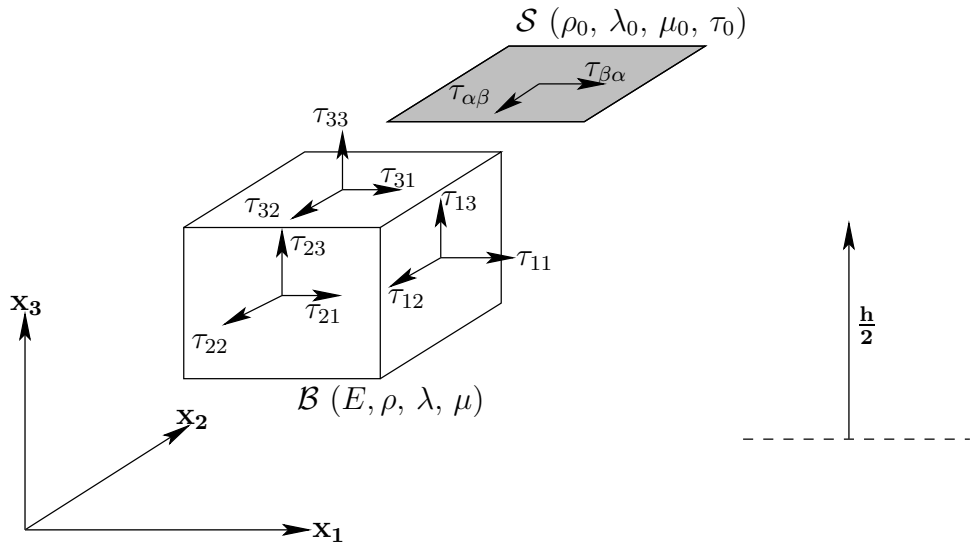

Figure 4.5: Half-space (surface and cubic element)

For the two dimensional surface continuum $\mathcal{S}$ the stresses [33] in the system are subject to boundary equilibrium, with equations determined as follows;

$$\tau^{\pm}_{\beta i,\beta} = \pm\tau_{i3} \qquad \text{at} \qquad x_3 = \pm\frac{h}{2} \tag{4.33}$$

where $\pm\tau_{i3}$ are bulk stress components which must equal the surface stress per unit area. Substituting equilibrium equation (4.33) into equation (4.31) and (4.32), the governing equations for the plate containing surface effects are obtained as follows;

$$N_{i\beta,\beta} + \tau^{+}_{\beta\alpha,\beta} + \tau^{-}_{\beta\alpha,\beta} = 0 \tag{4.34}$$

$$M_{\alpha\beta,\beta} - N_{\alpha 3} + \frac{h}{2}(\tau^{+}_{\alpha\beta,\beta} - \tau^{-}_{\alpha\beta,\beta}) = 0 \tag{4.35}$$

The plate is assumed to be composed of two physically distinct sections but within each continuum materials properties such that they are homogeneous, isotropic and linearly elastic, for both surface $\mathcal{S}$ and the bulk $\mathcal{B}$. From the compatibility of stress and strain equations, linear elasticity within the element, the stress components are expressed in terms of strain as follows;

$$\tau_{ij} = \lambda\delta_{ij}\epsilon_{kk} + 2\mu\epsilon_{ij} \tag{4.36}$$

where δ_{ij} denotes Kronecker delta such that;

$$\delta_{ij} = \begin{bmatrix} 1 & 0 & 0 \\ 0 & 1 & 0 \\ 0 & 0 & 1 \end{bmatrix}$$

and $\{i, j, k\} = \{1 \text{ or } 2 \text{ or } 3\}$.

Strain equations can be replaced by the concise version as follows;

$$\epsilon_{ij} = \frac{1}{2}\left(u_{i,j} + u_{j,i}\right)$$

where the nine components of strain are expressed as follows;

$$\epsilon_{ij} = \begin{cases} \frac{\partial u_i}{\partial x_i} & \text{if } i = j, \\ \frac{1}{2}\left(\frac{\partial u_i}{\partial x_j} + \frac{\partial u_j}{\partial x_i}\right) & \text{if } i \neq j. \end{cases}$$

Based on the fact that the material is isotropic the *Lamé* constants are specified as follows;

$$\mu = \frac{E}{2(1+\nu)}, \qquad \lambda = \frac{\nu E}{(1+\nu)(1-2\nu)}$$

and repeated subscripts implies summation such that with strain ϵ_{kk} the following is obtained;

$$\epsilon_{kk} = \epsilon_{11} + \epsilon_{22} + \epsilon_{33}$$

and this applies equally to stress τ_{ii}. Gurtin-Murdoch's [33] model for the constitutive relations at the surface layers with the top $\mathcal{S}^+$ and bottom $\mathcal{S}^-$ layers having the same material properties,the following is given;

$$\tau^{\pm}_{\alpha\beta} = \tau_0\,\delta_{\alpha\beta} + (\mu_0 - \tau_0)\left(u^{\pm}_{\alpha,\beta} - u^{\pm}_{\beta,\alpha}\right) + (\lambda_0 + \tau_0)\;\; u^{\pm}_{r,r}\delta_{\alpha\beta} + \tau_0\; u^{\pm}_{\alpha,\beta}, \tag{4.37}$$

$$\tau^{\pm}_{3\beta} = \tau_0\; u^{\pm}_{3,\beta} \tag{4.38}$$

where μ_0 and γ_0 are the Lamé moduli. The nonlocal constitutive relation for the isotropic plane stress and strain system is as follows;

$$\begin{Bmatrix} \tau_{11} \\ \tau_{22} \\ \tau_{12} \end{Bmatrix} - \eta^2\nabla^2 \begin{Bmatrix} \tau_{11} \\ \tau_{22} \\ \tau_{12} \end{Bmatrix} = \begin{bmatrix} \frac{E}{(1-\nu^2)} & \frac{\nu E}{(1-\nu^2} & 0 \\ \frac{\nu E}{(1-\nu^2} & \frac{E}{(1-\nu^2)} & 0 \\ 0 & 0 & 2G \end{bmatrix} \begin{Bmatrix} \varepsilon_{11} \\ \varepsilon_{22} \\ \varepsilon_{12} \end{Bmatrix}, \qquad (\eta^2 = e_0^2 a^2) \tag{4.39}$$

Using equations $(4.29, 4.30, 4.34, 4.35, 4.37, 4.38, 4.39)$ the governing equation is obtained as follows;

$$\left(D + \frac{1}{2}h^2\,E^s\right)\nabla^4 w - \frac{1}{2}\mu^2 h^2\,E^s\nabla^6 w = \left(1 - \mu^2\nabla^2\right)\left(2\tilde{\tau}_0\nabla^2 w + N_x\frac{\partial^2 w}{\partial x^2} + N_y\frac{\partial^2 w}{\partial y^2}\right) \tag{4.40}$$

where

$$D = \frac{Eh^3}{12(1-\nu^2)}, \qquad E^s = 2u_0 + \lambda_0. \tag{4.41}$$

Chapter 5

Final Discussion

A robust non-probabilistic modelling regime that demonstrated high levels of effectiveness in handling uncertainties has been presented. Using the Euclidean space and the inference from its geometric properties as a foundation, a set-theoretic formulation of uncertainty has been applied to nanostructures. The impact of variations in the loading and material properties has been the main objective of the study. Convex modelling methods consider variations within the bearing load as well as in the material properties to be uncertain-but-bounded. Inherent scale related material features dictates that small scale effects namely nonlocal and surface effects be considered for the analysis of nanostructures.

Summary of the research results

The main findings of each publication are summarised and presented as per the order of appearance of the respective papers in the dissertation.

Paper 1

The study of the effects of uncertainty using convex modelling has been applied to the deflection of a statically loaded beam. Fourier series expansion of the load into deterministic and uncertain components has been implemented in the beam problem. The elastic constants and the small scale parameter have also been expanded into deterministic and uncertain quantities, in order to determine the maximum deflection. Uncertain coefficients utilised in the constitutive equations were linearised and computed accordingly. Since these parameters were not independent a method of Lagrange multipliers has been applied in determining the solution with results showing increased uncertainty levels producing higher deflection. Sensitivity analysis of the deflection relative to the level of uncertainty in the material parameters has been investigated. Results demonstrate higher sensitivity of the deflection to the elastic

constant than to the small scale parameter with a ratio of about 5 : 1.

Remarks

The results produced in this beam problem proved beneficial in a sense that although theoretical formulation of the model was predictable it highlighted issues that were not expected otherwise. For instance the fact that there is a higher rate of sensitivity with respect to small scale parameter as opposed to that of the Young's modulus parameter is informative and highlights the importance of modelling appropriately for the relevant scale.

Paper 2

Buckling of the orthotropic nano-scale plate with material uncertainty and nonlocal effects has been presented. The buckling load expression has been expanded around its nominal value using the Taylor series expansion. The solution has been obtained by solving a min-max optimization problem subject to a set of extreme points in the domain. Material uncertainty properties investigated were the following; Young's modulus, shear modulus, in-plane Poisson's ratio, and the nonlocal small scale parameter. Correspondence between uncertainty levels to worst-case combination of material properties was implemented to determine the lowest buckling load. The least favourable buckling load computed by convex modelling lead to a five-dimensional ellipsoid bound for uncertainty. Relative sensitivity of the buckling load to uncertainty in the elastic constants investigated has been normalised with respect to the deterministic load. Sensitivity to Young's modulus was mostly influenced by the level of uncertainty.

Remarks

As in the previous case there is consistency when it comes to the small-scale effects on the model. Results also show some measure of sensitivity of the buckling load to the nonlocal parameter.

Paper 3

Buckling of isotropic nano-scale plates with material uncertainty and small scale effects was presented. Material uncertainty properties investigated were the following; Young's modulus, surface elastic modulus, residual surface elastic modulus, residual surface stress, and nonlocal small scale factor. The correspondence between uncertainty levels to worst-case combination of material properties to determine the lowest buckling load have been established in this case as well. The analysis of an isotropic

case led to a four-dimensional ellipsoid bounding for the convex model of uncertainty. Relative sensitivity of the buckling load and uncertainty in the elastic constants was given. Sensitivity results demonstrated that the buckling load is most sensitive to Young's modulus for the plate with some measure of sensitivity to small scale effects as well. Sensitivity to the nonlocal parameter and surface elastic modulus increased with the upwards scaling in the size of the plate.

Remarks

This study complemented the finding in the literature that deals with various statically loaded structures containing cases that assume loading and material properties to be deterministic.

Future research

The study of dynamically loaded structures did not form part of this investigation thus affording an opportunity for future research. This may entail issues around the fundamental frequency and resonance frequency of these nanostructures subject to uncertain dynamic load and material properties. Convex modelling of uncertain design parameters for various elements coupled with the optimisation of the same parameters, resulting from inadequate information presents another chance for further investigation. There are prospects of investigating relative sensitivity of the optimised uncertain design parameters to the loads and material properties. Optimum alignment of the design modelling regimes with design problem sets using convexity and the fine tuning of the manufacturing techniques will result with reliable products. The study of the interaction between small scale effects with various boundary conditions is still outstanding as far as the assessment of the literature and the opinion of the author is concerned. Convex modelling of approximate solution to clamped plate problems produces non-linear results, thus presents a challenge and opportunity for further studies.

Bibliography

[1] Sarp Adali. *Advanced Polymeric Materials*, chapter "Design Optimization of Composite Laminates under Deterministic and Uncertain Conditions", pages 31–47. CRC PRESS, 2003.

[2] Sarp Adali. "Variational principles for multi-walled carbon nanotubes undergoing buckling based on nonlocal elasticity theory". *Physics Letters A*, 372:5701–5705, 2008.

[3] Sarp Adali, Jr John C. Bruch, Ibrahim S. Sadek, and James M. Sloss. "Transient vibrations of cross-ply plates subject to uncertain excitations". *Applied Mathematical Modelling*, 19:56–63, 1995.

[4] P. M. Ajayan and Sumio Iijima. "Smallest carbon nanotube". *Nature*, 358:23, Jul 1992.

[5] Pulickel M. Ajayan. "How does a nanofibre grow?". *Nature*, 427:402–403, Jan 2004.

[6] Pulickel M. Ajayan and James M. Tour. "Nanotube composites". *Nature*, 447:1066–1068, Jun 2007.

[7] H. R. Analooei, M. Azhari, and A. Heidarpour. "Elastic buckling and vibration analyses of orthotropic nanoplates using nonlocal continuum mechanics and spline finite strip method". *Aplied Mathematical Modelling*, 37:6703–6717, 2013.

[8] R. Andrews, D. Jacques, A. M. Rao, T. Rantell, F. Derbyshire, Y. Chen, J. Chen, and R. C. Haddon. "Nanotube composite carbon fibers". *Applied Physics Letters*, 75(9):1329–1331, Aug 1999.

[9] R. Ansari and S. Sahmani. "Small scale effect on vibrational response of single-walled carbon nanotubes with different boundary conditions based on nonlocal beam models". *Commun Nonlinear Sci Numer Simulat*, 17:1965–1979, 2012.

[10] Donald R. Askeland, Pradeep P. Fulay, and Wendelin J. Wright. *"The Science and Engineering of Materials"*. CENGAGE Learning, 2011.

[11] Yakov Ben-Haim and Isaac Elishakoff. *"Convex Models of Uncertainty in Applied Mechanics"*. ELSEVIER, 1990.

[12] Jerzy Bernholc, Christopher Roland, and Boris I. Yakobson. "Nanotubes". *Current Opinion in Solid State and Materials Science*, 2:706–715, 1997.

[13] Stephen Boyd and Lieven Vandenberghe. *"Convex Optimization"*. CAMBRIDGE UNIVERSITY PRESS, 2004.

[14] Carlos Conceição António and Luísa N. Hoffbauer. "Uncertainty analysis based on sensitivity applied to angle-ply composite structures". *Reliability Engineering and System Safety*, 92:1353–1362, 2007.

[15] R. C. Cammarata. "Surface and interface stress effects on interfacial and nanostructured Materials". *Materials Science and Engineering*, A237:180–184, 1997.

[16] R. C. Cammarata. "Surface and interface stress effects on the growth of thin films". *Journal of Electronic Materials*, 26:966–968, 1997.

[17] L. Chernozatonskii. "Three-terminal junction of carbon nanotubes: synthesis, structures, properties and applications". *Journal of Nanoparticle Research*, 5:473–484, 2003.

[18] Richard Courant and David Hilbert. *"Methods of Mathematical Physics"*. WILEY-VCH, 2004.

[19] Thomas H. Courtney. *"Mechanical Behavior of Materials"*. McGRAW-HILL BOOK COMPANY, 2000.

[20] T. W. Ebbesen, P. M. Ajayan, H. Hlura, and K. Tanigaki. "Purification of nanotubes". *Nature*, 367:519, Feb 1994.

[21] M. C. Ece and M. Aydogdu. "Nonlocal elasticity effect on vibration of in-plane loaded double-walled carbon nano-tubes". *Acta Mechanica*, 190:185–195, 2007.

[22] Albert Einstein. "Geometry and Experience". *Address to the Prussian Academy of Sciences in Berlin on January 27th*, 1921.

[23] I Elishakoff and M. Zingales. "Contrasting probabilistic and anti-optimization approaches in an applied mechanics problem". *International Journal of Solids and Structures*, 40:4281–4297, 2003.

[24] Isaac Elishakoff. "Essay on uncertainties in elastic and viscoelastic structures: from A. M. Freudenthal's criticisms to modern convex modeling". *Computers and Structures*, 56(6):871–895, 1995.

[25] Isaac Elishakoff. "Uncertain buckling: its past, present and future". *International Journal of Solids and Structures*, 37:6869–6889, 2000.

[26] A. Cemal Eringen. "Nonlocal polar elastic continua". *Int.J.Engng. Sci*, 10(1-A):1–16, 1972.

[27] A. Cemal Eringen. "On differential equations of nonlocal elasticity and solutions of srew dislocation and surface waves". *J.Appl.Phys*, 54(9):4703–4710, 1983.

[28] A. Cemal Eringen and D. G. B. Edelen. "On nonlocal elasticity". *Int.J.Engng. Sci*, 10(3-B):233–248, 1972.

[29] Stanley J. Farlow. *"Partial Differential Equations for Scientist and Engineers"*. DOVER PUBLICATIONS, INC., 1993.

[30] Bodo Fiedler, Florian H. Gojny, Malte H. G. Wichmann, Mathias C. M. Nolte, and Karl Schulte. "Fundamental aspects of nano-reinforced composites". *Composites Science and Technology*, 66:3115–3125, 2006.

[31] S. A. M. Ghannadpour, B. Mohammadi, and J. Fazilati. "Bending buckling and vibration problems of nonlocal Euler beams using Ritz method". *Composite Structures*, 96:584–589, 2013.

[32] Morton E. Gurtin and A. Ian Murdoch. "A Continuum theory of elastic material surfaces". *Arch. Rat. Mech. Anal*, 57:291–323, 1975.

[33] Morton E. Gurtin and A. Ian Murdoch. "Surface stress in solids". *Int. J. Solids Structures*, 14:431–440, 1978.

[34] Stig helveg, Carlos Lopez-Cartes, Jens Sehested, Poul L. Hansen, Bjerne S. Clausen, Jens R. Rostrup-Nielsen, Frank Abild-Pedersen, and Jens K. Norskov. "Atomic-scale imaging of carbon nanofibre growth". *Nature*, 427:426–429, Jan 2004.

[35] I. N. Herstein. *"Abstract Algebra"*. JOHN WILEY AND SONS, INC, 1999.

[36] W. H. Horton, J. I. Craig, and D. E. Struble. "A simple, practical method for the experimental determination of the fixity of a column". *Proceedings of the Eighth International Symposium on Space Technology and Science*, 1969.

[37] Sumio Iijima. "Helical microtubule of graphitic carbon". *Nature*, 354:56–58, Nov 1991.

[38] Paul Joseph Kelly and Max L. Weiss. *"Geometry and Convexity: a study in mathematical methods"*. WILEY, 1979.

[39] Tapas Kuilla, Sambhu Bhadra, Daru Yao, Nam Hoon Kim, Saswata Bose, and Joong Hee Lee. "Recent advances in graphene based polymer composites". *Progress in Polymer Science*, 35:1350–1375, 2010.

[40] A. Labuschagne, N. F. J. van Rensburg, and A. J. van der Merwe. "Comparison of linear beam theories". *Mathematical and Computer Modelling*, 49:20–30, 2009.

[41] A. B. Levy and R. T. Rockafellar. "Sensitivity analysis of solutions to generalized equations". *American Mathematical Society*, 345(2):661–671, 1994.

[42] Chunyu Li, Erik T. Thostenson, and Tsu-Wei Chou. "Sensors and actuators based on carbon nanotubes and their composites: A review". *Composites Science and Technology*, 68:1227–1249, 2008.

[43] C. W. Lim and L. H. He. "Size-dependent nonlinear response of thin elastic films with nano-scale thickness". *International Journal of Mechanical Sciences*, 46:1715–1726, 2004.

[44] Ronald E. Miller and Vijay B. Shenoy. "Size-dependent elastic properties of nanosized Structural elements". *Nanotechnology*, 11:139–147, 2000.

[45] T. Murmu and S. Adhikari. "Nonlocal elasticity based vibration of initially pre-stressed couple nanobeam systems". *European Journal of Mechanics and Solids*, 34:52–62, 2012.

[46] D. R. Paul and L. M. Robeson. "Polymer nanotechnology: Nanocomposites". *Polymer*, 49:3187–3204, 2008.

[47] P.Lu, L. H. He, H. P. Lee, and C. Lu. "Thin plate theory including surface effects". *International Journal of Solids and Structures*, 43:4631–4647, 2006.

[48] Valentin N. Popov. "Carbon nanotubes: properties and application". *Materials Science and Engineering R*, 43:61–102, 2004.

[49] Jeffrey R. Potts, Daniel R. Dreyer, Christopher W. Bielawski, and Rodney S. Ruoff. "Graphene-based polymer nanocomposites". *Polymer*, 52:5–25, 2011.

[50] Zhiping Qiu and Isaac Elishakoff. "Anti-optimization technique - a generalization of interval analysis for nonprobabilistic treatment of uncertainty". *Chaos, Solutions and Fractals*, 12:1747–1759, 2001.

[51] J. N. Reddy. "Nonlocal theories for bending, buckling and vibration of beams". *International Journal of Engineering Science*, 45:288–307, 2007.

[52] J. N. Reddy. *"Theory and Analysis of Elastic Plates and Shells"*. CRC Press, 2007.

[53] J. N. Reddy and S. D. Pang. "Nonlocal continuum theories of beams for the analysis of carbon nanotubes". *Journal of Applied Physics*, 103(023511), 2008.

[54] Stephen M. Robinson. "An implicit-function theorem for a class of nonsmooth functions". *Mathematics of Operations Research*, 16(2):292–309, 1991.

[55] R. Tyrrell Rockafellar. *"Convex Analysis"*. PRINCETON UNIVERSITY PRESS, 1970.

[56] I. S. Sadek, J. M. Sloss, S. Adali, and Jr J. C. Bruch. "Nonprobabilistic modelling of dynamically loaded beams under uncertain excitations". *Mathl. Comput. Modelling*, 18:59–67, 1993.

[57] Hans Sagan. *"Introduction to the Calculus of Variations"*. DOVER PUBLICATIONS, INC., New York, 1969.

[58] Virendra Singh, Daeha Joung, Lei Zhai, Soumen Das, Saiful I. Khondaker, and Sudipta Seal. "Graphene based material: Past, present and future". *Progress in Materials Science*, 56:1178–1271, 2011.

[59] Barry Spain. *"Tensor Calculus"*. OLIVER AND BOYD, 1960.

[60] Jonghwan Suhr, Nikhil Koratkar, Pawel Keblinski, and Pulickel Ajayan. "Viscoelasticity in carbon nanotube composites". *Nature Materials*, 4, Feb 2005.

[61] Stephen R. Swanson. *"Introduction to Design and Analysis with Advanced Composite Materials"*. PRENTICE HALL, 1997.

[62] A. L. Sweet, J. Genin, and P. F. Mlakar. "Vibratory identification of beam boundary conditions". *Journal of Dynamic Systems, Measurement, and Control*, pages 387–394, 1976.

[63] A. L. Sweet, J. Genin, and P. F. Mlakar. "Determination of column-buckling criteria using vibratory data". *Experimental Mechanics*, 1977.

[64] S. P. Timoshenko and J. N. Goodier. *"Theory of Elasticity"*. McGRAW-HILL BOOK COMPANY, 1970.

[65] S. P. Timoshenko and S. Woinowsky-Krieger. *"Theory of Plates and Shell"*. McGRAW-HILL BOOK COMPANY, 1959.

[66] C. M. Wang, S. Kitipornchai, C. W. Lim, and Eisenberger. "Beam bending solutions based on nonlocal Timoshenko beam theory". *Journal of Engineering Mechanics*, 134(6):475–481, 2008.

[67] Kaifa F. Wang and Baolin L. Wang. "Combining effects of surface energy and non-local elasticity on the buckling of nanoplates". *Micro and Nano Letters*, 6:941–943, 2011.

[68] Q. Wang and K. M. Liew. "Application of nonlocal continuum mechanics to static analysis of micro-and nano-structures". *Physics Letters A*, 363:236–242, 2007.

[69] B. Q. Wei, R. Vajtai, and P. M. Ajayan. "Reliability and current carrying capacity of carbon nanotubes". *Applied Physics Letters*, 79(8):1172–1174, Aug 2001.

[70] Mingtian Xu. "Free transverse vibrations of nano-to-micron scale beams". *Proceedings of the Royal Society A*, 462(2074):2977–2995, 2006.

Part II

Publications

Paper 1

The paper was accepted for publication in the **Journal of Theoretical and Applied Mechanics (JTAM)**

STATIC AND SENSITIVITY ANALYSIS OF NONLOCAL NANOBEAMS SUBJECT TO LOAD AND MATERIAL UNCERTAINTIES BY CONVEX MODELING

ISAAC SFISO RADEBE

Department of Mechanical Engineering, Durban University of Technology, Durban, South Africa

Email: sfisor@dut.ac.za

SARP ADALI

Discipline of Mechanical Engineering, University of KwaZulu-Natal, Durban, South Africa

Email: adali@ukzn.ac.za

At the nano-scale, loads acting on a nanobeam and its material properties are likely to be not known precisely, i.e., uncertain. In the present the deflection of a nanobeam subject to load and material uncertainties is studied by convex modeling of the uncertainties. The level of uncertainty is taken to be bounded and the maximum deflection corresponding to the worst-case of loading or material properties is obtained, that is, the uncertainties are determined so as to maximize the deflection. The sensitivity of the deflection to the uncertainty in the material properties is also investigated. Numerical results are given relating the level of uncertainty to maximum deflection.

Key words: nanobeams, load uncertainty, material uncertainty, convex modeling, sensitivity

1. Introduction

Mechanics of nanobeams has been studied extensively using continuum based models in an effort to quantify their behavior under static, buckling and dynamic loads. Several studies focused on continuum modeling and mechanics of nano and micro-sized beams and carbon nanotubes using various beam theories (see Wang and Shindo, 2006; Reddy, 2007; Reddy and Pang, 2008; Adali, 2008; Zhang *et al*., 2010; Di Paola *et al*., 2011; Muc, 2011; Adali, 2011; Hosseini-Ara *et al*., 2012; Thai, 2012; Thai and Vo, 2012; Eltaher *et al*., 2013). These studies employed Euler-Bernoulli and Timoshenko beam models coupled with the nonlocal elastic theory (see Eringen, 2002) to formulate the variational principles and the governing equations for nanobeams undergoing static bending, buckling and vibrations.

The bending behavior of nano-scale structures has been the subject of several studies and, in particular, nanobeams under static transverse loads have been studied in (Wang and Shindo, 2006; Reddy, 2007; Reddy and Pang, 2008; Zhang *et al*., 2010; Di Paola *et al*., 2011; Thai, 2012; Thai and Vo, 2012; Eltaher *et al*., 2013; Challamel and Wang, 2008; Wang *et al*., 2008; Ansari and Sahmani, 2011; Fang *et al*., 2011; Roque *et al*., 2011; Li *et al*., 2012; Khajeansari *et al*., 2012). These studies took into account a number of effects such as shear deformation, surface stress, and elastic foundation but neglected the load and material uncertainties.

As such in the previous studies, the loading was taken as deterministic and the material properties were defined taking their average values. However, under operational conditions, the loads often have random characteristics making it difficult to predict their magnitude and distribution with accuracy. Similarly it is usually difficult to determine the elastic constants of nano-sized beams with some certainty. The scatter in the geometric and material properties of carbon nanotubes is known and has been discussed in (Kalamkarov *et al*., 2006, Huang *et al*., 2006, Scarpa and Adhikari, 2008, Lu and Zhong, 2012, Fereidoon *et al*., 2014).

The main trust of the present work is to study the bending of nanobeams in a non-deterministic setting by taking the load and material variations into account. Thus the maximum deflection of nanobeams is determined taking the transverse loading as non-deterministic and the material properties as uncertain. Problem analysis is conducted using convex modeling of uncertainties to determine the least favourable conditions to produce the highest deflection. Convex modeling has been used extensively in the past to

deal with various engineering problems containing data uncertainties (see Adali *et al*., 1995a, b, Pantelidis and Ganzerli, 1998, Jiang *et al*., 2007, Kang and Luo, 2009, Hu and Qiu, 2010, Radebe and Adali, 2013). For further information the reader is referred to the review articles by Wang *et al*. (2001) and the book by Ben-Haim and Elishakoff (1990).

In the present study, the effect of load and material uncertainties on the deflection of a nanobeam is studied based on the nonlocal Euler-Bernoulli beam theory. Previous work on the subject involves the study of the effect of material uncertainties on the buckling of a nonlocal plate by Radebe and Adali (2014). Load and material uncertainties are modeled as uncertain-but-bounded quantities. Explicit expressions are obtained for the least favorable deflection of a nanobeam for a given level of uncertainty. The sensitivity of the deflection to the level of uncertainty in material properties is also studied. Numerical results are given to investigate the effect of uncertainty on deflection and on the sensitivity to material properties.

2. Load uncertainty

The nanobeam under consideration is subject to a combination of deterministic and uncertain transverse loads denoted by $p(x)$ and $\tilde{q}(x)$, respectively, as well as a compressive axial load N_0 as shown in Fig. 1. The beam has a rectangular cross-section of dimensions $h \times b$ where h is the height and b is the width (Fig. 1).

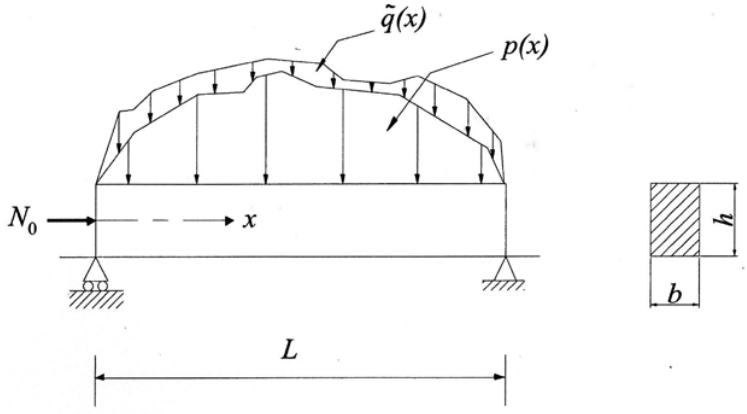

Fig. 1. Beam geometry and uncertain loading

The differential equation governing its deflection $w(x)$ based on the nonlocal elastic theory is given by (Reddy, 2007)

$$EIw_{xxxx} + N_0(w_{xx} - \eta^2 w_{xxxx}) = (p - \eta^2 p_{xx}) + (\tilde{q} - \eta^2 \tilde{q}_{xx}) \quad \text{for} \quad 0 \le x \le L \tag{2.1}$$

where E is the Young's modulus, I is the moment of inertia and η is the small-scale parameter. The subscript x denotes differentiation with respect to x. Compressive axial load N_0 satisfies the buckling constraint $N_0 < N_{cr}$ where the buckling load N_{cr} is given by (see Reddy, 2007)

$$N_{cr} = \frac{\mu^2 EI}{L^2 + \mu^2 \eta^2} \tag{2.2}$$

with μ denoting a coefficient depending on the boundary conditions.

The uncertain load $\tilde{q}(x)$ acting on the beam is unknown, and only limited information is available on its coefficients. The information required on the uncertain load is that it should have a finite norm, i.e., it should satisfy the constraint

$$\|\tilde{q}(x)\|_{L_2}^2 = \int_0^L [\tilde{q}(x)]^2 \, dx \le \varepsilon^2 \tag{2.3}$$

where $0 < \varepsilon < 1$ is a given constant which determines the level of uncertainty and the subscript L_2 denotes the L_2 norm. The solution of the deflection problem is obtained by expanding the deterministic and uncertain loads in terms of orthogonal functions $\psi_n(x)$ satisfying the boundary conditions, viz.

$$p(x) = \sum_{n=1}^{\infty} p_n \psi_n(x), \qquad \tilde{q}(x) = \sum_{n=1}^{\infty} \tilde{q}_n \psi_n(x) \tag{2.4}$$

where the coefficients are given by

$$p_n = \frac{1}{r}\int_0^L p(x)\psi_n(x)dx, \qquad \tilde{q}_n = \frac{1}{r}\int_0^L \tilde{q}(x)\psi_n(x)dx \tag{2.5}$$

with r given by

$$r = \|\psi_n(x)\|_{L_2}^2 = \int_0^L [\psi_n(x)]^2 \, dx \tag{2.6}$$

Here the coefficients p_n are known since the deterministic load $p(x)$ is given, however the coefficients $\tilde{q}_n$ are unknown and have to be determined to maximize the deflection corresponding to the least favourable (worst-case) loading. The solution for the deflection function $w(x)$ is also expanded in terms of $\psi_n(x)$ and can be expressed as

$$w(x) = \sum_{n=1}^{\infty} W_n \psi_n(x) \tag{2.7}$$

The coefficients W_n are computed by substituting Eq. (2.7) into the differential equation (2.1). Next the worst-case uncertain loading causing the highest deflection is obtained. From Eqs. (2.3) and (2.5), it follows that

$$\sum_{n=1}^{N} (\tilde{q}_n)^2 \le \frac{\varepsilon^2}{r} \tag{2.8}$$

where N is a large number. The highest load is obtained when $\sum_{n=1}^{N} (\tilde{q}_n)^2 = \varepsilon^2 / r$, i.e., the inequality is taken as an equality. Thus the deflection $w(x;\tilde{q})$ is to be maximized with respect to the uncertain load subject to the constraint $\sum_{n=1}^{N} (\tilde{q}_n)^2 = \varepsilon^2 / r$. For this purpose the method of Lagrange multipliers is employed with the Lagrangian at a point $x = x_0$ given by

$$L(x_0;\tilde{q}_n) = w(x_0;\tilde{q}(x_0)) + \lambda\left(\sum_{n=1}^{N} (\tilde{q}_n)^2 - \frac{\varepsilon^2}{r}\right) \tag{2.9}$$

where λ is a Lagrange multiplier and $0 \le x_0 \le L$ is a point which has to be determined such that $w(x_0;\tilde{q}(x_0))$ is maximum at $x = x_0$. The maximum of $L(x_0;\tilde{q}_n)$ with respect to $\tilde{q}_n$ produces the least favourable uncertain load, viz.

$$\max_{\tilde{q}_n} L(x_0;\tilde{q}_n) \tag{2.10}$$

which can be computed by setting its derivative with respect to $\tilde{q}_n$ to zero, viz.

$$\frac{\partial L(x_0;\tilde{q}_n)}{\partial \tilde{q}_n} = 0 \qquad \text{for} \qquad n = 1,2,...,N \tag{2.11}$$

This computation gives the coefficient $\tilde{q}_n$ at a point x_0 as

$$\tilde{q}_n(x_0) = -\frac{1}{2\lambda}\frac{\partial w(x_0;\tilde{q}_n(x_0))}{\partial \tilde{q}_n} \tag{2.12}$$

The point x_0 is an unknown and has to be determined to maximize the deflection.

2.1. Simply supported beam

The method of solution outlined above is now applied to a simply supported beam subject to a deterministic load $p(x) = p_0(x/L)^3$ and the uncertain load $\tilde{q}(x)$. The simply supported boundary conditions for the nonlocal nanobeam are given by (Reddy, 2007)

$$w(0) = 0\,, \qquad (-EI + \eta^2 N_0)w_{xx}(0) + \eta^2 k_0 b w(0) - \eta^2 p(0) - \eta^2 \tilde{q}(0) = 0 \tag{2.13}$$

$$w(L) = 0\,, \qquad (-EI + \eta^2 N_0)w_{xx}(L) + \eta^2 k_0 b w(L) - \eta^2 p(L) - \eta^2 \tilde{q}(L) = 0 \tag{2.14}$$

The deterministic and uncertain loads are expanded in terms of orthogonal functions $\psi_n(x) = \sin\alpha_n x$ where $\alpha_n = \dfrac{n\pi}{L}$. Thus

$$p(x) = \sum_{n=1}^{N} p_n \sin\alpha_n x\,, \qquad \tilde{q}(x) = \sum_{n=1}^{N} \tilde{q}_n \sin\alpha_n x \tag{2.15}$$

where the coefficients p_n are given by

$$p_n = (-1)^{n+1}\frac{2p_0}{(n\pi)^3}\left(n^2\pi^2 - 6\right) \tag{2.16}$$

The deflection $w(x)$ satisfying the boundary conditions Eqs. (2.13) and (2.14) can be obtained by expanding it in terms of $\sin\alpha_n x$ as

$$w(x) = \sum_{n=1}^{N} W_n \sin\alpha_n x \tag{2.17}$$

Substituting Eq. (2.17) into the differential equation (2.1), the coefficients W_n are computed as

$$W_n = \frac{(1+\eta^2\alpha_n^2)(p_n + \tilde{q}_n)}{EI\alpha_n^4 - (1+\eta^2\alpha_n^2)\alpha_n^2 N_0} \tag{2.18}$$

Lagrangian $L(x_0; \tilde{q}_n)$ given by Eq. (2.9) becomes

$$L(x_0; \tilde{q}_n) = \sum_{n=1}^{N} \frac{(1+\eta^2\alpha_n^2)(p_n + \tilde{q}_n)}{EI\alpha_n^4 - (1+\eta^2\alpha_n^2)\alpha_n^2 N_0} \sin\alpha_n x_0 + \lambda\left(\sum_{n=1}^{N}(\tilde{q}_n)^2 - \frac{2\varepsilon^2}{L}\right) \tag{2.19}$$

The coefficients $\tilde{q}_n(x_0)$ are computed from Eqs. (2.11) and (2.19) as

$$\tilde{q}_n(x_0) = -\frac{1}{2\lambda}\frac{A_n(x_0)}{B_n} \tag{2.20}$$

where

$$A_n(x_0) = (1+\eta^2\alpha_n^2)\sin\alpha_n x_0\,, \qquad B_n = EI\alpha_n^4 - (1+\eta^2\alpha_n^2)\alpha_n^2 N_0 \tag{2.21}$$

Noting that the worst case loading is given by

$$\sum_{n=1}^{N}(\tilde{q}_n)^2 = \frac{2\varepsilon^2}{L} \tag{2.22}$$

we can compute the Lagrange multiplier from Eqs. (2.20) and (2.22) as

$$\lambda = \pm\frac{L^{1/2}}{\sqrt{8}\varepsilon}\left(\sum_{n=1}^{N}\frac{A_n^2(x_0)}{B_n^2}\right)^{1/2} \tag{2.23}$$

where the plus and minus signs correspond to the least and most favourable loading cases. The coefficients $\tilde{q}_n$ can be computed by inserting the Lagrange multiplier (2.23) into Eq. (2.20). This computation gives

$$\tilde{q}_n(x_0) = \mp \frac{\sqrt{2}\varepsilon}{L^{1/2}} \left(\sum_{n=1}^{N} \frac{A_n^2(x_0)}{B_n^2} \right)^{-1/2} \frac{A_n(x_0)}{B_n} \tag{2.24}$$

The uncertain load producing the maximum deflection is given by Eq. (2.15) with the coefficients given by Eq. (2.24).

3. Material uncertainty

3.1. Uncertain constants

Next the effect of uncertainty in material properties on the deflection is investigated. The Young's modulus $\tilde{E}$ and the small scale parameter $\tilde{\eta}$ are taken as uncertain material parameters and they are defined as

$$\tilde{E} = E_0(1+\delta_1), \qquad \tilde{\eta} = \eta_0(1+\delta_2) \tag{3.1}$$

where E_0 and η_0 are the nominal (deterministic) values, and δ_1 and δ_2 are margins of error (uncertainty) to be determined to maximize the deflection. The unknown constants δ_1 and δ_2 are required to lie in an ellipse and satisfy the inequality $\sum_{i=1}^{2} \delta_i^2 \le \gamma^2$ which corresponds to the inequality (2.3) of the uncertain loading case. The least favourable solution is given when the constants lie on the boundary of the ellipse, i.e., they satisfy the equality constraint

$$\sum_{i=1}^{2} \delta_i^2 = \gamma^2 \tag{3.2}$$

Material uncertainty is studied for a simply supported nanobeam under a sinusoidal load $p(x) = p_1 \sin(\pi x / L)$. For this case the maximum deflection occurs at the mid-point and is given by

$$w\left(\frac{L}{2}; \tilde{E}, \tilde{\eta}\right) = \frac{(1+\alpha_1^2\tilde{\eta}^2)\, p_1}{\alpha_1^4 I\tilde{E} - (1+\alpha_1^2\tilde{\eta}^2)\alpha_1^2 N_0} \tag{3.3}$$

where $\alpha_1 = \pi / L$. Substituting Eq. (3.1) into Eq. (3.3), we obtain

$$w\left(\frac{L}{2}; \tilde{E}, \tilde{\eta}\right) = \frac{\left(1+\alpha_1^2\eta_0^2(1+\delta_2)^2\right) p_1}{\alpha_1^4 IE_0(1+\delta_1) - \left(1+\alpha_1^2\eta_0^2(1+\delta_2)^2\right)\alpha_1^2 N_0} \tag{3.4}$$

which can be linearized leading to the expression

$$w\left(\frac{L}{2}; \tilde{E}, \tilde{\eta}\right) = c_0 + c_1\delta_1 + c_2\delta_2 \tag{3.5}$$

where

$$c_0 = \frac{1+\alpha_1^2\eta_0^2}{\alpha_1^4 IE_0 - (1+\alpha_1^2\eta_0^2)\alpha_1^2 N_0}\, p_1 \tag{3.6}$$

$$c_1 = -\frac{IE_0\left(1+\alpha_1^2\eta_0^2\right)}{\left(\alpha_1^2 IE_0 - (1+\alpha_1^2\eta_0^2)N_0\right)^2}\, p_1 \tag{3.7}$$

$$c_2 = \frac{2\alpha_1^2 IE_0\eta_0^2}{\left(\alpha_1^2 IE_0 - (1+\alpha_1^2\eta_0^2)N_0\right)^2}\, p_1 \tag{3.8}$$

To derive the expression (3.5), the relation

$$(1 \pm \delta)^c \cong (1 \mp c\delta) + O(\delta^2) \tag{3.9}$$

was employed where the superscript c can take positive or negative values and $|\delta| << 1$. Lagrangian $L(\delta_1, \delta_2)$ to compute the maximum deflection subject to the constraint (3.2) is given by

$$L(\delta_1, \delta_2) = c_0 + c_1\delta_1 + c_2\delta_2 + \lambda\left(\sum_{n=1}^{2}\delta_i^2 - \gamma^2\right) \tag{3.10}$$

The constants δ_i are computed from Eq. (3.10) as

$$\delta_i = -\frac{c_i}{2\lambda} \tag{3.11}$$

Lagrange multiplier λ can be computed from Eqs. (3.2) and (3.11) as

$$\lambda = \pm\frac{1}{2\gamma}\left(\sum_{i=1}^{2}c_i^2\right)^{1/2} \tag{3.12}$$

where the plus and minus signs correspond to least and most favourable cases. The coefficients δ_i can be computed by inserting the Lagrange multiplier (3.12) into Eq. (3.11). This computation gives

$$\delta_i = \mp\gamma\left(c_1^2 + c_2^2\right)^{-1/2}c_i \tag{3.13}$$

The values of δ_i given by Eq. (3.13) are substituted into Eq. (3.5) to compute the mid-point deflection $w\left(L/2; \tilde{\tilde{E}}, \tilde{\eta}\right)$ subject to material uncertainty.

3.2. Sensitivity analysis

The sensitivity of the deflection to the level of uncertainty in material data can be studied by sensitivity analysis. In general the deflection shows different sensitivities to the material parameters $\tilde{\tilde{E}}$ and $\tilde{\eta}$ and this can be investigated by defining relative sensitivity indices $S_K(\delta_i)$ given by

$$S_K(\delta_i) = \left|\frac{\partial w\left(L/2; \tilde{\tilde{E}}, \tilde{\eta}\right)}{\partial \delta_i}\right| \frac{|\delta_i|}{w\left(L/2; E_0, \eta_0\right)} \tag{3.14}$$

which is normalized with respect to the deterministic mid-point deflection $w\left(L/2; E_0, \eta_0\right)$. In Eq. (3.14), the sensitivity $S_E(\gamma_1)$ denotes the relative sensitivity of the mid-point deflection with respect to uncertainty in $\tilde{\tilde{E}}$, and $S_\eta(\delta_2)$ with respect to uncertainty in $\tilde{\eta}$ so that the subscript K stands for the respective material property. The sensitivities $S_K(\delta_i)$ can be computed from Eqs. (3.5) and (3.14) as

$$S_K(\delta_i) = \frac{|c_i\ \delta_i|}{c_0} \tag{3.15}$$

noting that $w\left(L/2; E_0, \eta_0\right) = c_0$ where the values of c_i are given by equations Eqs. (3.6)-(3.8).

4. Numerical results

The effect of uncertain loads and material properties on deflection is studied in the present section. The cross-section of the nanobeam is taken as square, and the height and the length of the nanobeam are specified as $b = h = 1\,\text{nm}$ and $L = 10\,\text{nm}$. The material properties are specified as $E = 1000\,\text{GPa}$, $0 \le \eta \le 2\,\text{nm}$.

4.1. Load uncertainty

L_2 norms of the uncertain and the deterministic loads can be related as

$$\left\|\tilde{q}(x)\right\|_{L_2}^2 = \varepsilon^2 = R_0^2\left\|p(x)\right\|_{L_2}^2 \tag{4.1}$$

where R_0 is a proportionality constant and determines the degree of uncertainty relative to the deterministic load with $R_0 = 0$ corresponding to no uncertainty, i.e., the deterministic case. For the present case $\|p(x)\|_{L_2}^2 = \frac{1}{7} p_0^2 L$, hence

$$\varepsilon = \sqrt{\frac{L}{7}} p_0 R_0 \tag{4.2}$$

In the calculations the load coefficient p_0 is taken as $p_0 = 1$ N/m. Fig. 2 shows the curves of deflection vs *x*-axis for various uncertainty levels R_0 with $\eta = 2$ nm and $N_0 = 0$. In Fig. 2, and in the subsequent figures, the curves are obtained by setting $x_0 = x$ in equation (2.7) and consequently at every point x the deflection is the least favourable deflection.

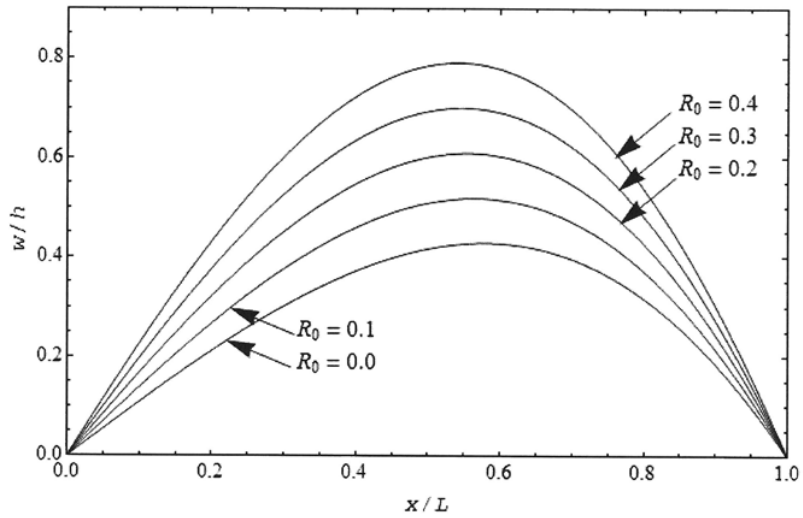

Fig. 2. The curves of deflection vs *x*-axis for various uncertainty levels with $\eta_0 = 2$ nm and $N_0 = 0$

Fig. 2 shows that, compared to the deterministic case corresponding to $R_0 = 0$, the deflection increases as the level of load uncertainty increases. The corresponding results for a beam subject to a compressive axial load of $N_0 = 0.5N_{cr}$ are given in Fig. 3 which shows the effect of compressive axial load on the uncertain deflection. For a simply supported beam the coefficient $\mu = \pi$ in (2.2) for N_{cr}.

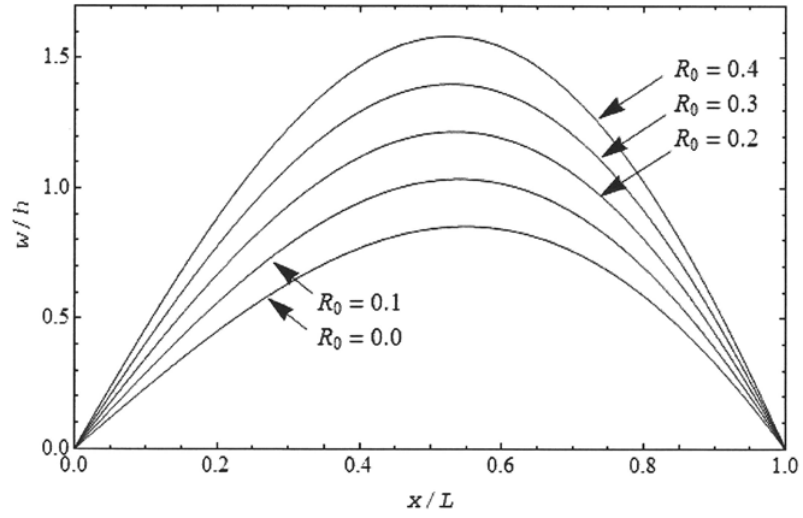

Fig. 3. Curves of deflection vs *x*-axis for various uncertainty levels with $\eta_0 = 2$ nm and $N_0 = 0.5N_{cr}$

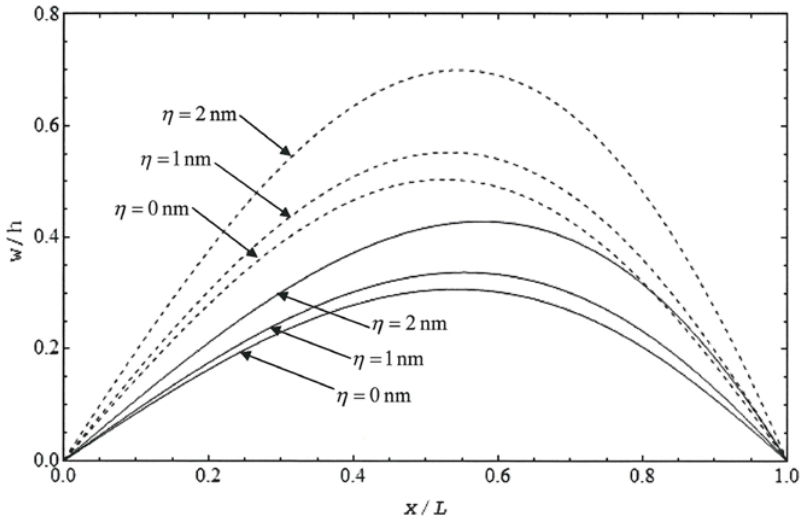

Fig. 4. The curves of deflection vs *x*-axis for the deterministic case (full lines) and for an uncertainty level of $R_0 = 0.3$ (dotted line) with $\eta_0 = 0,1,2$ nm and $N_0 = 0$

The effect of the small scale parameter η_0 on the deflection of the nanobeam subject to an uncertain load with $R_0 = 0.3$ is shown in Fig. 4. It is observed that both the small-scale parameter η_0 and the level of deflection are factors in increasing the mid-point deflection. Next the combined effect of the small-scale parameter and the axial load on the maximum deflection is studied in Fig. 5 which shows the contour plots of the maximum deflection with respect to $0 \le N_0 \le 0.6N_{cr}$ (*x*-axis) and $0 \le \eta_0 \le 2$ nm (*y*-axis) for uncertainty levels $0.0 \le R_0 \le 0.3$. The maximum deflection of the beam is computed by

$$\max_{0\le x\le L} w(x) = \max_{0\le x\le L}\left(\sum_{n=1}^{N} W_n \sin\alpha_n x\right) \tag{4.3}$$

using a minimization routine in Mathematica. Fig. 5 figure shows that an increase in the parameters η_0 or N_0 as well as in the level of load uncertainty leads to higher deflection.

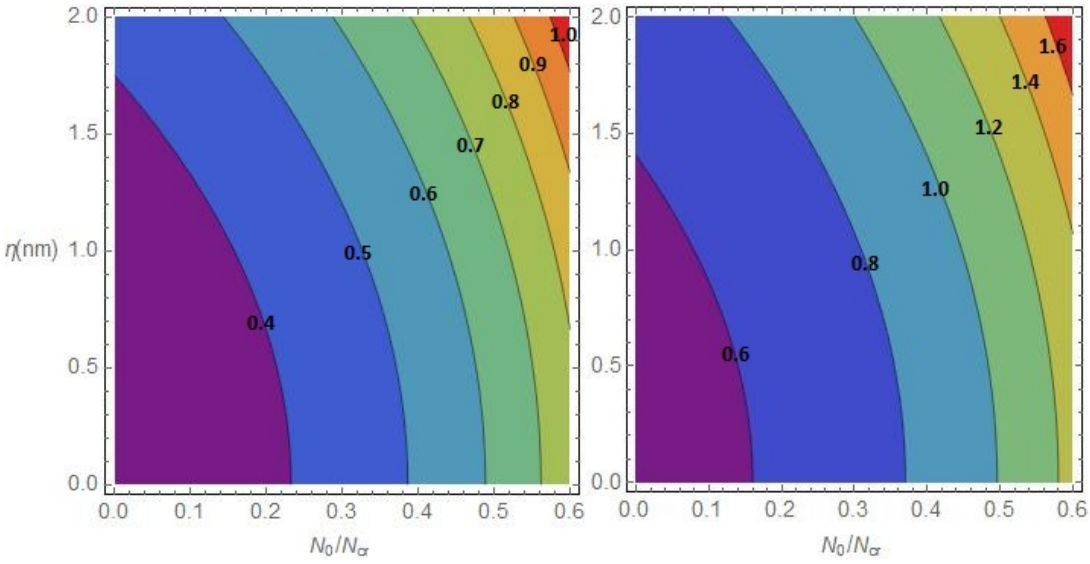

Fig. 5. Contour plots of maximum deflection with respect to N_0 (*x*-axis) and η (y-axis) for: (a) $R_0 = 0$, (b) $R_0 = 0.3$

4.2. Material uncertainty

Next numerical results are given for the problem studied in Section 3 for a square nanobeam of $b = h = 1\,\text{nm}$ and length $L = 10\,\text{nm}$ with $p_1 = 0.1\,\text{N/m}$ and $N_0 = 0$. The nominal (deterministic) value of the Young's modulus is taken as $E_0 = 1000\,\text{GPa}$. The results in the following figures are obtained by employing the exact expression (3.4) for the mid-point deflection of the nanobeam. In the figures the mid-point deflection is normalized by the height h by defining $w_0 = w\left(L/2; \tilde{\tilde{E}}, \tilde{\tilde{\eta}}\right)/h$.

Fig. 6 shows the curves of mid-point deflection w_0 plotted against the uncertainty level γ for various values of the uncertain small-scale parameter η_0. It is observed that the maximum deflection increases with increasing material uncertainty and the increase is given by a nonlinear curve. The effect of the small-scale parameter η_0 on the mid-point deflection is shown in Fig. 7. It is observed that the effect of uncertainty becomes more pronounced at higher values of the small-scale parameter.

Next the sensitivity of the deflection to material properties is studied in Fig. 8 which shows the contour plots of the mid-point deflection w_0 with respect to the level of uncertainty and the small-scale parameter. It is observed that the sensitivity of the deflection with respect to the Young's modulus is about 5 times more than the sensitivity to the small-scale parameter. Moreover the sensitivity with respect to the Young's modulus is not affected much with respect to the small-scale parameter, but the sensitivity with respect to the small-scale parameter increases with increasing η_0.

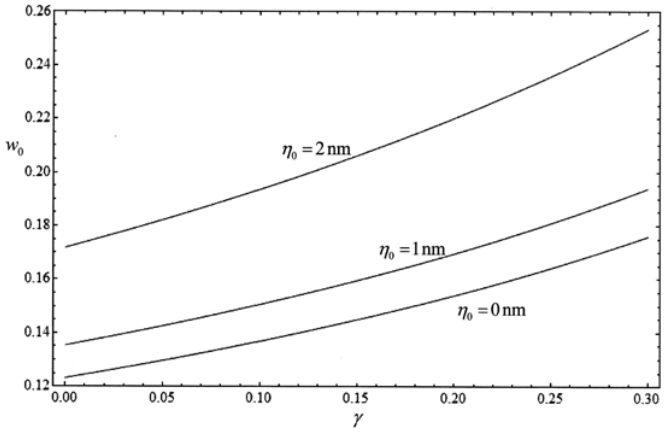

Fig. 6. Mid-point deflection vs the uncertainty parameter γ for various values of η_0

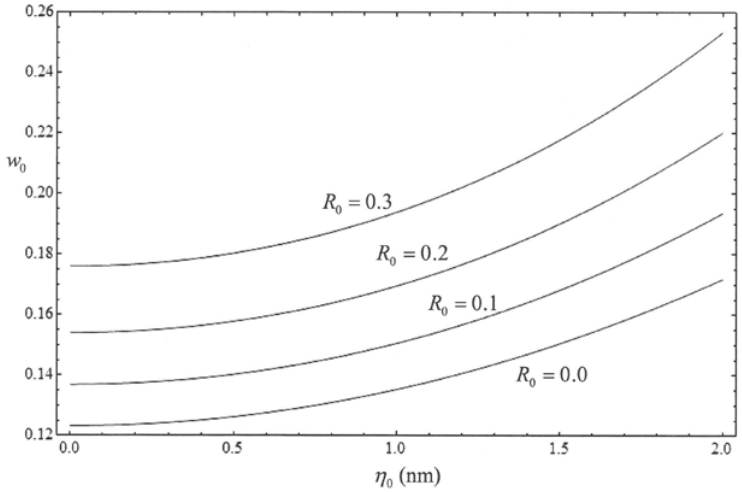

Fig. 7. Mid-point deflection vs the small-scale parameter for various levels of uncertainty

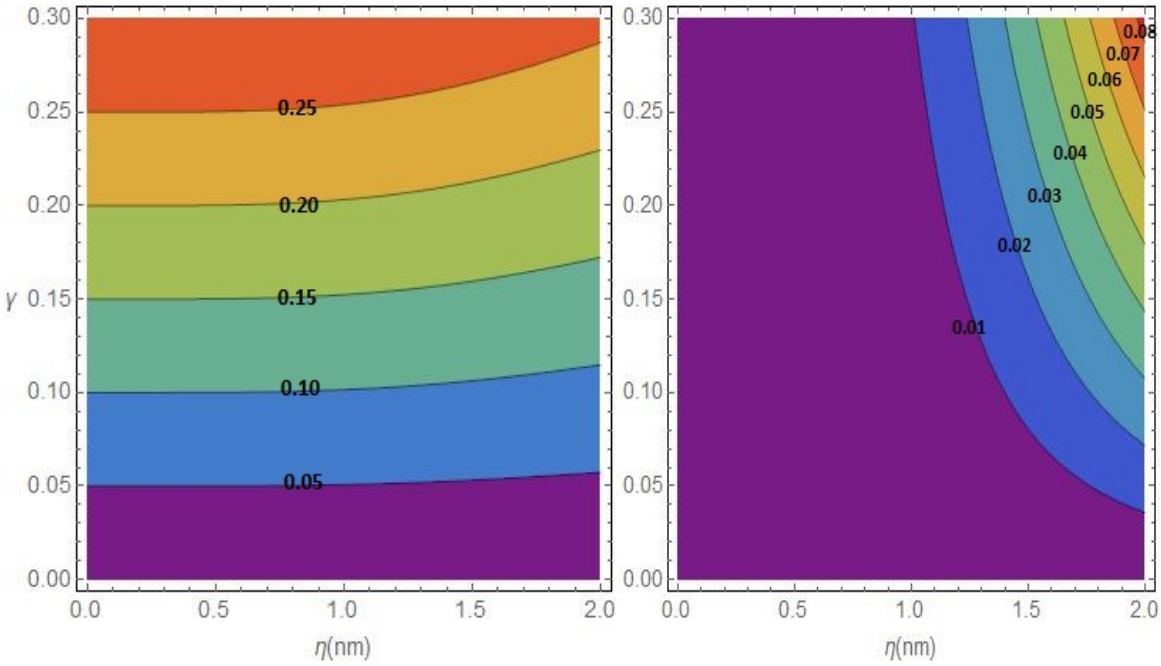

(a) (b)

Figure 8. Contour plots of sensitivities with respect to level of uncertainties and small-scale parameter: (a) S_E, (b) S_η

5. Conclusions

Non-probabilistic analysis of the uncertainties which can arise in the transverse loads and in the material properties of nanobeams was given using convex modelling. The variations in the uncertain quantities were taken as uncertain-but-bounded by imposing a constraint on the L_2 norm of the uncertainties. The nanobeam was modelled as a nonlocal Euler-Bernoulli beam and the effect of axial compression was taken into account. The uncertain load was approximated by a Fourier series expression and the coefficients of the series were determined to obtain the worst-case uncertain loading. Closed form solutions of the problems were given and the theory was illustrated for simply supported boundary conditions. It was observed that increasing uncertainty as manifested by increasing the L_2 norm of the uncertain load leads to higher deflections. The effect of uncertainties in the Young's modulus and the small-scale parameter was also studied and a sensitivity index was proposed to assess the sensitivity of the deflection to these parameters. Numerical results were given to observe the effect of various problem parameters on the deflection. The present study complements the studies in the literature on the static deflection of nanobeams which have taken the loads acting on the nanobeams and its properties as deterministic neglecting the uncertainties which can occur under operational conditions.

Acknowledgements
The research reported in this paper was supported by research grants from the University of KwaZulu-Natal (UKZN) and from National Research Foundation (NRF) of South Africa. The author gratefully acknowledges the supports provided by UKZN and NRF.

References

1. ADALI S., 2008, Variational principles for multi-walled carbon nanotubes undergoing buckling based on nonlocal elasticity theory, *Physics Letters A*, **372**, 5701-5705

2. ADALI S., 2011, Variational principles for vibrating carbon nanotubes modeled as cylindrical shells based on strain gradient nonlocal theory, *Journal of Computational and Theoretical Nanoscience*, **8**,1954-1962

3. ADALI S., RICHTER A., VERIJENKO V.E., 1995a, Minimum weight design of symmetric angle-ply laminates under multiple uncertain loads, *Structural Optimization*, **9**, 89-95

4. ADALI S., RICHTER A., VERIJENKO V.E., 1995b, Non-probabilistic modelling and design of sandwich plates subject to uncertain loads and initial deflections, *International Journal of Engineering Science*, **33**, 855-866

5. ANSARI R., SAHMANI S., 2011, Bending behavior and buckling of nanobeams including surface stress effects corresponding to different beam theories, *International Journal of Engineering Science*, **49**, 1244–1255

6. BEN-HAIM Y., ELISHAKOFF I., *Convex Models of Uncertainty in Applied Mechanics*. Elsevier Science Publishers, Amsterdam, The Netherlands, 1990.

7. CHALLAMEL N., WANG C.M., 2008, Small length scale effect in non-local cantilever beam: Paradox solved, *Nanotechnology*, **19**, 345703

8. DI PAOLA M., FAILLA G., SOFI A., ZINGALES M., 2011, A mechanically based approach to non-local beam theories, *International Journal of Mechanical Science*, **53**, 676–687

9. ELTAHER M.A., EMAM S.A., MAHMOUD F.F., 2013, Static and stability analysis of nonlocal functionally graded nanobeams, *Composite Structures*, **96**, 82-88

10. ERINGEN A.C., 2002, *Nonlocal Continuum Field Theories*. Springer, New York.

11. FANG C., KUMAR A., MUKHERJEE S., 2011, A finite element analysis of single-walled carbon nanotube deformation, *ASME Journal of Applied Mechanics*, **78**, 034502-1 - 034502-7

12. FEREIDOON A., RAJABPOUR M., HEMMATIAN H., 2014, Elastic moduli of carbon nanotubes with new geometry based on FEM, *Journal of Theoretical and Applied Mechanics*, **52**, to appear

13. HOSSEINI-ARA R., MIRDAMADI H.R., KHADEMYZADEH H., 2012, Buckling analysis of short carbon nanotubes based on a novel Timoshenko beam model, *Journal of Theoretical and Applied Mechanics*, **50**, 975-986

14. HU J., QIU Z., 2010, Non-probabilistic convex models and interval analysis method for dynamic response of a beam with bounded uncertainty, *Applied Mathematical Modelling*, **34**, 725–734

15. JIANG C., HAN X., LIU G.R., 2007, Optimization of structures with uncertain constraints based on convex model and satisfaction degree of interval, *Computer Methods in Applied Mechanics and Engineering*, **196**, 4791-4800

16. KALAMKAROV A.L., GEORGIADES A.V., ROKKAM S.K., VEEDU V.P., GHASEMI-NEJHAD M.N., 2006, Analytical and numerical techniques to predict carbon nanotubes properties, *International Journal of Solids and Structures*, **43**, 6832-6854

17. KANG Z., LUO Y., 2009, Non-probabilistic reliability-based topology optimization of geometrically nonlinear structures using convex models, *Computer Methods in Applied Mechanics and Engineering*, **198**, 3228-3238

18. KHAJEANSARI A., BARADARAN G.H., YVONNET J., 2012, An explicit solution for bending of nanowires lying on Winkler–Pasternak elastic substrate medium based on the Euler–Bernoulli beam theory, *International Journal of Engineering Science*, **52**,115-128

19. LI X.-F., WANG B.-L., TANG G.-J., LEE K.Y., 2012, Size effect in transverse mechanical behaviour of one-dimensional nanostructures, *Physica E, Low-dimensional Systems and Nanostructures*, **44**, 207–214

20. LU X., ZHONG H., 2012, Mechanical property evaluation of single-walled carbon nanotubes by finite element modeling, *Composites Part B: Engineering*, **43**, 1902-1913

21. MUC A., 2011, Modelling of carbon nanotubes behaviour with the use of a thin shell theory, *Journal of Theoretical and Applied Mechanics*, **49**, 531-540

22. PANTELIDIS C.P., GANZERLI S., 1998, Design of trusses under uncertain loads using convex models, *ASCE Journal of Structural Engineering*, **124**, 318-329

23. RADEBE I.S., ADALI S., 2014, Buckling and sensitivity analysis of nonlocal orthotropic nanoplates with uncertain material properties, *Composites Part B: Engineering*, **56**, 840-846

24. RADEBE I.S., ADALI S., 2013, Minimum weight design of beams against failure under uncertain loading by convex analysis, *Journal of Mechanical Science and Technology*, 27, 2071-2078.

25. REDDY J.N., 2007, Nonlocal theories for bending, buckling and vibration of beams, *International Journal of Engineering Science*, **45**, 288-307

26. REDDY J.N., PANG S.D., 2008, Nonlocal continuum theories of beams for the analysis of carbon nanotubes, *Journal of Applied Physics*, **103**, 023511

27. ROQUE C.M.C., FERREIRA A.J.M., REDDY J.N., 2011, Analysis of Timoshenko nanobeams with a nonlocal formulation and meshless method, *International Journal of Engineering Science*, **49**, 976–984

28. SCARPA F., ADHIKARI S., 2008, Uncertainty modeling of carbon nanotube terahertz oscillators, *Journal of Non-Crystalline Solids*, **354**, 4151–4156

29. THAI H.-T., VO T.P., 2012, A nonlocal sinusoidal shear deformation beam theory with application to bending, buckling, and vibration of nanobeams, *International Journal of Engineering Science*, **54**, 58–66

30. THAI, H.-T., 2012, A nonlocal beam theory for bending, buckling, and vibration of nanobeams, *International Journal of Engineering Science*, **52**, 56–64

31. WANG C.M., KITIPORNCHAI S., LIM C.W., EISENBERGER M., 2008, Beam bending solutions based on nonlocal Timoshenko beam theory, *ASCE Journal of Engineering Mechanics*, 134, 475–481

32. WANG Q., SHINDO Y., 2006, Nonlocal continuum models for carbon nanotubes subjected to static loading, *Journal of Mechanics of Materials and Structures*, **1**, 663-680

33. WANG X., WANG L., ELISHAKOFF I., QIU Z., 2011, Probability and convexity concepts are not antagonistic, *Acta Mechanica*, **219**, 45–64

34. ZHANG Y.Y., WANG C.M., CHALLAMEL N., 2010, Bending, buckling, and vibration of micro/nanobeams by hybrid nonlocal beam model, *ASCE Journal of Engineering Mechanics*, **136**, 562–574

LIST OF FIGURE CAPTIONS

Figure 1. Beam geometry and uncertain loading

Figure 2. The curves of deflection vs *x*-axis for various uncertainty levels with $\eta_0 = 2$ nm and $N_0 = 0$

Figure 3. Curves of deflection vs *x*-axis for various uncertainty levels with $\eta_0 = 2$ nm and $N_0 = 0.5N_{cr}$

Figure 4. The curves of deflection vs *x*-axis for the deterministic case (full lines) and for an uncertainty level of $R_0 = 0.3$ (dotted line) with $\eta_0 = 0,1,2$ nm and $N_0 = 0$

Figure 5. Contour plots of maximum deflection with respect to N_0 (*x*-axis) and η (y-axis) for: (a) $R_0 = 0$, (b) $R_0 = 0.3$

Figure 6. Mid-point deflection vs the uncertainty parameter γ for various values of η_0

Figure 7. Mid-point deflection vs the small-scale parameter for various levels of uncertainty

Figure 8. Contour plots of sensitivities with respect to level of uncertainties and small-scale parameter: (a) S_E, (b) S_η

Paper 2

The paper has been published in the journal **Composite: Part B 56 (2014) 840-846**.

Composites: Part B 56 (2014) 840–846

Contents lists available at ScienceDirect

Composites: Part B

journal homepage: www.elsevier.com/locate/compositesb

Buckling and sensitivity analysis of nonlocal orthotropic nanoplates with uncertain material properties

Isaac Sfiso Radebe [a,1], Sarp Adali [b,*]

[a] Department of Mechanical Engineering, Durban University of Technology, Durban, South Africa
[b] School of Mechanical Engineering, University of KwaZulu-Natal, Durban, South Africa

ARTICLE INFO

Article history:
Received 20 March 2013
Accepted 12 August 2013
Available online 22 August 2013

Keywords:
A. Nano-structures
A. Plates
B. Buckling
C. Analytical modeling
Material uncertainty

ABSTRACT

Accurate estimates of the orthotropic properties of nano-materials are usually not available due to the difficulties in making measurements at nano-scale. However the values of the elastic constants may be known with some level uncertainty. In the present study an ellipsoidal convex model is employed to study the biaxial buckling of a rectangular orthotropic nanoplate with the material properties displaying uncertain-but-bounded variations around their nominal values. Such uncertainties are not uncommon in nano-sized structures and the convex analysis enables to determine the lowest buckling loads for a given level of material uncertainty. The nanoplate considered in the present study is modeled as a nonlocal plate to take the small-size effects into account with the small-scale parameter also taken to be uncertain. Method of Lagrange multipliers is applied to obtain the worst-case variations of the orthotropic constants with respect to the critical buckling load. The sensitivity of the buckling load to the uncertainties in the elastic constants is also investigated. Numerical results are given to study the effect of material uncertainty on the buckling load.

1. Introduction

In the deterministic analysis, variations in the material properties are neglected and the average values of the elastic constants are used to obtain a mean value for the structural response. This approach does not take the deviations from the average into account even though it is usually difficult to determine the properties of a material with any certainty. This is more so for nano-sized structures which exhibit large variations in their material properties due to defects and imperfections in their molecular structures. Moreover experimental difficulties in making accurate measurements at the nano-scale lead to significant scatter in the values of elastic constants. For example the values of Young's modulus of carbon nanotubes have been reported between 1 and 5 TPa in the literature [1–3].

Nanoplates, made of mono or multilayer graphene, are often employed in nanotechnology applications as sensors [4] and actuators [5] as well as in many other capacities and their usage is expected to increase [6]. Quite often they are subject to in-plane loads making them susceptible to buckling due to their extremely small thickness measured in nanometers. This situation has led to several studies on the subject and the buckling of single layer graphene has been studied in [7] without taking small-scale effects into account and in [8,9] employing the nonlocal theory. Buckling of isotropic nanoplates has been studied in [10,11] and orthotropic plates in [12–17] employing nonlocal constitutive relations and taking various effects such as nonuniform thickness [10], temperature [13], shear deformation [14] and nonuniform in-plane loads [15] into account. Variational principles for vibrating multi-layered orthotropic graphenes sheets were given in [16,17]. Studies on the vibrations of orthotropic nanoplates include [18–21]. The nonlocal theory developed in the 1970s [22,23] includes the small-scale effects by expressing stress as a function of strain at all points of the continuum.

Buckling and vibration results given in [10–21] for graphene and nanoplates are based on the deterministic values of the elastic constants and as such neglect the variations in the material properties even though such variations are common. Nominal buckling load, corresponding to a deterministic model, could be higher than the applied compressive loads, indicating a safe design. However, a safe design based on deterministic material values is not robust due to inherent uncertainties in elastic constants [24]. This situation necessitates taking the data uncertainties into account in a non-deterministic model which will improve the reliability of the results by providing conservative load-carrying estimates.

Such a model could be probabilistic or statistical requiring information on the probability distributions of random variables.

* Corresponding author. Tel.: +27 312603203; fax: +27 312603217.
E-mail address: adali@ukzn.ac.za (S. Adali).
[1] Post-graduate student, Mechanical Engineering, University of KwaZulu-Natal, Durban, South Africa.

1359-8368/$ - see front matter © 2013 Elsevier Ltd. All rights reserved.
http://dx.doi.org/10.1016/j.compositesb.2013.08.054

Obtaining this information in many cases is a difficult task. However, data on upper and lower bounds of uncertain parameters may be known or can be estimated with reasonable accuracy in which case an approach based on convex modeling would yield the reliable results. In this case the total level of uncertainties is bounded by an n-dimensional ellipsoid where the number of dimensions is equal to the number of uncertain parameters [25]. Examples of convex modeling applied to engineering problems with uncertain data include [24–32]. A comparison of convex modeling with probabilistic methods is given in [33] and the book by Ben-Haim and Elishakoff [34] details the techniques of convex modeling.

The present study involves the computation of the buckling load of an orthotropic nanoplate in the presence of material uncertainties using convex modeling with the L_2 norm of the uncertainties bounded. The constitutive relations are based on the nonlocal theory of plates which takes nano-scale effects into account. The sensitivity of the critical load to uncertainty is also investigated by defining relative sensitivities in terms of uncertainty parameters [35,36]. Further information on sensitivity indices can be found in [37–39]. Numerical results are given to investigate the effect of uncertainty on the buckling loads and the dependence of the relative sensitivities on the aspect ratio is studied by means of contour plots.

2. Convex modeling

In this section, the method of solution to compute the uncertainty parameters corresponding to the least-favorable buckling load is summarized. Let $\widetilde{U}_i = U_{0i}(1+\gamma_i)$ denote the ith uncertain material property ($i = 1,2,\ldots,n$) where U_{0i} is the nominal value of $\widetilde{U}_i$ and γ_i is an unknown parameter to be computed to minimize (the least favorable solution) or to maximize (the most favorable solution) the critical buckling load. The convex model of uncertainties can be described by an n-dimensional uncertainty vector $\Phi = (\gamma_1,\gamma_2,\gamma_3,\ldots,\gamma_n)^T$ defined on a convex set S such that $\Phi \in S$. In the present study uncertainty parameters γ_i belong to a bounded quadratic convex set defined as

$$S(\Phi,\beta) = \{\Phi | \Phi \in R^n, \Phi^T\Phi \leqslant \beta^2\} \tag{1}$$

where β is the prescribed measure of uncertainty satisfying the inequality $\beta < 1$. Thus

$$S(\Phi,\beta) = \left\{\Phi | \Phi \in R^n, \sum_i^n \gamma_i^2 \leqslant \beta^2\right\} \tag{2}$$

Here β is the radius of the n-dimensional ellipsoid. The problem investigated involves the computation of the unknown parameters γ_i such that the buckling load becomes the lowest or highest possible subject to the constraint $\sum_i^n \gamma_i^2 \leqslant \beta^2$. The buckling load can be expressed as a function of the uncertain quantities $\widetilde{U}_i$, *viz.*

$$N_{cr} = f(\widetilde{U}_i) \tag{3}$$

Since the variations of the uncertain parameters around their nominal values are small, the function $f(\widetilde{U}_i)$ can be expanded around U_{0i} by substituting $\widetilde{U}_i \cong U_{0i}(1+\gamma_i)$ into Eq. (3) and keeping only the terms which are of zero and first order in γ_i and neglecting the higher order terms. This computation can be carried out using the Taylor series expansion of the expression

$$(1 \pm \varepsilon)^c \cong (1 \mp c\varepsilon) + O(\varepsilon^2) \tag{4}$$

where the superscript c can take positive or negative values and $|\varepsilon| \ll 1$. The expansion of the buckling load around U_{0i} using Eq. (4) leads to

$$N_{cr} \cong f_0(U_{01},U_{02},\ldots,U_{0n}) + \sum_{i=1}^n f_i(U_{01},U_{02},\ldots,U_{0n})\gamma_i \tag{5}$$

where $f_0(U_{01},U_{02},\ldots,U_{0n})$ is the deterministic (nominal) value of the buckling load. The solutions are obtained by solving the following optimization problems

$$\min_{\gamma_i} \sum_{i=1}^n f_i(U_{01},U_{02},\ldots,U_{0n})\gamma_i \text{ and } \max_{\gamma_i} \sum_{i=1}^n f_i(U_{01},U_{02},\ldots,U_{0n})\gamma_i \tag{6}$$

subject to the constraint $\sum_i^n \gamma_i^2 \leqslant \beta^2$. It is noted that every affine functional whose domain is a compact convex set takes on its maximum value on the set of extreme points of its domain which is the boundary of the ellipsoid in the present case [31,32]. Thus the inequality (2) can be replaced by the equality

$$\sum_{i=1}^n \gamma_i^2 = \beta^2 \tag{7}$$

and the problem can be solved by introducing the Lagrangian

$$L(\widetilde{U}_i,\gamma_i) = \sum_{i=1}^n f_i(U_{01},U_{02},\ldots,U_{0n})\gamma_i + \lambda\left(\sum_{i=1}^n \gamma_i^2 - \beta^2\right) \tag{8}$$

where λ is the Lagrange multiplier. By taking the derivatives of $L(\widetilde{U}_i,\gamma_i)$ with respect to γ_i, we obtain

$$\frac{\partial L(\widetilde{U}_i,\gamma_i)}{\partial \gamma_i} = f_i(U_{01},U_{02},\ldots,U_{0n}) + 2\lambda\gamma_i = 0 \tag{9}$$

Thus

$$\gamma_i = -\frac{1}{2\lambda} f_i(U_{01},U_{02},\ldots,U_{0n}), \quad i = 1,2,\ldots n \tag{10}$$

The Lagrange multiplier is computed by substituting Eq. (10) into Eq. (7). This computation gives

$$\lambda = \pm\frac{1}{2\beta}\sqrt{\sum_{i=1}^n (f_i(U_{01},U_{02},\ldots,U_{0n}))^2} \tag{11}$$

In Eq. (11) the plus and minus values of λ correspond to the minimum and maximum values of the buckling load. The uncertain parameters γ_i are computed from Eqs. (10) and (11).

3. Orthotropic nanoplate with material uncertainty

The basic formulation is given next for an orthotropic rectangular plate subject to material uncertainty and biaxial buckling loads. Let $\widetilde{E}_1$ and $\widetilde{E}_2$ denote Young's moduli in the material coordinates, $\widetilde{G}_{12}$ in-plane shear modulus, and $\tilde{\nu}_{12}$ and $\tilde{\nu}_{21}$ in-plane Poisson's ratios where a tilde indicates an uncertain quantity. The plate has the length a, width b and thickness h in the x, y and z directions, respectively, with the aspect ratio denoted as $r = a/b$. The axial loads in the x and y directions are denoted as N_x and N_y, and the deflection function as $w(x,y;\widetilde{\Psi})$ where $\widetilde{\Psi}$ is the set of uncertain material constants defined as

$$\widetilde{\Psi} = \{\widetilde{\Psi} | \widetilde{E}_1, \widetilde{E}_2, \widetilde{G}_{12}, \tilde{\nu}_{12}, \tilde{\eta}\} \tag{12}$$

noting $\tilde{\nu}_{21} = \tilde{\nu}_{12}\widetilde{E}_2/\widetilde{E}_1$. The differential equation governing the biaxial buckling of an orthotropic nanoplate based on nonlocal constitutive relations can be expressed as [12]

$$\widetilde{D}_{11}\frac{\partial^4 w}{\partial x^4} + 2(\widetilde{D}_{12} + 2\widetilde{D}_{66})\frac{\partial^4 w}{\partial x^2 \partial y^2} + \widetilde{D}_{22}\frac{\partial^4 w}{\partial y^4} + (1 - \tilde{\eta}^2\nabla^2)\left(N_x\frac{\partial^2 w}{\partial x^2} + N_y\frac{\partial^2 w}{\partial y^2}\right) = 0 \tag{13}$$

where

$$\widetilde{D}_{11} = \frac{d\widetilde{E}_1}{1 - \tilde{\nu}_{12}\tilde{\nu}_{21}}, \quad \widetilde{D}_{12} = \frac{d\tilde{\nu}_{12}\widetilde{E}_2}{1 - \tilde{\nu}_{12}\tilde{\nu}_{21}}, \quad \widetilde{D}_{22} = \frac{d\widetilde{E}_2}{1 - \tilde{\nu}_{12}\tilde{\nu}_{21}},$$
$$\widetilde{D}_{66} = d\widetilde{G}_{12}, \quad d = \frac{h^3}{12} \tag{14}$$

and $\tilde{\eta} = e_0 a$ is the uncertain small-scale parameter [XX]. The differential Eq. (13) is subject to the simply supported boundary conditions given by

$$w = 0, \quad \widetilde{D}_{11}\frac{\partial^2 w}{\partial x^2} + \widetilde{D}_{12}\frac{\partial^2 w}{\partial y^2} = 0 \quad \text{for } x = 0, a \tag{15}$$

$$w = 0, \quad \widetilde{D}_{12}\frac{\partial^2 w}{\partial x^2} + \widetilde{D}_{22}\frac{\partial^2 w}{\partial y^2} = 0 \quad \text{for } y = 0, b \tag{16}$$

The uncertain material constants are defined as

$$\widetilde{E}_1 = E_1^0(1+\gamma_1),\ \widetilde{E}_2 = E_2^0(1+\gamma_2),\ \widetilde{G}_{12} = G_{12}^0(1+\gamma_3),$$
$$\tilde{\nu}_{12} = \nu_{12}^0(1+\gamma_4),\ \tilde{\eta} = \eta_0(1+\gamma_5) \tag{17}$$

where the superscript "0" denotes the nominal quantities for $\widetilde{E}_1, \widetilde{E}_2, \widetilde{G}_{12}, \tilde{\nu}_{12}$ and η_0 is the nominal value for the small-scale parameter $\tilde{\eta}$. The variations γ_i, satisfying the inequalities $|\gamma_i| \ll 1$, are unknown constants to be determined by convex analysis to yield the least favorable buckling load. The bending stiffnesses $\widetilde{D}_{ij}$ can be expressed in terms of γ_i using the first-order approximation

$$(1 \pm \varepsilon)^c \cong (1 \pm c\varepsilon) + O(\varepsilon^2) \tag{18}$$

where the superscript c can take positive or negative values and $|\varepsilon| \ll 1$. For this purpose we first linearize $\tilde{\nu}_{21} = \tilde{\nu}_{12}\widetilde{E}_2/\widetilde{E}_1$ in terms of γ_i by noting that

$$\tilde{\nu}_{21} = \frac{\nu_{12}^0 E_2^0}{E_1^0}\frac{(1+\gamma_4)(1+\gamma_2)}{1+\gamma_1} \cong \frac{\nu_{12}^0 E_2^0}{E_1^0}(1-\gamma_1+\gamma_2+\gamma_4) \tag{19}$$

Similarly,

$$1 - \tilde{\nu}_{12}\tilde{\nu}_{21} \cong (1-a_1)(1+a_2\gamma_1 - a_2\gamma_2 - 2a_2\gamma_4) \tag{20}$$

where

$$a_1 = \nu_{12}^0\nu_{21}^0, \quad a_2 = \frac{a_1}{1-a_1} \tag{21}$$

Substituting Eqs. (17) and (20) into Eq. (14), using Eq. (18) and keeping only the terms linear in γ_i, we obtain

$$\widetilde{D}_{11} \cong D_{11}^0(1+(1-a_2)\gamma_1 + a_2\gamma_2 + 2a_2\gamma_4) \tag{22}$$
$$\widetilde{D}_{12} \cong D_{12}^0(1-a_2\gamma_1 + (1+a_2)\gamma_2 + (1+2a_2)\gamma_4) \tag{23}$$
$$\widetilde{D}_{22} \cong D_{22}^0(1-a_2\gamma_1 + (1+a_2)\gamma_2 + 2a_2\gamma_4) \tag{24}$$
$$\widetilde{D}_{66} \cong D_{66}^0(1+\gamma_3) \tag{25}$$

where

$$D_{11}^0 = \frac{dE_1^0}{1-\nu_{12}^0\nu_{21}^0}, \quad D_{12}^0 = \frac{d\nu_{12}^0 E_2^0}{1-\nu_{12}^0\nu_{21}^0}, \quad D_{22}^0 = \frac{dE_2^0}{1-\nu_{12}^0\nu_{21}^0},$$
$$D_{66}^0 = dG_{12}^0 \tag{26}$$

4. Least favorable solution

In this section the least favorable buckling load is computed by convex analysis. The variations γ_i are subject to the constraint

$$\sum_i^5 \gamma_i^2 \leqslant \beta^2 \tag{27}$$

where $\beta < 1$ determines the level of uncertainty and $\beta = 0$ corresponds to the deterministic case. Thus the set of uncertain-but-bounded variations can be defined as

$$S(\Phi,\beta) = \left\{ \Phi | \Phi \in R^n, \sum_i^5 \gamma_i^2 \leqslant \beta^2 \right\} \tag{28}$$

where $\Phi = (\gamma_1, \gamma_2, \gamma_3, \ldots, \gamma_5)^T$. Thus $\Phi \in S$ and β is the radius of the 5-dimensional ellipsoid.

Let $N_x = N_{cr}$ and $N_y = \mu N_{cr}$, $\mu = N_y/N_x$, where N_{cr} is the non-deterministic buckling load corresponding to the solution of the eigenvalue problem (2) subject to the boundary conditions (15) and (16) and is given by [12]

$$N_{\rm cr}(\beta) = \min_{m,n} \frac{\pi^2(m^4\widetilde{D}_{11} + 2m^2n^2(\widetilde{D}_{12}+2\widetilde{D}_{66})r^2 + n^4\widetilde{D}_{22}r^4)}{\tilde{\eta}^2(m^4 + m^2n^2(\mu+1)r^2 + n^4\mu r^4) + m^2 + n^2\mu r^2} \tag{29}$$

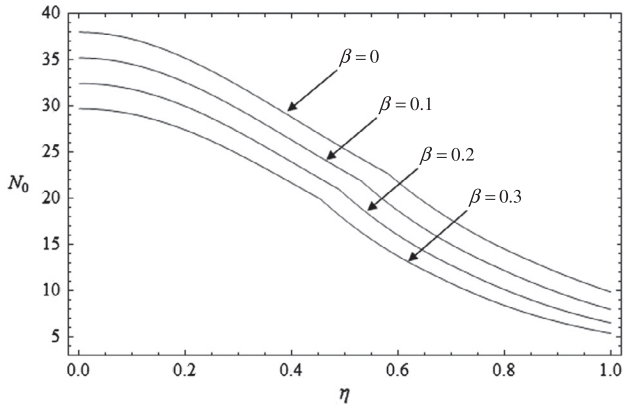

Fig. 1. Buckling load vs small-scale parameter for various uncertainty levels with $\mu = 0$ and $a/b = 1$.

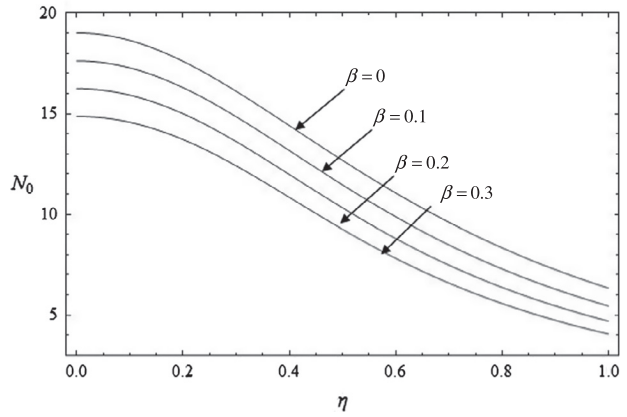

Fig. 2. Buckling load vs small-scale parameter for various uncertainty levels with $\mu = 1$ and $a/b = 1$.

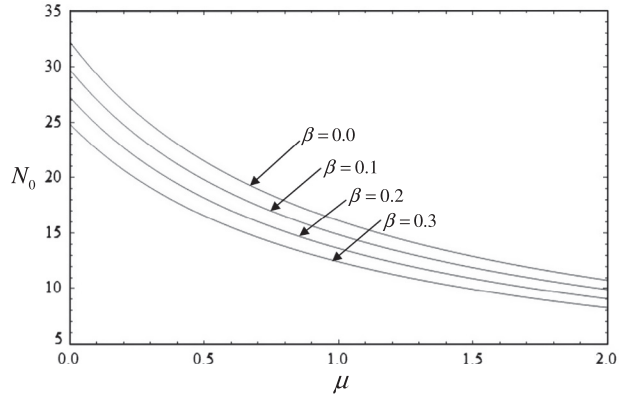

Fig. 3. Buckling load vs the buckling load ratio μ for various uncertainty levels with $\eta/a = 0.3$ and $a/b = 1$.

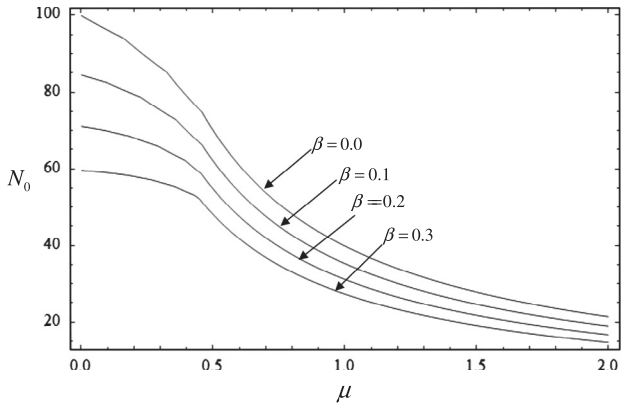

Fig. 4. Buckling load vs the buckling load ratio μ for various uncertainty levels with $\eta/a = 0.3$ and $a/b = 2.5$.

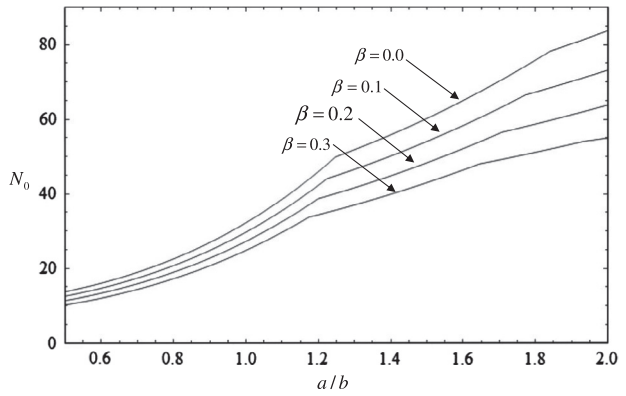

Fig. 5. Buckling load vs the aspect ratio a/b for various uncertainty levels with $\eta/a = 0.3$ and $\mu = 0$.

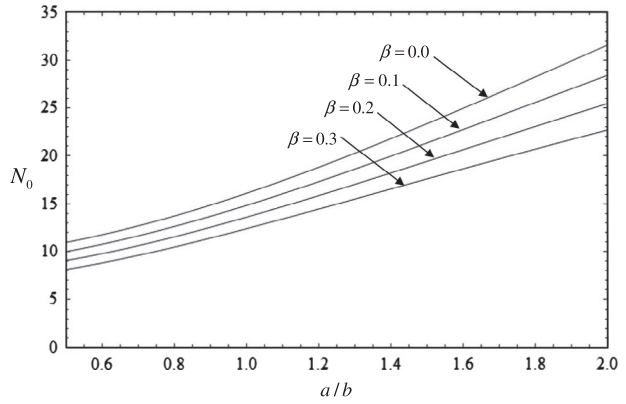

Fig. 6. Buckling load vs the aspect ratio a/b for various uncertainty levels with $\eta/a = 0.3$ and $\mu = 1$.

where m and n are the mode numbers and $N_{cr}(0)$ corresponds to the deterministic buckling load. The buckling load depends on the level of material uncertainty as measured by β and its least favorable value corresponding to the worst-case material uncertainty can be determined by convex analysis. Substituting Eqs. (11)–(14) and $\tilde{\eta} = \eta_0(1+\gamma_5)$ into Eq. (29), using Eq. (18) and keeping only the terms linear in γ_i, we obtain

$$N_{cr} \equiv \frac{\pi^2}{p_{mn}}(b_{0mn} + b_{1mn}\gamma_1 + b_{2mn}\gamma_2 + b_{3mn}\gamma_3 + b_{4mn}\gamma_4 + b_{5mn}\gamma_5) \tag{30}$$

where the terms b_{imn}, $i = 1,2,\ldots,5$ and p_{mn} are given in Appendix A. The expression (30) has to be minimized subject to the constraint (27) to compute the constants γ_i. For this purpose, the following Lagrangian is formulated

$$L(b_{imn},\gamma_i) = \frac{\pi^2}{p_{mn}}\left(b_{0mn} + \sum_{i=1}^{5} b_{imn}\gamma_i\right) + \lambda\left(\sum_{i=1}^{5}\gamma_i^2 - \beta^2\right) \tag{31}$$

The minima and the maxima of the Lagrangian are determined from

$$\frac{\partial L(b_{imn},\gamma_i)}{\partial \gamma_i} = 0 \tag{32}$$

The parameters γ_i and the Lagrange multiplier λ are computed from Eq. (32) as

$$\gamma_i = -\frac{\pi^2}{p_{mn}}\frac{b_{imn}}{2\lambda}, \quad \lambda = \pm\frac{\pi^2}{2\beta_{mn}}\frac{1}{\beta}\left(\sum_{i=1}^{5} b_{imn}^2\right)^{1/2} \tag{33}$$

Thus

$$\gamma_i = \mp\beta\, b_{imn}\left(\sum_{i=1}^{5} b_{imn}^2\right)^{-1/2} \quad \text{for } i = 1,2,\ldots,5 \tag{34}$$

where the plus and minus signs correspond to the lowest and highest buckling loads.

5. Sensitivity analysis

The sensitivity of the buckling load to uncertainty can be investigated by defining relative sensitivity indices $S_K(\gamma_i)$ given by

$$S_K(\gamma_i) = \left|\frac{\partial N_{cr}(\beta)}{\partial \gamma_i}\right| \frac{|\gamma_i|}{N_{cr}(0)} \tag{35}$$

which is normalized with respect to the deterministic buckling load $N_{cr}(0)$. In Eq. (35), the sensitivities of the buckling load with respect to the uncertainty in the ith constant indicated by γ_i, $i = 1,2,\ldots,5$ are denoted by $S_{E_1}(\gamma_1)$, $S_{E_2}(\gamma_2)$, $S_{G_{12}}(\gamma_3)$, $S_{\nu_{12}}(\gamma_4)$ and $S_\eta(\gamma_5)$, respectively, so that the subscript K indicates the respective material property. Eq. (35) indicates that the buckling load will have zero sensitivity for $\gamma_i = 0$ corresponding to the deterministic case as expected. The sensitivities $S_K(\gamma_i)$ can be computed from Eqs. (30) and (35) as

Table 1
Sensitivities $S_K(\gamma_i)$ with respect to a/b for the sensitivity level $\beta = 0.1$ with $\eta/a = 0.3$.

a/b	$\mu = 0$					$\mu = 1$				
	m, n	$S_{E_1}(\gamma_1)$	$S_{E_2}(\gamma_2)$	$S_{\nu_{12}}(\gamma_4)$	$S_\eta(\gamma_5)$	m,n	$S_{E_1}(\gamma_1)$	$S_{E_2}(\gamma_2)$	$S_{\nu_{12}}(\gamma_4)$	$S_\eta(\gamma_5)$
0.5	1, 1	0.075	0.004	0.003	0.005	1, 1	0.075	0.004	0.003	0.005
1.0	1, 1	0.041	0.023	0.004	0.012	1, 1	0.041	0.023	0.004	0.012
1.5	2, 1	0.046	0.009	0.003	0.049	1, 1	0.015	0.047	0.003	0.023
2.0	3, 1	0.040	0.005	0.002	0.087	1, 1	0.005	0.059	0.003	0.037
2.5	5, 1	0.038	0.002	0.002	0.128	1, 1	0.001	0.063	0.003	0.052

Table 2
Sensitivities $S_K(\gamma_i)$ with respect to a/b for the sensitivity level $\beta = 0.3$ with $\eta/a = 0.3$.

a/b	$\mu = 0$					$\mu = 1$				
	m, n	$S_{E_1}(\gamma_1)$	$S_{E_2}(\gamma_2)$	$S_{\nu_{12}}(\gamma_4)$	$S_\eta(\gamma_5)$	m,n	$S_{E_1}(\gamma_1)$	$S_{E_2}(\gamma_2)$	$S_{\nu_{12}}(\gamma_4)$	$S_\eta(\gamma_5)$
0.5	1, 1	0.225	0.013	0.010	0.014	1, 1	0.225	0.013	0.010	0.014
1.0	1, 1	0.123	0.070	0.011	0.035	1, 1	0.123	0.070	0.011	0.035
1.5	2, 1	0.137	0.026	0.008	0.147	1, 1	0.044	0.140	0.010	0.070
2.0	4, 1	0.127	0.007	0.006	0.322	1, 1	0.014	0.176	0.008	0.112
2.5	10, 1	0.116	0.002	0.005	0.485	1, 1	0.004	0.190	0.007	0.157

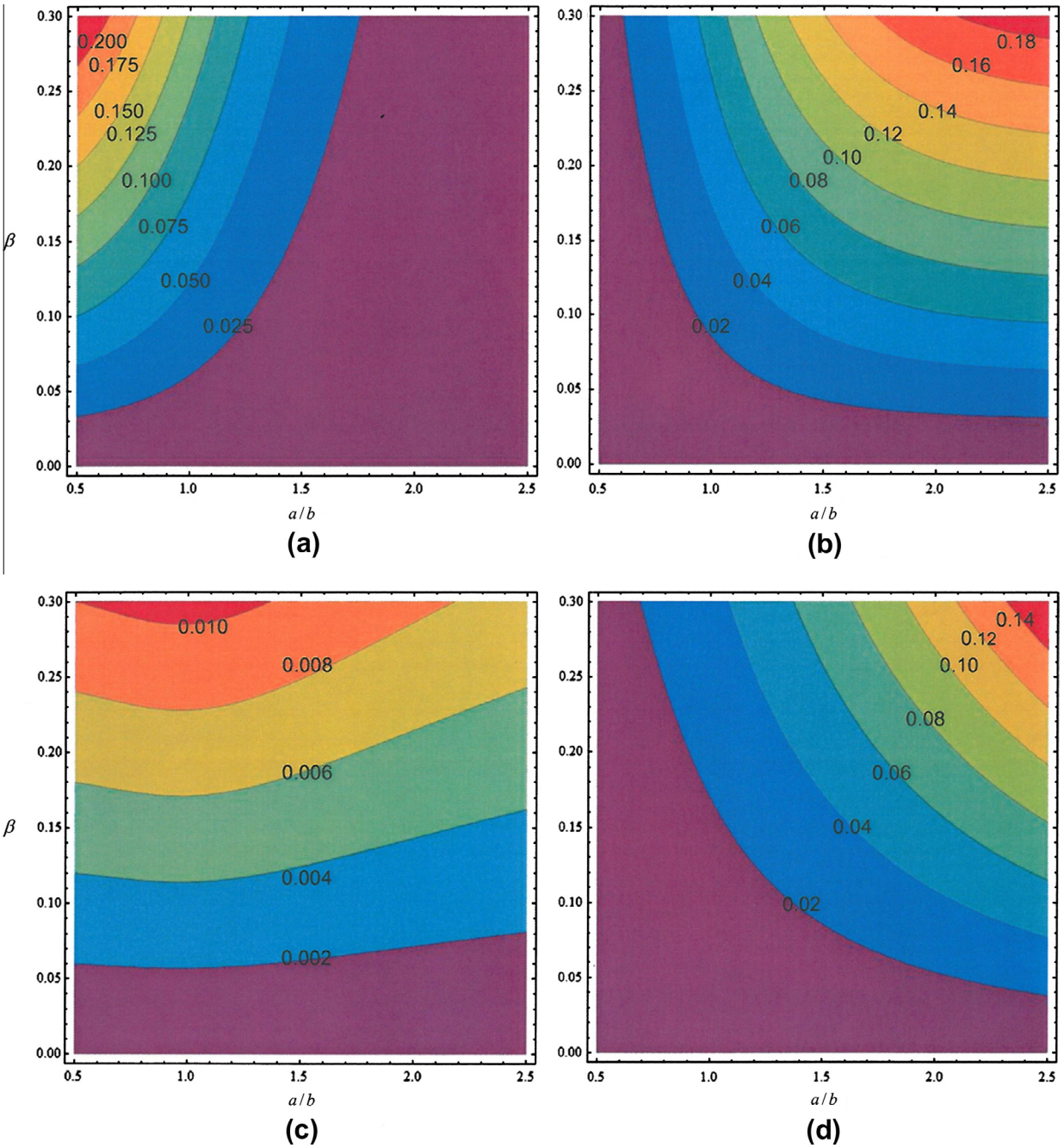

Fig. 7. Contour plots of sensitivities with respect to level of uncertainties and aspect ratio for $\eta/a = 0.3$ and $\mu = 1$, (a) S_{E_1}, (b) S_{E_2}, (c) $S_{\nu_{12}}$, and (d) S_η.

$$S_K(\gamma_i) = \frac{|b_{imn}\gamma_i|}{b_{0mn}} \tag{36}$$

noting that $N_{cr}(0) \equiv \frac{\pi^2}{p_{mn}} b_{0mn}$. In Eq. (36), the mode numbers m and n correspond to the modes (m,n) minimizing the buckling load $N_{cr}(\beta)$.

6. Numerical results

The nanoplates based on graphene sheets exhibit different Young's moduli in different directions due to zigzag and armchair configurations of the atomic structure. In a zig-zag configuration,

one third of the bonds are aligned with the loading direction, while every bond stays at an angle with the loading direction in the armchair configuration. There have been estimates of the product $E \times h$ for zig-zag and armchair nanotubes by Hernandez et al. [40] and Wang [41] with Young's modulus for the armchair direction yielding a higher value. As the nanotube diameter increases, Young's modulus of the nanotube approaches that of graphene since a carbon nanotube can be viewed as a sheet of graphene that has been rolled into a tube (Li and Chou [42]). For the graphene sheet the values of Young's modulus were obtained as $E_1 = 1765$ GPa and $E_2 = 1588$ GPa for the two orientations corresponding to the zig-zag and armchair configurations with the other elastic constants specified as $\nu_{12} = 0.3$ and $G_{12} = 0.5E_1/(1 + \nu_{12})$ in several publications [12–15]. In the present study these values are adopted in the numerical calculations with the thickness of the nanoplate taken as $h = 0.34$ nm. The dependence of the shear modulus G_{12} on E_1 reduces the number of independent elastic constants from four to three, that is, the independent orthotropic constants are now E_1, E_2 and ν_{12}. As the solution given in Section 3 is for the general case of four independent constants, new expressions for b_{imn} have to be given reflecting the fact that for this case $G_{12} = 0.5E_1/(1 + \nu_{12})$. The results for this calculation are given in Appendix A. In the numerical results, the non-dimensional buckling load N_0 normalized by the expression

$$N_0 = \frac{N_{cr}a^2}{D_{11}^0} \tag{37}$$

is used.

6.1. Buckling load

The effect of the small-scale parameter on the buckling load is shown for square plates in Figs. 1 and 2 for the buckling ratios of $\mu = 0$ and $\mu = 1$, respectively, for various uncertainty levels. The lines for $\beta = 0$ in these figures correspond to the deterministic cases given in [12]. It is observed that the buckling load corresponding to the least-favorable combination of the material properties decreases as the uncertainty increases. Next the variation of the buckling load with respect to the buckling load ratio μ is shown for various uncertainty levels in Fig. 3 for $a/b = 1$ and in Fig. 4 for $a/b = 2.5$. Mode changes as μ increases can be observed from Fig. 4. Figs. 5 and 6 show the curves of non-dimensional buckling load N_0 vs the aspect ratio a/b for various uncertainty levels for $\mu = 0$ (Fig. 5) and $\mu = 1$ (Fig. 6).

6.2. Sensitivity

The sensitivity of the buckling load to the level of uncertainties are investigated in Table 1 for $\beta = 0.1$ and in Table 2 for $\beta = 0.3$ which show the sensitivity values $S_K(\gamma_i)$ for various aspect ratios a/b. It is observed from Table 1 ($\beta = 0.1$) that for $\mu = 1$, $S_{E_1}(\gamma_1)$ monotonically decreases, and $S_{E_2}(\gamma_2)$ and $S_\eta(\gamma_5)$ monotonically increase with increasing aspect ratio. For low aspect ratios $S_{E_1}(\gamma_1)$ is higher than $S_{E_2}(\gamma_2)$, and $S_{E_2}(\gamma_2)$ exceeds $S_{E_1}(\gamma_1)$ as the aspect ratio increases. Thus the magnitude of the relative sensitivity for E_1 could be larger or smaller than that of E_2 depending on the aspect ratio due to orthotropy. $S_{\nu_{12}}(\gamma_4)$ is not monotonically increasing as a/b increases as it reaches a maximum and then decreases. It is noted that for $\mu = 1$, the mode numbers do not change and $m = 1$, $n = 1$ for all a/b. For the case $\mu = 0$, only $S_\eta(\gamma_5)$ shows a monotonic increase with increasing aspect ratio. The other sensitivities show a non-monotonic behavior. $S_{E_2}(\gamma_2)$ decreases with increasing a/b after an initial increase which is different from the case of $\mu = 1$. The differences in the dependence of the sensitivities on a/b for the two cases of $\mu = 0$ and $\mu = 1$ are the result of changes in the mode numbers which go from $m = 1$, $n = 1$ for $a/b = 0.5$ and $a/b = 1$ to $m = 5$, $n = 1$ for $a/b = 2.5$ when $\mu = 0$. It is observed from Table 2 that the sensitivity trends for $\beta = 0.3$ are similar to the ones for $\beta = 0.1$. An interesting observation is that for $\mu = 1$, the sensitivity $S_{E_1}(\gamma_1)$ is higher for low aspect ratios and the sensitivity $S_{E_2}(\gamma_2)$ is higher for high aspect ratios and the cross-over point is around $a/b = 1.3$. However for $\mu = 0$, $S_{E_1}(\gamma_1)$ is higher than $S_{E_2}(\gamma_2)$ for all aspect ratios as E_1 contributes more to the stiffness of the nanoplate when the compressive loads are axial as opposed to biaxial ($\mu = 1$).

Next the relative sensitivities S_{E_1}, S_{E_2}, $S_{\nu_{12}}$ and S_η are plotted against the level of uncertainty and the aspect ratio in Fig. 7 for $\mu = 1$ by means of contour plots. It is observed that S_{E_1} is higher for low aspect ratios (Fig. 7a) and S_{E_2} is higher for high aspect ratios (Fig. 7b) due to the orthotropy of the graphene. On the other hand $S_{\nu_{12}}$ is not affected much by the aspect ratio (Fig. 7c), but by the level of uncertainty and its value is much lower than the sensitivities of Young's moduli. Fig. 7d shows the corresponding counter plot for S_η. It is observed that the buckling load is fairly sensitive to the small-scale parameter η.

7. Conclusions

The effect of variations in the material properties of a rectangular orthotropic nanoplate have been studied with respect to the critical buckling load. Small-scale effect was taken into account by employing the nonlocal theory for the governing equation. The uncertain quantities were identified as the elastic constants and the small-scale parameter and treated as uncertain-but-bounded quantities. Convex modeling of the uncertainties led to a five-dimensional ellipsoid bounding the uncertainties and the method of Lagrange multipliers were implemented in obtaining the least favorable solution, i.e., the most conservative buckling load given the bound on the uncertainties. Numerical results are given for various levels of uncertainty.

Acknowledgements

The research reported in this paper was supported by research grants from the University of KwaZulu-Natal (UKZN) and from National Research Foundation (NRF) of South Africa. The authors gratefully acknowledge the support provided by UKZN and NRF.

Appendix A

In the case of four independent orthotropic constants $\widetilde{E}_1, \widetilde{E}_2, \widetilde{G}_{12}, \tilde{\nu}_{12}$, the expressions for b_{imn}, $i = 1,2,\ldots,5$, p_{mn} and q_{mn} appearing in the buckling load (19) are given by

$$b_{0mn} = m^4 D_{11}^0 + 2m^2n^2r^2D_{12}^0 + 4m^2n^2r^2D_{66}^0 + n^4r^4D_{22}^0 \tag{A1}$$

$$b_{1mn} = m^4(1-a_2)D_{11}^0 - 2m^2n^2r^2a_2D_{12}^0 + n^4r^4(1-a_2)D_{22}^0 \tag{A2}$$

$$b_{2mn} = m^4a_2D_{11}^0 + 2m^2n^2r^2(1+a_2)D_{12}^0 + n^4r^4a_2D_{22}^0 \tag{A3}$$

$$b_{3mn} = 4m^2n^2r^2D_{66}^0 \tag{A4}$$

$$b_{4mn} = 2m^4a_2D_{11}^0 + 2m^2n^2r^2(1+2a_2) + 2n^4r^4a_2D_{22}^0 \tag{A5}$$

$$b_{5mn} = -b_{0mn}q_{mn} \tag{A6}$$

where

$$p_{mn} = \eta_0^2 s_{mn} + m^2 + n^2\mu r^2, \quad q_{mn} = \frac{2\eta_0^2 s_{mn}}{p_{mn}},$$
$$s_{mn} = m^4 + m^2n^2(\mu+1)r^2 + n^4\mu r^4 \tag{A7}$$

In the case of three independent orthotropic constants $\widetilde{E}_1, \widetilde{E}_2, \tilde{\nu}_{12}$ with $\widetilde{G}_{12}$ given in terms of $\widetilde{E}_1$ and $\tilde{\nu}_{12}$ as $\widetilde{G}_{12} = \frac{\widetilde{E}_1}{2(1+\tilde{\nu}_{12})}$, the corresponding expressions are

$$b_{0mn} = m^4 D_{11}^0 + 2m^2 n^2 r^2 D_{12}^0 + 4m^2 n^2 r^2 D_{66}^0 + n^4 r^4 D_{22}^0 \quad \text{(A8)}$$

$$b_{1mn} = m^4(1-a_2)D_{11}^0 - 2m^2 n^2 r^2 a_2 D_{12}^0 + 4m^2 n^2 r^2 D_{66}^0 - n^4 r^4 a_6 a_2 \quad \text{(A9)}$$

$$b_{2mn} = m^4 a_2 D_{11}^0 + 2m^2 n^2 r^2 (1+a_2) D_{12}^0 + n^4 r^4 (1+a_2) D_{22}^0 \quad \text{(A10)}$$

$$b_{3mn} = 0 \quad \text{(A11)}$$

$$b_{4mn} = 2m^4 a_3 a_2 D_{11}^0 + 2m^2 n^2 r^2 (1+2a_2) D_{12}^0 - 4m^2 n^2 r^2 a_3 D_{66}^0 + 2n^4 r^4 a_2 D_{22}^0 \quad \text{(A12)}$$

$$b_{5mn} = -k_0 q_{mn} \quad \text{(A13)}$$

where $a_3 = \frac{\nu_{12}^0}{1+\nu_{12}^0}$.

References

[1] Yakobson BI, Avouris P. Mechanical properties of carbon nanotubes. Topics Appl Phys 2001;80:287–327. Dresselhaus Mildred S., Dresselhaus Gene, Avouris Phaedon, editors. Carbon nanotubes: synthesis, structure, properties, and applications.

[2] Kis A, Zetti A. Nanomechanis of carbon nanotubes. Philos Trans R Soc A 2008;366:1591–611.

[3] Lee C, Wei X, Kysar JW, Hone J. Measurement of the elastic properties and intrinsic strength of monolayer graphene. Science 2008;321:385–8.

[4] Xu Y, Guo Z, Chen H, Yuan Y, Lou J, Lin X, et al. In-plane and tunneling pressure sensors based on graphene/hexagonal boron nitride heterostructures. Appl Phys Lett 2011;99:133109.

[5] Rogers G, Liu J. Graphene actuators: quantum-mechanical and electrostatic double-layer effects. J Am Chem Soc 2011;133:10858.

[6] Moon J, Gaskill D. Graphene: its fundamentals to future applications. IEEE Trans Microw Theory Tech 2011;59:2702.

[7] Sakhaee-Pour A. Elastic buckling of single-layered graphene sheet. Comput Mater Sci 2009;45:266–70.

[8] Pradhan SC, Murmu T. Small scale effect on the buckling of single-layered graphene sheets under biaxial compression via nonlocal continuum mechanics. Comput Mater Sci 2009;47:268–74.

[9] Pradhan SC. Buckling of single layer graphene sheet based on nonlocal elasticity and higher order shear deformation theory. Phys Lett A 2009;373:4182–8.

[10] Farajpour A, Danesh M, Mohammadi M. Buckling analysis of variable thickness nanoplates using nonlocal continuum mechanics. Physica E 2011;44:719–27.

[11] Murmu T, Sienz J, Adhikari S, Arnold C. Nonlocal buckling of double-nanoplate-systems under biaxial compression. Compos Part B Eng 2013;44:84–94.

[12] Murmu T, Pradhan SC. Buckling of biaxially compressed orthotropic plates at small scales. Mech Res Commun 2009;36:933–8.

[13] Malekzadeh P, Setoodeh AR, Alibeygi Beni A. Small scale effect on the thermal buckling of orthotropic arbitrary straight-sided quadrilateral nanoplates embedded in an elastic medium. Compos Struct 2011;93:2083–9.

[14] Narendar S, Gopalakrishnan S. Scale effects on buckling analysis of orthotropic nanoplates based on nonlocal two-variable refined plate theory. Acta Mech 2012;223:395–413.

[15] Farajpour A, Shahidi AR, Mohammadi M, Mahzoon M. Buckling of orthotropic micro/nanoscale plates under linearly varying in-plane load via nonlocal continuum mechanics. Compos Struct 2012;94:1605–15.

[16] Adali S. Variational principles and natural boundary conditions for multilayered orthotropic graphene sheets undergoing vibrations and based on nonlocal elastic theory. J Theor Appl Mech 2011;49(3):621–39.

[17] Adali S. Variational principles for nonlocal continuum model of orthotropic graphene sheets embedded in an elastic medium. Acta Math Sci 2012;32B(1):325–38.

[18] Pradhan SC, Kumar A. Vibration analysis of orthotropic graphene sheets embedded in Pasternak elastic medium using nonlocal elasticity theory and differential quadrature method. Comput Mat Sci 2010;50:239–45.

[19] Pradhan SC, Kumar A. Vibration analysis of orthotropic graphene sheets using nonlocal elasticity theory and differential quadrature method. Compos Struct 2011;93:774–9.

[20] Satish N, Narendar S, Gopalakrishnan S. Thermal vibration analysis of orthotropic nanoplates based on nonlocal continuum mechanics. Physica E 2012;44:1950–62.

[21] Pouresmaeeli S, Fazelzadeh SA, Ghavanloo E. Exact solution for nonlocal vibration of double-orthotropic nanoplates embedded in elastic medium. Compos Part B Eng 2012;43:3384–90.

[22] Eringen AC. Linear theory of nonlocal elasticity and dispersion of plane waves. Int J Eng Sci 1972;10:425–35.

[23] Eringen AC. On differential equations of nonlocal elasticity and solutions of screw dislocation and surface waves. J Appl Phys 1983;54:4703.

[24] Au FTK, Cheng YS, Tham LG, Zeng GW. Robust design of structures using convex models. Comput Struct 2003;81:2611–9.

[25] Luo Y, Kang Z, Luo Z, Li A. Continuum topology optimization with non-probabilistic reliability constraints based on multi-ellipsoid convex model. Struct Multidisc Optim 2009;39:297–310.

[26] Sadek IS, Sloss JM, Adali S, Bruch Jr JC. Non-probabilistic modelling of dynamically loaded beams under uncertain excitations. Math Comput Modell 1993;18:59–67.

[27] Adali S, Bruch Jr JC, Sadek IS, Sloss JM. Transient vibrations of cross-ply plates subject to uncertain excitations. Appl Math Model 1995;19:56–63.

[28] Qiu Z, Ma L, Wang X. Unified form for static displacement, dynamic response and natural frequency analysis based on convex models. Appl Math Model 2009;33:3836–47.

[29] Jiang C, Han X, Lu GY, Liu J, Zhang Z, Bai YC. Correlation analysis of non-probabilistic convex model and corresponding structural reliability technique. Comput Methods Appl Mech Eng 2011;200:2528–46.

[30] Kang Z, Luo Y, Li A. On non-probabilistic reliability-based design optimization of structures with uncertain-but-bounded parameters. Struct Saf 2011;33:196–205.

[31] Luo Y, Li A, Kang Z. Reliability-based design optimization of adhesive bonded steel–concrete composite beams with probabilistic and non-probabilistic uncertainties. Eng Struct 2011;33(7):2110–9.

[32] Radebe IS, Adali S. Minimum weight design of beams against failure under uncertain loading by convex analysis. J Mech Sci Technol 2013;27(7):1–8.

[33] Wang X, Wang L, Elishakoff I, Qiu Z. Probability and convexity concepts are not antagonistic. Acta Mech 2011;219:45–64.

[34] Ben-Haim Y, Elishakoff I. Convex models of uncertainty in applied mechanics. Amsterdam: Elsevier Science; 1990.

[35] Conceição António CA, Hoffbauer LN. Uncertainty analysis based on sensitivity applied to angle-ply composite structures. Reliab Eng Syst Saf 2007;92:1353–62.

[36] Conceição António CA, Hoffbauer LN. Uncertainty assessment approach for composite structures based on global sensitivity indices. Compos Struct 2012. doi: http://dx.doi.org/10.1016/j.compstruct.2012.12.001.

[37] Sobol IM. Global sensitivity indices for nonlinear mathematical models and their Monte Carlo estimates. Math Comput Simul 2001;55:271–80.

[38] Cacuci DG. Sensitivity and uncertainty analysis. Theory, vol. 1. Boca Raton (FL): Chapman & Hall/CTC Press; 2003.

[39] Qiu Z, Hu J, Yang J, Lu Q. Exact bounds for the sensitivity analysis of structures with uncertain-but-bounded parameters. Appl Math Model 2008;32:1143–57.

[40] Hernandez E, Goze C, Bernier P, Rubio A. Elastic properties of C and $B_xC_yN_z$ composite nanotubes. Phys Rev Letters 1998;80:4502–5.

[41] Wang Q. Effective in-plane stiffness and bending rigidity of armchair and zigzag carbon. Int J Solids Struct 2004;41:5451–61.

[42] Li C, Chou TW. A structural mechanics approach for the analysis of carbon nanotubes. Int J Solids Struct 2003;40:2487–99.

Paper 3

The paper was accepted for publication in the **Latin American journal of Solid and Structures (LAJSS)**.

Latin American Journal of Solids and Structures
www.lajss.org

Effect of surface stress on the buckling of nonlocal nanoplates subject to material uncertainty

Abstract
At the nano scale, the effect of surface stress becomes prominent as well as the so-called small scale effect. Further complicating the phenomenon is the uncertainty involved in the determination of the material properties of nano structures due to difficulties in making accurate measurements at nano scale and also due to molecular defects and manufacturing tolerances. This introduces some degree of uncertainty in the computation of the mechanical response of the nano-scale components. In the present study a convex model is employed to take surface tension, small scale parameter and the elastic constants as uncertain-but-bounded quantities in the buckling analysis of nanoplates. The objective is to determine the lowest buckling load for a given level of uncertainty to obtain a conservative estimate by taking the worst-case variations of material properties. Moreover the sensitivity of the buckling load to material uncertainties is also investigated.

Keywords
Nanoplates, surface stress, buckling, material uncertainty, nonlocal theory, sensitivity analysis.

I. S. Radebe[a]
S. Adali[b,*]

[a] Department of Mechanical Engineering, Durban University of Technology, Durban, South Africa, email: sfisor@dut.ac.za

[b] Mechanical Engineering, University of KwaZulu-Natal, Durban, South Africa,

Author email: adali@ukzn.ac.za

1 INTRODUCTION

At nano scales, surface area to volume ratio increases to the extent that the surface stress effects can no longer be ignored as noted by Miller and Shenoy (2000) and Sun and Zhang (2003). This phenomenon has been observed and noted in a number of studies and, in particular, the effect of surface tension on the properties of nano-sized structures in (Cuenot et al 2004; Jing et al 2006; Park and Klein, 2008; Stan et al 2008; Eremeyev et al 2009; Wang et al 2010). These effects arise due to the fact that atoms at or near a free surface behave differently as compared to the atoms in the bulk of the material leading to a higher elastic modulus and mechanical strength (Murdoch, 2005). A review of the effect of surface stress on nanostructures was given by Wang et al (2011).

Nano-sized structures include nanowires, nanobeams and nanoplates. Recent work on the effect of surface energy on the mechanical behavior of nanowires include (Jiang and Yan 2010; Hasheminejad and Gheshlaghi 2010; Lee and Chang 2011; Samaei et al 2012). Vibrations of nanobeams with surface effects have been studied by Gheshlaghi and Hasheminejad (2011), Sharabiani and Yazdi (2013), Hosseini-Hashemi and Nazemnezhad (2013), Malekzadeh and Shojaee (2013).

High area to volume ratio of nanoplates makes them particularly susceptible to surface effects and the accuracy of solutions improves by including these effects in the governing equations. Theory of

plates with surface effects has been developed in (Lu et al 2006). The effect of surface stress on the stiffness of cantilever plates was studied by Lachut and Sader (2007). Buckling of nanoplates including the effects of surface energy as well as the small scale effect was studied by Wang and Wang (2011a) and Farajpour et al 2014, employing the nonlocal elastic theory. Several studies on the vibrations and dynamics of nanoplates were conducted taking the surface effects into account in (Ansari and Sahmani, 2011; Wang and Wang 2011b; Assadi 2013; Narendar and Gopalakrishnan 2012).

In the above studies only the average values of the material properties were used and the possibility of variations and/or inaccuracies in the data was not considered. Main drawback of the studies using deterministic material properties of the nano-sized structures is that the elastic constants and other material properties such as surface tension and the small-scale parameter often cannot be determined with a high degree of accuracy. The values of these constants may be known with some degree of uncertainty for a number of reasons such as processing difficulties, measurement inaccuracies, and defects and imperfections in the molecular structures. For example experimental difficulties for making accurate measurements at the nano scale can lead to significant scatter in material data as noted by Kis and Zetti (2008) and Lee et al (2008).

Results obtained by neglecting the possibility of uncertainty in material properties are, in general, not reliable in the sense that the load carrying capacity of the structure may be overestimated (Au et al 2003). In the case of buckling, premature buckling may occur when these uncertainties affect the structure in a negative way. However structural reliability can be improved by calculating a conservative buckling load by incorporating the uncertain data in a non-deterministic model of the problem. In the present study this is done by convex modeling which requires that the uncertain quantities are bounded by an ellipsoid (Luo et al 2009). Examples of convex modeling applied to various engineering problems with uncertain data can be found in (Sadek et al 1993; Adali et al 1995; Qiu et al 2009; Kang et al 2011; Luo et al 2011; Radebe and Adali 2013), where beams, plates and columns have been studied with respect to static and dynamic response, vibration and buckling response.

Nanoplates are used in several nanotechnology applications and often subjected to in-plane loads which can lead to failure by buckling, especially considering their extremely small thickness (Asemi et al 2014). Buckling behavior and sensitivity of nonlocal orthotropic nanoplates with material uncertainty have been investigated by Radebe and Adali (2014) neglecting the surface effect. In the present study buckling of isotropic nanoplates is studied including the effect of surface stress. The material parameters taken as uncertain are residual surface stress, surface elastic modulus, the small scale parameter of the nonlocal theory and Young's modulus. The sensitivity of the critical load to uncertainty including the surface effect is investigated by defining relative sensitivities (Cacuci 2003; Conceição António and Hoffbauer 2013). The effect of uncertainty on the buckling load is studied in the numerical examples and the sensitivity to uncertainty is studied by means of contour plots.

2 NONLOCAL NANOPLATE WITH SURFACE EFFECTS

We consider a rectangular nanoplate subject to biaxial buckling loads N_x and N_y acting in the x and y directions, respectively. The dimensions of the plate are specified as a in the x-direction and b in the y-direction with the plate thickness given by h. The differential equation governing the buckling of the nanoplate based on nonlocal elastic theory and including the effect of surface energy is given in (Wang and Wang 2001a) as

$$\left(\widetilde{D}+\frac{1}{2}h^2\widetilde{E}^s\right)\nabla^4 w-\frac{1}{2}\widetilde{\mu}^2h^2\widetilde{E}^s\nabla^6 w-(1-\widetilde{\mu}^2\nabla^2)\left(2\widetilde{\tau}_0\nabla^2 w+N_x\frac{\partial^2 w}{\partial^2 x}+N_y\frac{\partial^2 w}{\partial^2 y}\right)=0 \qquad (1)$$

where $w(x,y)$ is the deflection of the plate, $\nabla^2 = \frac{\partial^2 v}{\partial^2 x} + \frac{\partial^2 v}{\partial^2 y}$, $\widetilde{D} = \frac{\widetilde{E}h^3}{12(1-\nu^2)}$, $\widetilde{\mu}$ is the uncertain small-scale parameter of the nonlocal theory and ν is the Poisson's ratio. The uncertain material constants are denoted by $\widetilde{E}$ (Young's modulus), $\widetilde{E}^s$ (surface elastic modulus) and $\widetilde{\tau}_0$ (residual surface stress). For a simply supported plate, the solution is given by

$$w(x,y) = \sum_m \sum_n c_{mn} \sin(m\pi x/a)\sin(n\pi y/b) \tag{2}$$

The buckling load can be obtained by substituting Eq. (2) into Eq. (1). This computation gives [24]

$$N_{\mathrm{cr}} = \min_{m,n} \frac{\eta^4(\widetilde{D} + 0.5h^2\widetilde{E}^s + 2\widetilde{\tau}\widetilde{\mu}^2) + 0.5h^2\eta^6\widetilde{E}^s\widetilde{\mu}^2 + 2\eta^2\widetilde{\tau}_0}{(\xi^2 + R\zeta^2)\left(1+\eta^2\widetilde{\mu}^2\right)} \tag{3}$$

where $\xi = m\pi/a$, $\zeta = n\pi/b$, $\eta^2 = \xi^2 + \zeta^2$, $R = N_y/N_x$ and $m,n = 1,2,3\ldots$ The buckling load can be expressed as

$$N_{\mathrm{cr}} = \min_{m,n} \frac{\eta^4(g_1\widetilde{E} + g_2\widetilde{E}^s + 2\widetilde{\tau}\widetilde{\mu}^2) + g_2\eta^6\widetilde{E}^s\widetilde{\mu}^2 + 2\eta^2\widetilde{\tau}_0}{(\xi^2 + R\zeta^2)\left(1+\eta^2\widetilde{\mu}^2\right)} \tag{4}$$

where the constants g_1 and g_2 appearing in Eq. (4) are given by

$$g_1 = \frac{h^3}{12(1-\nu^2)}, \qquad g_2 = 0.5\,h^2 \tag{5}$$

Introducing the uncertainty parameters ε_i, the uncertain material constants can be expressed as

$$\widetilde{E} = E_0(1+\varepsilon_1), \qquad \widetilde{E}^s = E_0^s(1+\varepsilon_2), \qquad \widetilde{\tau} = \tau_0(1+\varepsilon_3), \qquad \widetilde{\mu} = \mu_0(1+\varepsilon_4) \tag{6}$$

where the subscript "0" denotes the nominal quantities. The parameters ε_i are unknown and have to be determined to obtain the so-called "worst-case" buckling load which is the lowest buckling load for a given level of uncertainty. Substituting Eq. (6) into Eq. (4) and keeping only the terms linear in ε_i, we obtain

$$N_{\mathrm{cr}}(\varepsilon_i) = \min_{m,n} \frac{A_0 + g_1\,\eta^4 E_0\,\varepsilon_1 + g_2\,\eta^4 E_0^s\gamma\,\varepsilon_2 + 2\eta^2\tau_0\,\gamma\,\varepsilon_3 + 2\eta^4\mu_0^2(2\tau_0 + g_2\,\eta^2 E_0^s)\,\varepsilon_4}{(\xi^2 + R\zeta^2)\gamma^2\left(1+2\eta^2\mu_0^2\gamma^{-1}\varepsilon_4\right)} \tag{7}$$

where

$$A_0 = \eta^4(g_1E_0 + g_2E_0^s) + 2\eta^4\tau_0\mu_0^2 + g_2\eta^6E_0^s\mu_0^2 + 2\eta^2\tau_0, \qquad \gamma = 1+\eta^2\mu_0^2 \tag{8}$$

The expression (7) for $N_{\mathrm{cr}}(\varepsilon_i)$ can be approximated as

$$N_{\mathrm{cr}}(\varepsilon_i) \cong \min_{m,n}\left(a_{0mn} + \sum_{i=1}^{4} a_{imn}\varepsilon_i\right) \tag{9}$$

by linearizing it using the relation $(1\pm\varepsilon)^c \cong (1\mp c\varepsilon)+O(\varepsilon^2)$ where the superscript c can take positive or negative values and $|\varepsilon| << 1$. The values of a_{imn} appearing in Eq. (8) are given in the Appendix.

2.1 Simply supported beam

The method of solution outlined above is now applied to a simply supported beam subject to a deterministic load $p(x)=p_0(x/L)^3$ and the uncertain load $\tilde{q}(x)$. The simply supported boundary conditions for the nonlocal nanobeam are given by (Reddy 2007)

$$w(0)=0, \qquad (-EI+\eta^2 N_0)w_{xx}(0)+\eta^2 k_0 b w(0)-\eta^2 p(0)-\eta^2\tilde{q}(0)=0 \tag{13}$$

$$w(L)=0, \qquad (-EI+\eta^2 N_0)w_{xx}(L)+\eta^2 k_0 b w(L)-\eta^2 p(L)-\eta^2\tilde{q}(L)=0 \tag{14}$$

The deterministic and uncertain loads are expanded in terms of orthogonal functions $\psi_n(x)=\sin\alpha_n x$ where $\alpha_n = n\pi/L$. Thus

$$p(x)=\sum_{n=1}^{N} p_n \sin\alpha_n x, \qquad \tilde{q}(x)=\sum_{n=1}^{N}\tilde{q}_n \sin\alpha_n x \tag{15}$$

where the coefficients p_n are given by

$$p_n=(-1)^{n+1}\frac{2p_0}{(n\pi)^3}\left(n^2\pi^2-6\right) \tag{16}$$

The deflection $w(x)$ satisfying the boundary conditions (13) and (14) can be obtained by expanding it in terms of $\sin\alpha_n x$ as

$$w(x)=\sum_{n=1}^{N} W_n \sin\alpha_n x \tag{17}$$

Substituting Eq. (17) into the differential equation (1), the coefficients W_n are computed as

$$W_n=\frac{(1+\eta^2\alpha_n^2)(p_n+\tilde{q}_n)}{EI\alpha_n^4-(1+\eta^2\alpha_n^2)\alpha_n^2 N_0} \tag{18}$$

Lagrangian $L(x_0;\tilde{q}_n)$ given by Eq. (9) becomes

$$L(x_0;\tilde{q}_n)=\sum_{n=1}^{N}\frac{(1+\eta^2\alpha_n^2)(p_n+\tilde{q}_n)}{EI\alpha_n^4-(1+\eta^2\alpha_n^2)\alpha_n^2 N_0}\sin\alpha_n x_0+\lambda\left(\sum_{n=1}^{N}(\tilde{q}_n)^2-\frac{2\varepsilon^2}{L}\right) \tag{19}$$

The coefficients $\tilde{q}_n(x_0)$ are computed from Eqs. (11) and (19) as

$$\tilde{q}_n(x_0)=-\frac{1}{2\lambda}\frac{A_n(x_0)}{B_n} \tag{20}$$

where

$$A_n(x_0) = (1+\eta^2\alpha_n^2)\sin\alpha_n x_0\,, \qquad B_n = EI\alpha_n^4 - (1+\eta^2\alpha_n^2)\alpha_n^2 N_0 \tag{21}$$

Noting that the worst case loading is given by

$$\sum_{n=1}^{N}(\tilde{q}_n)^2 = \frac{2\varepsilon^2}{L} \tag{22}$$

we can compute the Lagrange multiplier from Eqs. (20) and (22) as

$$\lambda = \pm\frac{L^{1/2}}{\sqrt{8}\varepsilon}\left(\sum_{n=1}^{N}\frac{A_n^2(x_0)}{B_n^2}\right)^{1/2} \tag{23}$$

where the plus and minus signs correspond to the least and most favourable loading cases. The coefficients $\tilde{q}_n$ can be computed by inserting the Lagrange multiplier (23) into Eq. (20). This computation gives

$$\tilde{q}_n(x_0) = \mp\frac{\sqrt{2}\varepsilon}{L^{1/2}}\left(\sum_{n=1}^{N}\frac{A_n^2(x_0)}{B_n^2}\right)^{-1/2}\frac{A_n(x_0)}{B_n} \tag{24}$$

The uncertain load producing the maximum deflection is given by Eq. (15) with the coefficients given by Eq. (24).

3 CONVEX MODELING

Next the unknown constants ε_i are determined to obtain the most conservative buckling load in the presence of material uncertainties. The convex modeling of the uncertainties is expressed as requiring that the unknown parameters ε_i are bounded such that they satisfy the inequality

$$\sum_{i=1}^{4}\varepsilon_i^2 \le \beta^2 \tag{10}$$

where β is the radius of a 4-dimensional ellipsoid. As such β is a measure of the level of uncertainty and satisfies the inequality $\beta < 1$ since $|\varepsilon| << 1$. It is known that the buckling load takes on its extreme values on the boundary of the ellipsoid defined by Eq. (10) (see Sadek et al 1993, Adali et al 1995). Thus the inequality (10) can be replaced by the equality

$$\sum_{i=1}^{n}\varepsilon_i^2 = \beta^2 \tag{11}$$

The expression (9) for $N_{\rm cr}$ is to be minimized subject to the constraint (11) to compute the constants ε_i and to obtain the lowest buckling load. For this purpose, the following Lagrangian is introduced

$$L(a_i, \varepsilon_i) = a_{0mn} + \sum_{i=1}^{4}a_{imn}\varepsilon_i + \lambda\left(\sum_{i=1}^{4}\varepsilon_i^2 - \beta^2\right) \tag{12}$$

By setting $\partial L(a_{imn},\varepsilon_i)/\partial\varepsilon_i = 0$ and using Eq. (11), the parameters ε_i and the Lagrange multiplier λ are computed as

$$\varepsilon_i = -\frac{a_{imn}}{2\lambda}, \qquad \lambda = \pm\frac{1}{2\beta}\left(\sum_{i=1}^{4} a_{imn}^2\right)^{1/2} \tag{13}$$

Thus

$$\varepsilon_i = \mp\beta a_{imn}\left(\sum_{i=1}^{4} a_{imn}^2\right)^{-1/2} \qquad \text{for} \quad i = 1,2,3,4 \tag{14}$$

where the plus and minus signs correspond to the lowest and highest buckling loads.

4 SENSITIVITY ANALYSIS

The sensitivity of the buckling load to uncertainty can be investigated by defining relative sensitivity indices $S_K(\varepsilon_i)$ given by

$$S_K(\varepsilon_i) = \left|\frac{\partial N_{cr}(\beta)}{\partial\varepsilon_i}\right| \frac{|\varepsilon_i|}{N_{cr}(0)} \tag{15}$$

which is normalized with respect to the deterministic buckling load $N_{cr}(0)$. In Eq. (15), the sensitivities of the buckling load to $\widetilde{E}$, $\widetilde{E}^s$, $\widetilde{\tau}$ and $\widetilde{\mu}$ with respect to uncertainty parameters ε_i, $i = 1,2,3,4$ are denoted by $S_E(\varepsilon_1)$, $S_{E^s}(\varepsilon_2)$, $S_\tau(\varepsilon_3)$ and $S_\mu(\varepsilon_4)$, respectively, so that the subscript K stands for the respective material property. Equation (15) indicates that the buckling pressure has zero sensitivity for $\varepsilon_i = 0$ corresponding to the deterministic case as expected. The sensitivities $S_K(\varepsilon_i)$ can be computed from Eqs. (9) and (15) as

$$S_K(\gamma_i) = \frac{|a_{imn}\varepsilon_i|}{a_{0mn}} \tag{16}$$

noting that $N_{cr}(0) \equiv a_{0mn}$.

5 NUMERICAL RESULTS

The effect of uncertain loads and material properties on deflection is studied in the present section. The results are given for a square silver nanoplate of thickness $h = 5$ nm. The nominal values of the elastic constants are taken as $E_0 = 76$ GPa, $\nu = 0.3$, $E_0^s = 1.22$ N/m and $\tau_0 = 0.89$ N/m which are the values used in (Wang and Wang 2011a). The buckling load is normalized by the buckling load N_{L} of a plate without surface and nonlocal effects and with deterministic constants which can be obtained from Eq. (7) by setting $E_0^s = \tau_0 = \mu_0 = \varepsilon_i = 0$. Thus the normalized buckling load is given by $N_R = N_{cr}(\varepsilon_i)/N_L$.

Figure 1 shows the curves of N_R plotted against the length a for various uncertainty levels with $\mu_0 = 2$ nm under the biaxial loading $N_x = N_y$ ($R = 1$). It is noted that the buckling load curve for

the deterministic case ($\beta = 0.0$) corresponds to the result given in Figure 1 of Wang and Wang (2011a). The corresponding results for the uniaxial loading with $N_y = 0$ ($R = 0$) are given in Figure 2. It is observed that the buckling load decreases as the level of uncertainty increases as expected.

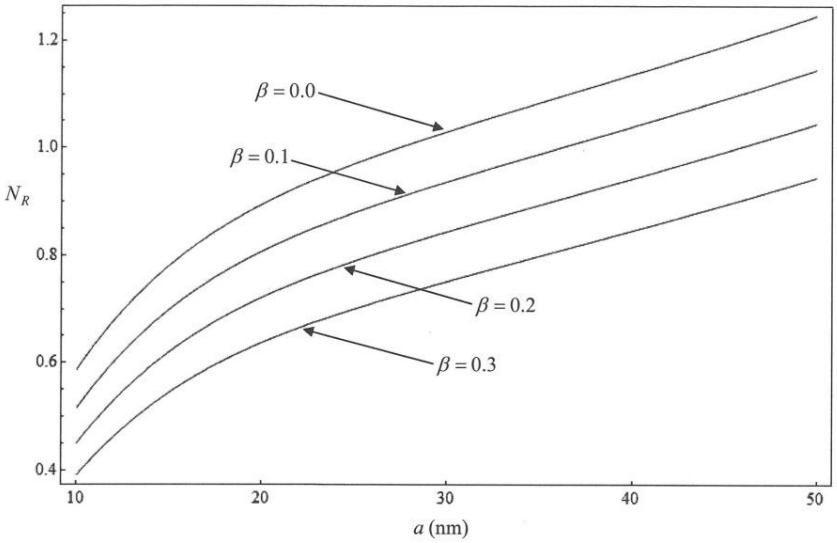

Figure 1 Curves of N_R plotted against a for various uncertainty levels with $b = a$, $\mu_0 = 2$ nm and $N_y / N_x = 1$

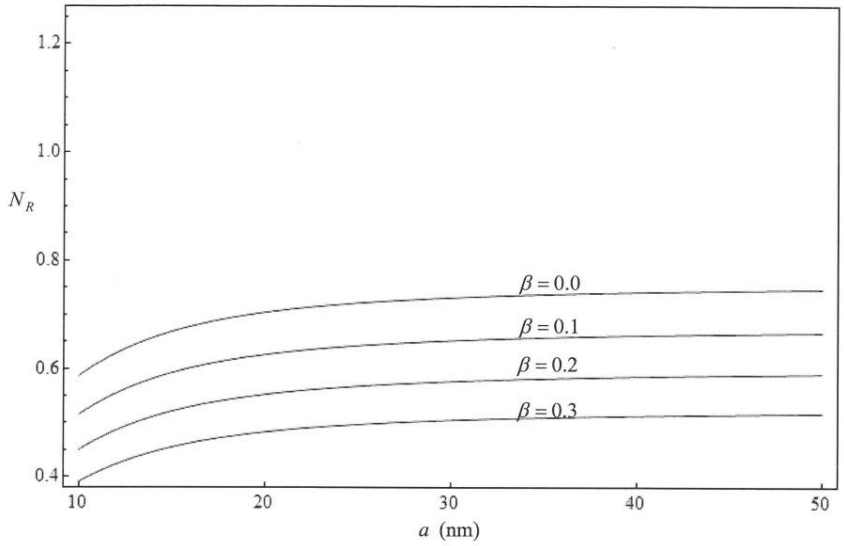

Figure 2 Curves of N_R plotted against a for various uncertainty levels with $b = a$, $\mu_0 = 2$ nm and $N_y = 0$

The sensitivity results are given in Figure 3 with respect to $\tilde{E}$, $\tilde{E}^s$, and Figure 4 with respect to $\tilde{\tau}$ and $\tilde{\mu}$ which show the contour plots of the sensitivity indices plotted against the level of uncertainty and the length a for a square nanoplate with $N_y / N_x = 1$. In all cases the sensitivity of the buckling load to elastic constants increases with increasing uncertainty, but the buckling load shows the most sensitivity to $\tilde{E}$ (Figure 3a). The second most sensitivity is observed towards the uncertain small-scale parameter $\tilde{\mu}$ (Figure 4b). This sensitivity, as well as the sensitivity to surface elastic modulus

$\tilde{E}^s$ (Figure 3b), increases as the size of the nanoplate becomes smaller, i.e., as $a \to 0$. On the other hand the sensitivity towards the residual surface stress $\tilde{\tau}_0$ increases as the nanoplate becomes larger (Figure 4a).

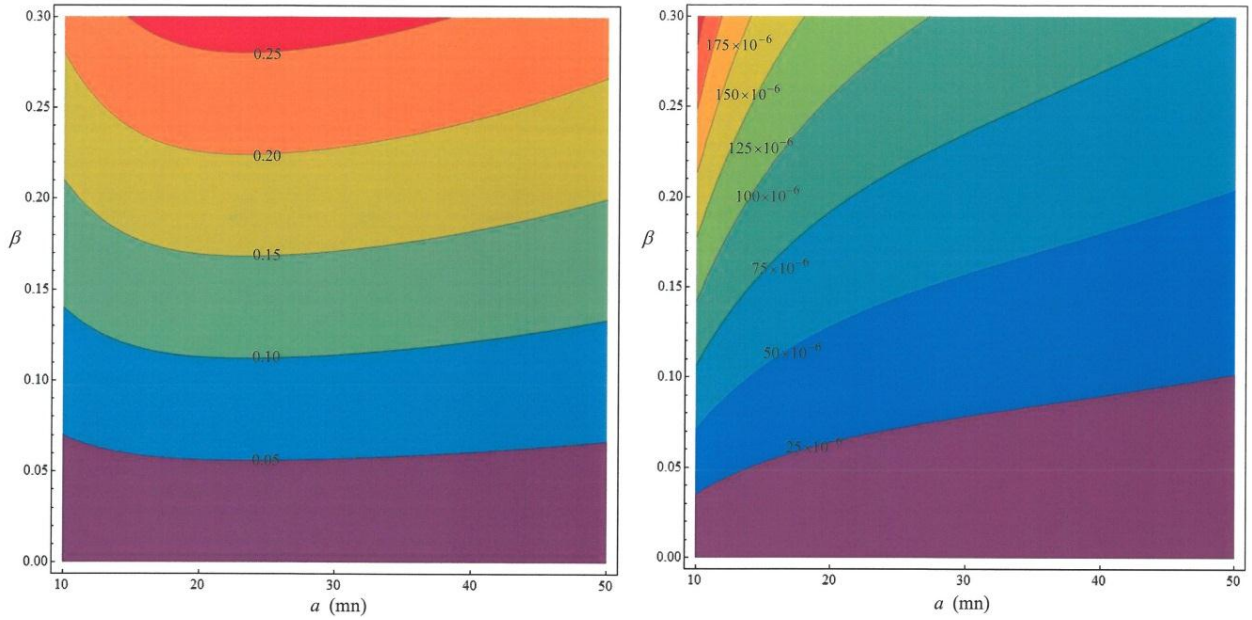

Figure 3 Contour plots of sensitivities plotted against uncertainty level β and a with $b = a$, $\mu_0 = 2$ nm and $N_y / N_x = 1$, a) $S_E(\varepsilon_1)$, b) $S_{E^s}(\varepsilon_2)$

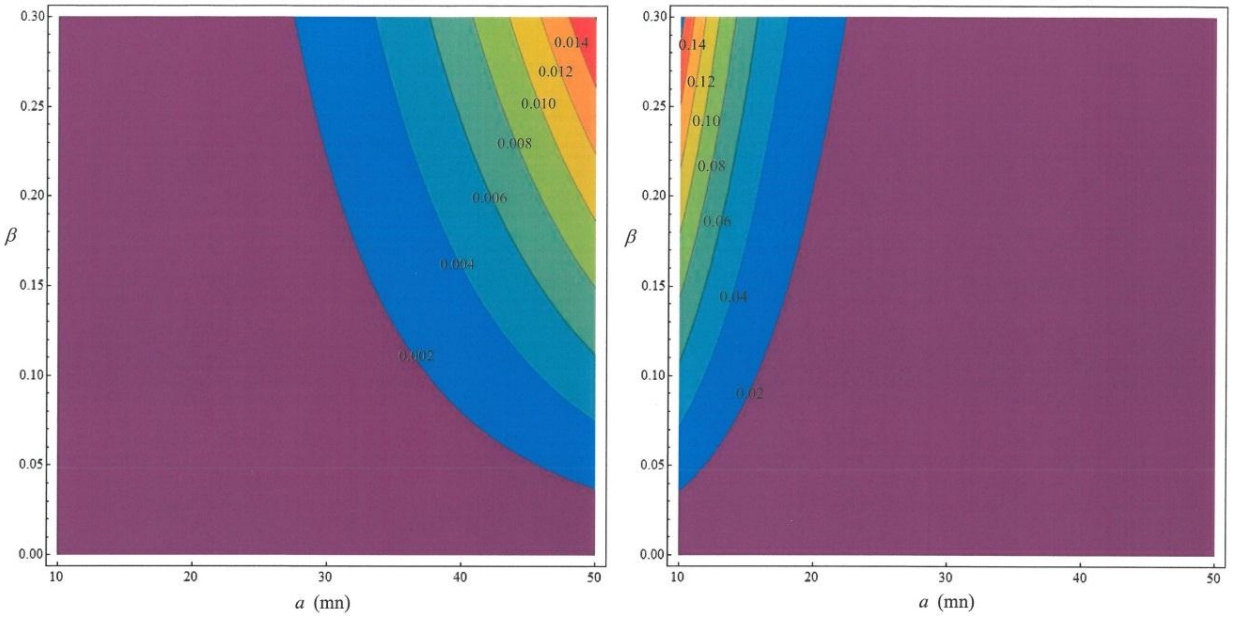

Figure 4 Contour plots of sensitivities plotted against uncertainty level β and a with $b = a$, $\mu_0 = 2$ nm and $N_y / N_x = 1$, a) $S_\tau(\varepsilon_3)$, b) $S_\mu(\varepsilon_4)$

6 CONCLUSIONS

The study is directed to the buckling of nano-scale plates with material uncertainties and including the effect of surface stress. The uncertain parameters are the Young's modulus, surface elastic modulus, residual surface stress and small scale parameter of the nonlocal theory. The effect of uncertainty in these constants is studied with respect to the buckling of an isotropic nanoplate. The uncertainty is taken into account by convex modeling which determines the worst-case combination of material properties to determine the lowest buckling load for a given level of uncertainty.

In the present case convex modeling leads to a four-dimensional ellipsoid bounding the uncertainties and the method of Lagrange multipliers is implemented to compute the uncertainty parameters. Moreover sensitivity indices are developed to investigate the relative sensitivity of the buckling load to the uncertainties in the elastic constants. The numerical results show the effect of increasing uncertainty on the buckling load for biaxial and uniaxial buckling loads (Figures 1 and 2). The sensitivity studies indicate that the buckling load is most sensitive to uncertainty in Young's modulus and the size of the nanoplate affects various sensitivities in different ways. The sensitivity to small-scale parameter and surface elastic modulus increases as the nanoplate gets smaller and the sensitivity to residual surface stress increases as the nanoplate becomes larger (Figures 3a and 4). Sensitivity to Young's modulus is mostly influenced by the level of uncertainty (Figures 4a).

Acknowledgements

The research reported in this paper was supported by research grants from the University of KwaZulu-Natal (UKZN) and from National Research Foundation (NRF) of South Africa. The author gratefully acknowledges the supports provided by UKZN and NRF.

References

Adali, S., Bruch, Jr., J. C., Sadek, I. S., Sloss, J. M. (1995). Transient vibrations of cross-ply plates subject to uncertain excitations. Applied Mathematical Modelling 19: 56–63.

Ansari, R., Sahmani, S. (2011). Surface stress effects on the free vibration behavior of nanoplates. International Journal of Engineering Science 49: 1204–1215.

Assadi, A. (2013). Size dependent forced vibration of nanoplates with consideration of surface effects. Applied Mathematical Modelling 37: 3575–3588.

Asemi, A. S., Farajpour, A., Borghei, M., Hassani, A. H. (2014). Thermal effects on the stability of circular graphene sheets via nonlocal continuum mechanics. Latin American Journal of Solids and Structures 11: 704-724.

Au, F. T. K., Cheng, Y. S., Tham, L. G., Zeng, G. W. (2003). Robust design of structures using convex models. Computers and Structures 81: 2611–2619.

Cacuci, D. G. (2003). Sensitivity and Uncertainty Analysis, Vol. 1: Theory. Boca Raton, FL: Chapman & Hall/CTC Press.

Conceição António, C. A., Hoffbauer, L. N. (2013). Uncertainty assessment approach for composite structures based on global sensitivity indices. Composite Structures 99: 202–212.

Cuenot, S., Frétigny, C., Demoustier-Champagne, S., Nysten, B. (2004). Surface tension effect on the mechanical properties of nano materials measured by atomic force microscopy. Physical Reviews B 69: 165410–165413.

Eremeyev, V. A., Altenbach, H., Morozov, N. F. (2009). The influence of surface tension on the effective stiffness of nanosize plates. Doklady Physics 54: 98–100.

Farajpour, A., Dehghany, M., Shahidi, A.R. (2013). Surface and nonlocal effects on the axisymmetric buckling of circular graphene sheets in thermal environment. Composites Part B: Engineering 50: 333–343.

Gheshlaghi, B., Hasheminejad, S. M. (2011). Surface effects on nonlinear free vibration of nanobeams. Composites Part B: Engineering 42: 934–937.

Hasheminejad, S. M., Gheshlaghi, B. (2010). Dissipative surface stress effects on free vibrations of nanowires. Applied Physics Letters 97: 253103.
Hosseini-Hashemi, S., Nazemnezhad, R. (2013). An analytical study on the nonlinear free vibration of functionally graded nanobeams incorporating surface effects. Composites Part B: Engineering 52: 199–206.
Jiang, L. Y., Yan, Z. (2010). Timoshenko beam model for static bending of nanowires with surface effects. Physica E 42: 2274–2279.
Jing, G. Y., Duan, H. L., Sun, X. M., Zhang, Z. S., Xu, J., Li, Y. D., Wang, J. X., Yu, D. P. (2006). Surface effects on elastic properties of silver nanowires: Contact atomic-force microscopy. Physical Reviews B 73: Art. 235409.
Kang, Z., Luo, Y., Li, A. (2011). On non-probabilistic reliability-based design optimization of structures with uncertain-but-bounded parameters. Structural Safety 33: 196–205.
Kis, A., Zetti, A. (2008). Nanomechanics of carbon nanotubes. Philosophical Transactions of Royal Society A 366: 1591–1611.
Lachut, M. J., Sader, J. E. (2007). Effect of surface stress on the stiffness of cantilever plates. Physics Review Letters 99: 206102.
Lee, C., Wei, X., Kysar, J.W., Hone, J. (2008). Measurement of the elastic properties and intrinsic strength of monolayer graphene. Science 321: 385–388.
Lee, H. L., Chang, W. J. (2011). Surface effects on axial buckling of nonuniform nanowires using non-local elasticity theory. Micro and Nano Letters 6: 19–21.
Lu, P., He, L. H., Lee, H. P., Lu, C. (2006). Thin plate theory including surface effects. International Journal of Solids and Structures 43: 4631–4647.
Luo, Y., Kang, Z., Luo, Z., Li, A. (2009). Continuum topology optimization with non-probabilistic reliability constraints based on multi-ellipsoid convex model. Structural and Multidisciplinary Optimization 39: 297–310.
Luo, Y., Li, A., Kang, Z. (2011). Reliability-based design optimization of adhesive bonded steel-concrete composite beams with probabilistic and non-probabilistic uncertainties. Engineering Structures 33: 2110–2119.
Malekzadeh, P., Shojaee, M. (2013). Surface and nonlocal effects on the nonlinear free vibration of non-uniform nanobeams. Composites Part B: Engineering 52: 84–92.
Miller, R. E., Shenoy, V. B. (2000). Size-dependent elastic properties of nanosized structural elements. Nanotechnology 11: 139–147.
Murdoch, A. I. (2005). Some fundamental aspects of surface modelling. Journal of Elasticity 80: 33–52.
Narendar, S., Gopalakrishnan, S. (2012). Study of terahertz wave propagation properties in nanoplates with surface and small scale effects. International Journal of Mechanical Science 64: 221–231.
Park, H. S., Klein, P. A., (2008). Surface stress effects on the resonant properties of metal nanowires: The importance of finite deformation kinematics and the impact of the residual surface stress. Journal of Mechanics and Physics of Solids 56:3144–3166.
Qiu, Z., Ma, L., Wang, X. (2009). Unified form for static displacement, dynamic response and natural frequency analysis based on convex models, Applied Mathematical Modelling 33:3836–3847.
Radebe, I. S., Adali, S. (2013). Minimum weight design of beams against failure under uncertain loading by convex analysis. Journal of Mechanical Science and Technology 27:2071–2078.
Radebe, I. S., Adali, S. (2014). Buckling and sensitivity analysis of nonlocal orthotropic nanoplates with uncertain material properties. Composites Part B: Engineering 56:840–846.
Reddy, J. N. (2007). Nonlocal theories for bending, buckling and vibration of beams. International Journal of Engineering Science 45: 288-307.
Sadek, I. S., Sloss, J. M., Adali, S., Bruch, Jr., J. C. (1993). Nonprobabilistic modelling of dynamically loaded beams under uncertain excitations. Mathematical and Computer Modelling 18: 59–67.
Samaei, A. T., Bakhtiari, M., Wang, G.-F. (2012). Timoshenko beam model for buckling of piezoelectric nanowires with surface effects. Nanoscale Research Letters 7: 201 (6 pages).
Sharabiani, P. A., Yazdi, M. R. H. (2013). Nonlinear free vibrations of functionally graded nanobeams with surface effects. Composites Part B: Engineering 45: 581–586.
Stan, G., Krylyuk, S., Davydov, A. V., Vaudin, M., Bendersky, L. A., Cook, R. F. (2008). Surface effects on the elastic modulus of Te nanowires. Applied Physics Letters 92: 241908.

Sun, C. T., Zhang, H. (2003). Size-dependent elastic moduli of platelike nanomaterials. Journal of Applied Physics 93: 1212–1218.
Wang, J., Huang, Z., Duan, H., Yu, S., Wang, X. G., Zhang, W., Wang, T. (2011). Surface stress effect in mechanics of nano structured materials. Acta Mechanica Solida Sinica 24: 52–82.
Wang, K. F., Wang, B. L. (2011a). Combining effects of surface energy and non-local elasticity on the buckling of nanoplates. Micro and Nano Letters 6: 941–943.
Wang, K. F., Wang, B. L. (2011b). Vibration of nanoscale plates with surface energy via nonlocal elasticity. Physica E 44: 448–453.
Wang, Z. Q., Zhao, Y. P., Huang, Z. P. (2010). The effects of surface tension on the elastic properties of nano structures. International Journal of Engineering Science 48: 140–150.